8-2004

Measurement of Charge Storage Decay Time and Resistivity of Spacecraft Insulators

Prasanna V. Swaminathan

MEASUREMENT OF CHARGE STORAGE DECAY TIME AND RESISTIVITY OF SPACECRAFT INSULATORS

by

Prasanna V. Swaminathan

A thesis submitted in partial fulfillment
of the requirements for the degree

of

MASTER OF SCIENCE

in

Electrical Engineering

Approved:

_____	_____
Dr. Randy J. Jost Major Professor	Dr. John R. Dennison Committee Member
_____	_____
Dr. Alan W. Shaw Committee Member	Dr. Laurens H. Smith, Jr. Interim Dean of Graduate Studies

UTAH STATE UNIVERSITY
Logan, Utah
2004

ABSTRACT

Measurement of Charge Storage Decay Time and Resistivity

of Spacecraft Insulators

by

Prasanna V. Swaminathan, Master of Science

Utah State University, 2004

Major Professor: Dr. Randy J. Jost
Department: Electrical and Computer Engineering

Insulators used in the construction of spacecraft are irradiated with high-energy electrons in the space environment and this sometimes causes the insulators to charge to very high voltages. Such charged insulators can generate spontaneous electric partial-discharge pulses of the order of mA to tens of A. These pulses sometimes last enough time to destroy the expensive micro-circuitry present in the spacecraft. In evaluating the threat to the spacecraft due to these discharges, calculation of the resistivity becomes a critical parameter since it determines how accumulated charge will distribute across the spacecraft and how rapidly charge imbalance will dissipate. So far, resistivity values for the insulators for spacecraft applications have been simply imported from tabulated results measured using standard American Society for Testing and Materials (ASTM) and International Electro-technical Commission (IEC) methods. This thesis work provides the details of the *charge storage method* which has been found to be more appropriate in calculating the

resistivity of spacecraft insulators by emulating the space environment better. This method is based on the concept that the resistivity is better measured as the decay of the charge deposited on the surface of an insulator, rather than by the flow of current across two electrodes around the sample which is the case with the classical method of measurements.

From the results obtained from the charge storage method, it has been found that the ASTM resistivity values for thin film insulating spacecraft materials have been found to under-predict charge transport values applicable to many spacecraft charging problems, by 10 to 10^4 times. The charge storage method has only one side of the insulator in vacuum exposed to charged particles, light and plasma, with a metal electrode attached to the other side of the insulator. The chamber for measuring the charge storage decay has been designed with the capability to measure 32 samples simultaneously. The details of the apparatus, instrumentation, test methods, data acquisition methods, and data analysis for measuring resistivity of the spacecraft insulators are given here. Details about the vacuum environment, sample mounting, isolation of the samples, charging of the samples, measurement of the surface charge, rotary motion of the sample carousel, etc., are also given. The report also includes differences between the classical methods and the charge storage method both in terms instrumentation and methodology. The results obtained from both methods are tabulated showing the superiority of the charge storage method. Recommendations for future work are also included.

(142 pages)

ACKNOWLEDGMENTS

I am greatly indebted to Dr. J.R. Dennison, under whose supervision I chose this topic and began the thesis. He has been the epitome of patience, especially considering the amount of lab equipment I have broken over the last two years and the infinite number of times I knocked at his door citing some problem or other in the lab. His enthusiasm and help have been instrumental in making this project successful. I thank him for his collegial support and assistance for the spacecraft conference, which was a fabulous experience. Dr. Randy Jost, my major advisor, has been abundantly helpful in numerous ways, both in terms of research and the writeup of this thesis work. His suggestions and comments played an extremely vital role in the outcome of the project. I also thank Dr. Alan Shaw for his constant encouragement and support.

I would also like to thank the late Dr. Robb Frederickson of JPL whose research work was the prime motivation of this project. In his absence, Mr. Nelson Green of JPL was of great help and the discussions with him over the phone led me to understand the results that I obtained, better. I will have to acknowledge the efforts of different members of my research group under Dr. Dennison. They have always lent a helping hand whenever I required, especially Alec Sim and Clint Thomson. Alec developed the LabVIEW program required for the complete automation of my system and he was always there to make sure things went smoothly for me. Clint has also been of great help, especially in building the electron gun and the controller. I had a lot of fun with these guys around. I should also

thank the staff members at both the Department of Physics and the ECE office for assisting me in times of need.

I cannot end without thanking my family and friends, on whose constant encouragement and love I have relied throughout my time here. Someone long back said "A happy family is a closer heaven." I have been lucky enough to be a part of one such family. They have always provided me with the right environment to study and relax. I am what I am today because of my family. Their unflinching courage and conviction will continue to inspire me. I would consider myself blessed if I could reciprocate even an ounce of the love and affection they have showered on me.

Prasanna V. Swaminathan

CONTENTS

LIST OF TABLES

LIST OF FIGURES

CHAPTER I

INTRODUCTION

In the space environment, a spacecraft can get charged to large potentials relative to the ambient plasma. This charging can also enhance surface contamination, which degrades thermal properties of the insulator used. It also compromises scientific missions seeking to measure properties of the space environment. Insulators like Kapton^{TM}, Teflon^{TM} , and polyethylene are generally used in the construction of spacecrafts. The value of resistivity of these insulators in space environment, differ from the values obtained in atmospheric conditions. It is vital to characterize resistivity especially with respect to the spacecraft charging problem because the insulators do not behave in the same way in both the space and the atmospheric conditions. This project aims to improve the measurement of resistivity of thin film insulators using the charge storage method. This was motivated by prior research showing that such methods were more appropriate for many spacecraft charging applications and yield resistivity values 10 to 10^4 higher than standard resistivity methods [1]. As interaction with the space environment builds up charge on spacecraft surfaces, the rate at which further charge accumulates will be affected. In the simplest scenario, for a fully conductive spacecraft the charge will readily redistribute over the entire satellite and will charge to the point where the incident currents from the environment fluxes are equal to emission currents. By contrast, as insulating spacecraft materials accumulate charge, their low charge mobility causes that charge to accumulate where deposited and local electric fields to rise until the leakage current from the insulators to conductors equals the accumulation current from the

environment (or until the insulator actually breaks down and generates a charge pulse).

Hence, resistivity of insulating materials is a key parameter to determine how accumulated charge will distribute across the spacecraft, how rapidly charge imbalance will dissipate, and what equilibrium potential an insulator will adopt under given environmental conditions [2].

A. Spacecraft Charging and Its Effects

Spacecraft charging is defined as the buildup of charge on spacecraft surfaces or in the spacecraft interior. The spacecraft charging is driven by charged particle motion near the spacecraft surface from the nearby plasma. These plasma energies are from eV to keV levels. The spacecraft surface potential is a function of the net current flow to and from the spacecraft surface. A spacecraft placed in the plasma will assume a floating potential different from the plasma itself. Since electrons move at higher velocities than ions, the negative electron current to the surface is greater than the positive ion current. Therefore, in the absence of sunlight, a spacecraft surface will tend to charge negatively from the ambient plasma electrons. Though exposure to sunlight provides photoemission, not all parts of the spacecraft surface is exposed to sunlight which causes *differential charging*, when parts of the spacecraft are charged to different potentials relative to one another [3]. *Absolute charging* occurs when the satellite potential relative to the ambient plasma is changed uniformly. A uniformly charged spacecraft does not affect spacecraft systems referenced to structure ground except as mentioned above.

However, spacecraft surfaces are not uniform in their material properties and surfaces will be either shaded or sunlit, and the ambient fluxes may be anisotropic. The

spacecraft environment itself affects the spacecraft and its charging behavior. The plasma affects spacecraft by inducing charges on the spacecraft surface due to the flux of electrons and positive ions. The motion of a spacecraft through plasma may give rise to a local environment which may also contribute to spacecraft charging. When a significant plasma environment and photoelectrons arising from solar radiation are not present, the potential to which a spacecraft will charge is directly proportional to the electron temperature and varies between 1 to 20 kV. Electrons with energies between 1- 100 keV contribute to surface charging, while trapped electrons with energies above 100 keV penetrate the surface and contribute to internal charging effects. Photons emitted from the sun have an important effect in surface charging. Ultra-Violet (UV) and Extreme UV photon impacts on spacecraft surfaces result in the emission of photoelectrons (by the photoelectric effect). These photoelectrons constitute a current out of the spacecraft surface, which can reduce the effect of negative surface charging and hence it can be an important contributor to the surface charging mechanism. The Earth's magnetic field is approximately a magnetic dipole which is displaced from the center of the Earth by ~ 436 km. The geomagnetic axis is inclined at 11.5° with respect to the rotational axis of the Earth. The Earth's magnetic field has great influence on plasma motions and on trapped high-energy charged particles, which lead to spacecraft charging and damage to electronics. The magnetic field determines the regions of the space environment where spacecraft charging can occur. It also plays a role in the surface charging mechanism since it can affect the escape of electrons (such as photoelectrons) emitted from the spacecraft surface [4]. Up to one third of all spacecraft system anomalies and component failures are known to result from spacecraft charging [3].

Charging to high potentials can also lead to satellite material alterations and degraded instrumentation performance, as well as potential safety hazards for astronauts. The extent and configurations of spacecraft charge buildup depends on spacecraft position and orientation, local environment parameters such as incident charged particle and photon flux, and material properties such as electrical properties (*e.g.*, resistivity and capacitance) and electron emission rates [5].

The most important effect of spacecraft charging is the resulting Electro Static Discharge (ESD). ESD can be in the form of surface discharge or in the form of bulk discharge [6]. A surface discharge occurs when the surface voltage exceeds the breakdown voltage of the surface material and as a result it can generate currents up to a few hundred amps. On the other hand, dielectric discharge is triggered when dielectrics are exposed to space radiation. The charge involved in bulk discharge is small relative to surface discharge, but nevertheless presents a direct hazard to electronics. Arc discharges result mainly from differential charging and internal charging of spacecraft. Discharges may lead to anomalies such as erroneous logic changes in semiconductor devices, command errors or component failures. Degradation of sensors and solar cell panels is also a serious possibility and it may cause decreased amounts of power generation. Discharges may also cause serious physical damage to surfaces. Localized heating and material loss can result from arc discharges. Material loss may cause structural damage to the spacecraft. In addition, surface contamination can alter and degrade the properties of the surface materials. The three types of discharges that can occur are "flashover," "punch-through" and "discharge to space." Flashover is the term given to the discharge from one surface to another. Punch-through is a discharge from the interior structure of a

spacecraft through its surface, while discharge to space is the discharge from spacecraft to the surrounding plasma [7].

In the space environment, charge is deposited on the surface of the spacecraft as it orbits. Hence, the orbital periodicity sets the relevant time scale for the problem; typical orbits of near-earth satellites range from 1 to 24 hours [5]. For example, satellite orbit or rotation period determines the time surfaces are exposed to sunlight and subject to photoemission. Charge accumulated on the insulating spacecraft surfaces typically dissipates through the insulator to a conducting substrate. To understand the charging phenomena better, one then needs to relate resistivity or charge mobility to a suitable time scale. The charge storage decay time to the conducting substrate depends on the (macroscopic) conductivity or equivalently the (microscopic) charge mobility for the insulator. If the charge decay time exceeds the orbit time, not all charge will be dissipated before orbital conditions again charge the satellite, and charge can accumulate. As the insulator accumulates charge, the electric field rises until the insulator breaks down and generates a pulse [2]. Ohm's law is not sufficient to characterize the resistivity of the insulators for space applications. To prevent the electrostatic discharges, the electric field must relax at least as fast as the space environment injects new charge into the insulator. The relaxation time is given as product of bulk resistivity and the permittivity.

The charge on satellite surfaces accumulates in such a way as to produce an electric field that modifies the incident and emitted charge particle fluxes so that a net current balance and charge equilibrium is achieved. This current balance is depicted in fig. 1.1 [5]. As mentioned earlier, this model is plausible, if simplistic, for a fully conductive

spacecraft for which the charge will readily redistribute over the entire satellite in the case of absolute charging (or over isolated sections, for differential charging). The surface of conductors will charge to the point where the incident currents from the environment fluxes are equal to emission currents. Treating a thin film insulator as a simple capacitor, charge decay time is proportional to resistivity. As a first approximation, the thin-film insulator can be treated as a planar capacitor (with the charged front surface and conducting rear electrode acting as the electrodes). As with all capacitors, all charge resides at the interfaces, and the charge dissipates in an ohmic fashion through the bulk of the insulator.

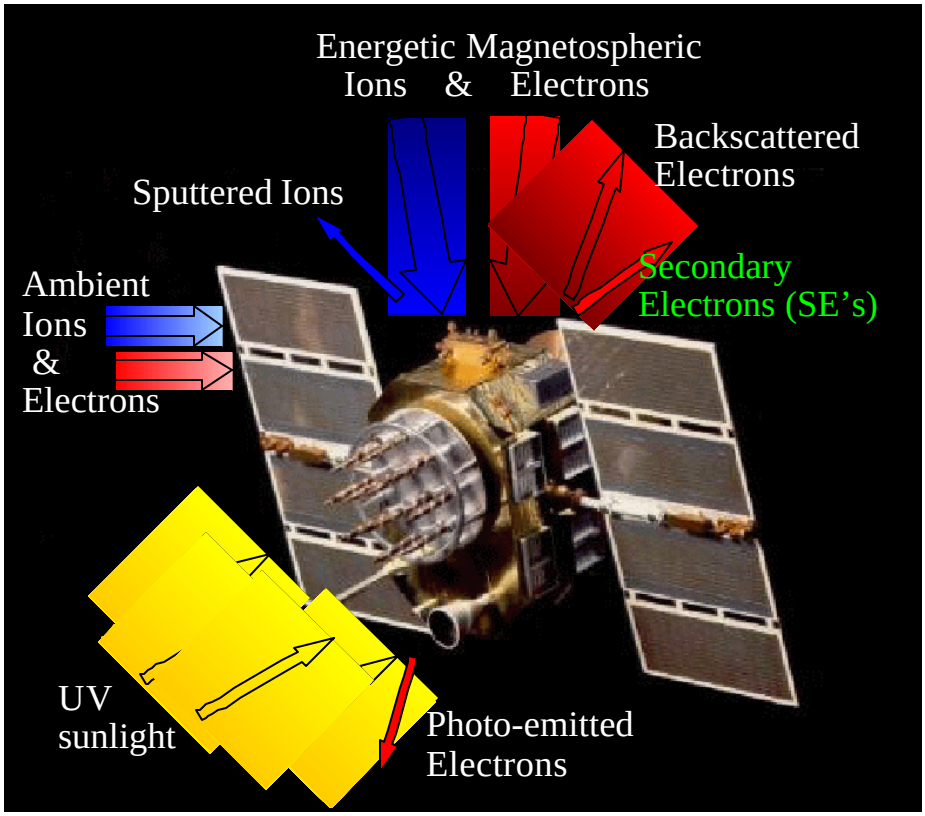

Fig. 1.1. Schematic representation of the current balance of incident and emitted charged particle fluxes.

In this approximation, the RC-time constant or relaxation time, t, for discharging insulator can be written as:

$$t = ?e_0e_r \qquad (1.1)$$

where ? is the material resistivity and e_o is the permittivity of free space. The relative dielectric constants, e_r, of nearly all spacecraft insulators lie within a narrow range, 2-10, and is well known for most materials; thus, determination of the resistivity follows directly from measuring the relaxation time. The decaying surface potential can then be estimated as a function of time as $s(t) = s_0 \cdot e^{-t/t}$, where s_o is the initial sample surface charge induced by electron beam irradiation, and s is the decayed surface charge after a time interval, t.

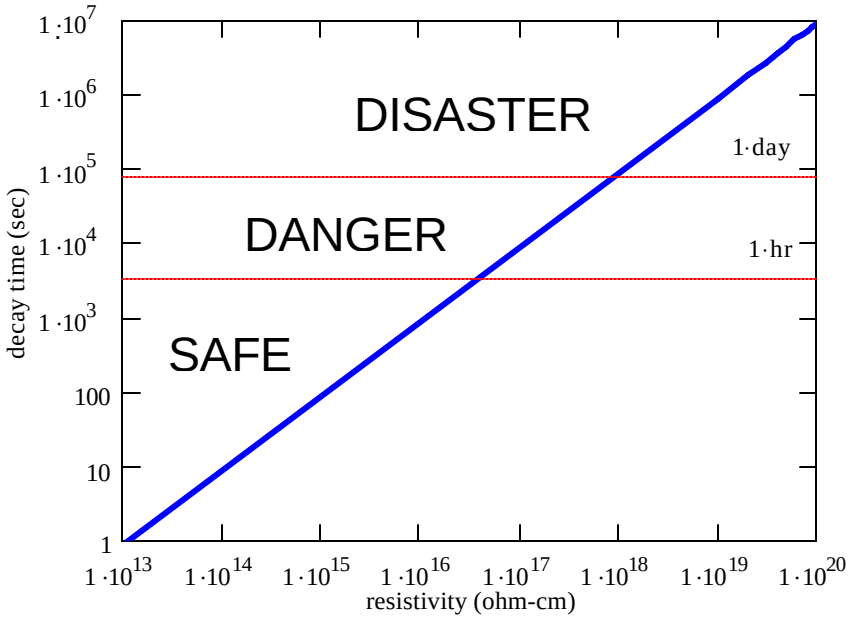

Fig. 1.2. Decay time as a function of resistivity base on a simple capacitor model showing safe, danger, and disaster zones based on resistivity of insulators.

Therefore, t is equivalently the relaxation time or the charge storage decay time, the time it takes for the surface charge to drop to 1/e of its initial value. Note that in this simple model, decay time is an intrinsic material property, independent of surface area or thickness. Figure 1.2 shows a plot of decay time as a function of resistivity, based on equation (1.1), for a relevant range of resistivity values. Values of typical spacecraft insulator material resistivities found in handbooks are in the range of 10^{11} to 10^{15} O-m [5]. This corresponds to decay times of ~1 sec to ~2 hr, suggesting that in most cases charge collected by common spacecraft insulators will dissipate faster than the charge is renewed. Considering these results, dangerous conditions occur for materials with resistivities in excess of ~10^{15} O-m, when t exceeds ~2 hr. Disastrous conditions occur for ? = 10^{16} O-m, when decay times exceed 1 day. Thus, it becomes critical for reliable spacecraft charging modeling to determine appropriate values of resistivity for typical thin film insulating materials [2]. The bulk resistivity values of insulators used to model spacecraft charging have traditionally been obtained from the handbook values found by the classical ASTM/IEC methods [8, 9]. However, recent work [10] has shown that these classical methods are often not applicable to situations encountered in spacecraft charging. The charge storage method was developed to measure the resistivity in a more applicable configuration.

B. Problem Statement

The resistivity of insulating materials is a key parameter to determine how accumulated charge will distribute across the spacecraft and how rapidly charge imbalance will dissipate. Classical ASTM and IEC methods measure thin film insulator

resistivity by applying a constant voltage to two electrodes around the sample and measure the resulting current for tens of minutes. However, resistivity is more appropriately measured for spacecraft charging applications as the "decay" of charge deposited on the surface of an insulator. Charge decay methods expose one side of the insulator in vacuum to sequences of charged particles, light, and plasma, with a metal electrode attached to the other side of the insulator. Data are obtained by capacitive coupling to measure both the resulting voltage on the open surface and emission of electrons from the exposed surface, as well monitoring currents to the electrode.

The objective of this project is to develop the instrumentation and methods at Utah State University (USU) for the measurement of the charge storage decay time and resistivity of spacecraft insulators. This includes preparing the necessary samples, testing the set-up, acquisition and analysis of data. This will enable us to compare data obtained with the existing standard methods [8, 9] for the measurement of resistivity.

The bulk resistivity of the spacecraft insulators is normally obtained from the values found by the classical ASTM/IEC methods. But it has been found that the ASTM/IEC methods are not applicable to this spacecraft problem for the following reasons:

1. The charge injection methods, resulting internal charge profile, and E field are fundamentally different for the classical and charge storage methods. The voltages developed in space are generated by impressing charge into the insulation, not by the application of voltage from a power supply onto electrodes [2].

2. The ASTM methods use classical ground conditions and are basically designed

for the problems associated with power loss through the dielectric and not how long charge can be stored on an insulator.

3. Conductors are placed on both surfaces of the insulators in ASTM/IEC tests whereas the spacecraft has only one surface of the insulator in contact with the conductor.

4. The measurement of the leakage current is made only after few minutes of bias application in the classical methods while the spacecraft experiences a fairly steady bias, for much longer periods. Classical methods fail to measure the movement of charge within tens of minutes after the application of electric field. The dielectric constant of the insulator increases with time (typically over tens of minutes) [5]. The resistivity data in handbooks do not take into consideration the fact that the resistivity continues to increase even after the measurement is taken. But in spacecraft modeling we need to know the how the leakage decays for as long as a year or more.

The typical orbits of the satellites in earth orbit range from 1 to 24 hours. This orbit time sets a critical time scale since this decides the amount of time the spacecraft is exposed to sunlight or other periodic charging conditions. Resistivity values based on the charge storage method have recently been used to correctly predict charging events observed in real satellite data, through modeling of pulses occurring aboard the Combined Release and Radiations Effects Satellite (CRRES) [11]. The classical method of measurement of resistivity is based upon measuring current flowing through a well defined structure from which the sample resistivity can be measured. Classical methods use a parallel plate capacitor configuration to determine the resistivity by application of a

constant voltage (E-field) and the measurement of the leakage current across plates through the insulator [2, 8]. Figure 1.3 [5] shows the schematic of current across the plates and through the insulator [2, 8] of the resistivity test conditions for both the classical method and the charge storage method. Details of the classical resistivity measurement are given in section III.B.

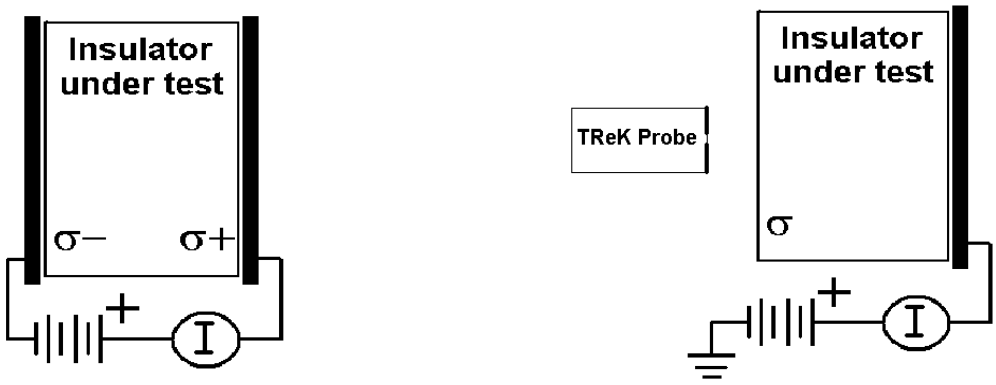

(a) (b)

Fig. 1.3. Schematic diagrams representing the set up for measurement of resistivity by (a) classical method (b) charge storage method.

C. Solution Approach

Robb Frederickson at the Jet Propulsion Laboratory (JPL) proposed a new system by keeping the aforementioned measurement differences in mind and made a resistivity measurement, wherein an insulator was charged and the surface voltage was measured continuously for a period of 38 days [5]. When the resistivity data obtained was compared to existing ASTM data for some spacecraft insulators, the resistivity calculated by this method was found to be higher by at least four orders of magnitude than the classical ASTM methods leading to predictions of 10^4 longer decay times [2].

Frederickson and Brautigam have recently completed a study [11] of Internal Discharge Monitor (IDM) pulse data from samples aboard the CRRES, which provides compelling evidence for the validity of using charge storage resistivity values in spacecraft charging modeling. The project used only basic laboratory-derived material properties (including resistivity) and data from on-board environmental charge flux monitors as inputs to models for internal charge deposition and migration within test samples to successfully predict the sample electrostatic discharge (ESD) pulsing amplitude and frequency over a time scale of hundreds of days and more than a thousand orbits. Central to the success of the project was the use of the charge storage resistivity in place of the classical value of resistivity. Specifically, data records were mined for IDM pulse data as a function of elapsed time for a variety of insulator samples, including a 0.8 mm thick FR4 printed circuit board sample, shown in the of fig. 1.3(b).

Concurrent electron environmental data over a range of energies from ~0.1 to 5 MeV were also mined and parameterized to obtain a dosage profile impinging on the sample as a function of elapsed time over the ~15 month lifetime of the satellite. These parameterized dosage profiles for each half-orbit (~5 hr period) were used, together with stopping power and resistivity data for the sample materials, to model the charge deposition profile, the charge transport, and the time evolution of the internal charge distribution. The NUMIT code [12] was then used to calculate a time-evolving E-field profile. The graphs in fig. 1.4 (a) and (c) show the predicted E-field at the front and rear of the sample as a function of elapsed time. The top panel is based on the classical resistivity value of FR4 board and an estimated value of the radiation-induced conductivity based on results for similar materials (values are listed in Table I). Note that

at no time does the E-field in the fig. 1.4(a) exceed 25% of the value of $1x\ 10^7$ V/m, which is typically needed to induce occasional pulsing. This prediction of no pulsing is consistent with the observation that the relaxation time from the total resistivity (dark resistivity and radiation-induced resistivity added in parallel) based on equation (1.1) of ~5 hr is less than the orbit time of ~10 hr. However, when the measured charge storage resistivity is used to predict the E-field evolution (see fig. 1.4. bottom plot); the E-field exceeds $0.6x10^7$ V/m near orbits numbered 600, 790, 850 and 1050. In each case, there is corresponding pulse activity observed in the center plot of fig. 1.4. with the pulse rate amplitude correlated to the magnitude of the E-field. Again, the prediction of pulsing is consistent with the predicted relaxation time of ~31 hrs from equation (1.1), which is well in excess of the orbit time. Finally, a value of dark resistivity that best fits the pulse data was determined. Note that because the charge storage resistivity and the estimated radiation-induced resistivity are comparable, the total resistivity of the best fit is only a factor of two larger than the total resistivity using the measured charge storage resistivity. Given these results, it has been concluded that charge storage resistivity methods are more appropriate than classical methods for many spacecraft charging problems.

TABLE I

RESISTIVITY VALUES FOR CRRES FROM FR4 CIRCUIT BOARD SAMPLES

Method Used to Determine Resistivity	Dark Resistivity (O-m)	Radiation-Induced Resistivity (O-m)	Total Resistivity (O-m)	Relaxation Time (hr)
Classical method	$5x10^{15}$	$3x\ 10^{16}$	$2x10^{15}$	5
Charge storage method	$2x10^{16}$	same	$1x10^{16}$	31
Best fit to pulse data	$6x10^{16}$	same	$2x10^{16}$	52

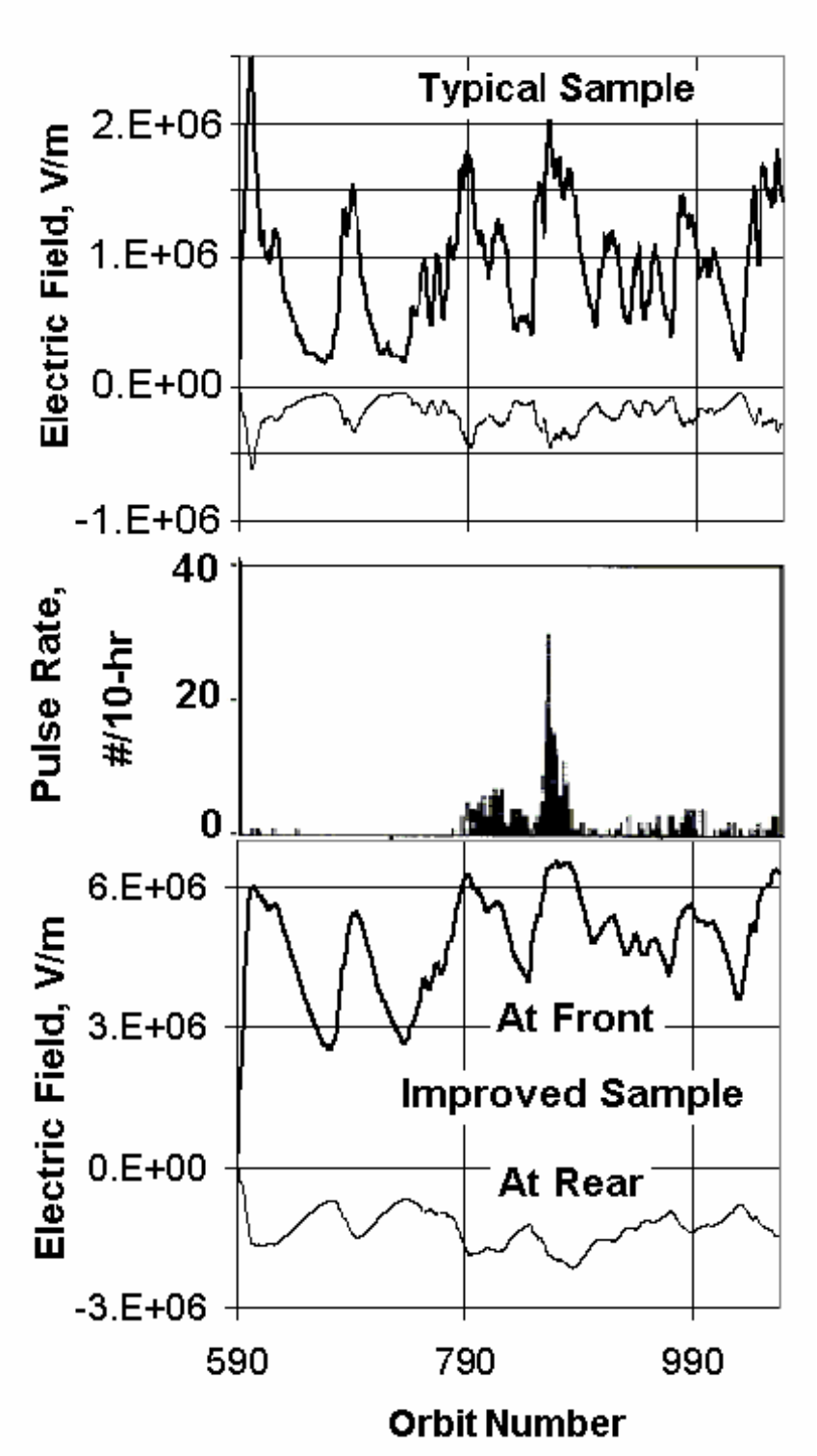

Fig. 1.4. Modeling of IDM pulse data from an FR4 printed circuit board sample aboard the CRRES satellite.

Table I shows the comparison of resistivity values for the two methods and also the huge difference in the relaxation times from both methods. Hence a correction is required in the existing database before further problems occur in space.

To summarize, the project objectives were as follows:

1.) To design and construct a vacuum chamber and a sample carousel.

2.) To assemble a vacuum and temperature control system for the chamber.

3.) To design and construct a sample holder system so that the samples can be accessed from outside the chamber.

4.) To design and build a rotary feedthrough design which would enable the movement of the samples in front of various monitoring devices.

5.) To define methodologies to charge the sample using an electron flood gun and to monitor the decay through the sample.

6.) To set up an arrangement to transfer the surface voltage of the samples to outside of the vacuum chamber.

7.) To automate the entire system to monitor the sample behavior under different environmental conditions.

8.) To document the data obtained and compare the results with that of classical resistivity measurements.

Instrumentation for both classical and charge storage decay methods has been developed and tested at JPL and at USU. The JPL charge storage decay chamber is a first-generation instrument, designed to make detailed measurements on only three to five samples at a time. Because samples must typically be tested for over a month, a second-generation high sample throughput charge storage decay chamber was developed at USU

with the capability of testing up to 32 samples simultaneously.

D. Review of Charge Storage Decay Literature

This section provides a detailed background study of the experimental setup used in the measurement of resistance and charge decay in insulators over the years by different researchers all over the world. The environment in which the measurement was taken and the kind of samples used is also noted. Most of the previous measurements of the resistivity were done using the capacitive coupling method. Here the insulator sample is placed between two electrodes, voltage is applied to the one electrode, and the other is grounded and used for the measurement of current through the sample using a picoammeter. This method was later made into a standard by the American Society for Testing and Materials (ASTM) in 1925 as D 257-25T and International Electro-technical Commission (IEC) for the measurement of resistivity of insulators [8]. Taylor and Lewis in 1971 [13] measured the electrical conduction of polyethylene terephthalate (PET) and polyethylene films to understand the mechanism of conduction in these insulators using two electrodes with the insulator in between them. They showed the influence of temperature on the insulator current decay at constant electric fields. A study on the nature of transient and discharge currents in PET films was done by Das Gupta and Joyner [14]. It discusses the variation of the currents due to changes in the electrode material and the sample thickness. They also used a very similar system of measurement mentioned above. Das Gupta concluded that the steady state current decay may be many orders of magnitude lower than the initial value of the transient current and that the discharge current flowing on the removal of the voltage on the top electrode is the mirror

image of the charging current except that the steady state current does not occur. This decay was attributed to processes like: electrode polarization, dipole orientation, charge injection leading to trapped space charge effects, tunneling of charge from the electrodes to empty traps and the hopping of charge carriers from one localized state to another.

The idea of charging one free insulator surface and grounding the other surface termed as the *surface potential decay method* was developed by Sonnonstine and Perlman [15] where the amount of decay was measured by a capacitative voltage probe. An insulator was placed in a plane parallel geometry equipped with a grounded electrode on one surface, while the free surface was corona charged to some initial potential. Neglecting carrier trapping, diffusion, thermal generation and allowing the drift mobility to be field dependent with time, the evolution of the surface potential was found to be governed by the Poisson's equation, the continuity equation, Ohm's law and the spatial integral of the electric field. At the highest initial surface potentials all the surface charge is injected into the insulator in a time small compared to the time scale of the measurement, and the injected charge drifts under its own self field to the collecting electrode by means of a field-dependent transport process without significant range limitation. At the lowest initial surface potentials little or no charge is injected, and the surface potential is constant in time. It was concluded that the decay of the surface charges may be due to the presence of a bulk insulator resistivity, i.e., due to the migration of thermally generated carriers within the bulk of the insulator.

The bulk of the measurements were made with 23 μm thick samples; however, a few measurements were made with samples 36, 75, and 190 μm thick. The samples were cleaned with ethyl alcohol before metal electrodes of thickness 250 Å were vacuum

deposited onto their surfaces. In addition to the two measuring electrodes, a guard ring around the low-tension electrode was also formed to reduce the effects of surface currents to a minimum. The effective area of the measuring electrode was 2 cm^2. The majority of the measurements were made using gold electrodes except for a few measurements which were made on samples provided with indium electrodes. The samples were conditioned for 24 hours by short-circuiting the electrodes in an evacuated measuring chamber and at a temperature of 140°C. The temperature of the preconditioned sample was then reduced to the lowest value to be used in the experiment. Constant electric field was applied to the sample at this temperature and the charging current monitored from 1 s after the application of the field for 5 hours. The field was then removed and the discharge current of the short circuited sample was recorded over a similar period of time. The temperature was then increased in steps of 15°C and the procedure repeated at each temperature. All measurements were made at a chamber pressure of less than 10^{-6} Torr. A Brandenburg photomultiplier power supply provided stabilized DC voltages, and currents were measured using a Keithley vibrating capacitor electrometer, type 640. The sample temperature could be controlled to ± 0.2 °C over the temperature range 80-440 K. It was observed that the charging and the discharging transient currents were mirror images of one another over most of the time and temperature changes. It is also indicated that the magnitude of the absorption currents in PET was independent of the electrode material and within the range of fields employed. It was found that the transient currents are also independent of the thickness of the sample.

The decay characteristics of the surface potential of corona-charged polyethylene films exhibited a striking feature, that is, in some situations surface potentials which are

high immediately after corona charging, decay with time to cross rather than merge into decay curves which start from lower initial potentials. Experimental evidence for this surprising result was given by Baum *et al.* [16]. The experimental procedure is done in such a way that charge depositions were more carefully monitored and the probe used for determining surface potential decay had much greater resolution. Samples of polyethylene film without additives and 25 μm thick were held firmly onto an earthed metal backing electrode mounted on a turntable. They could be charged on their free surface by exposure to a corona point discharge situated above the surface and behind a grid electrode and circular aperture which defined the area to be charged as shown in fig. 1.5. [16]. The grid was a fine metal mesh (0.5 x 0.5 mm) situated approximately 5 mm above the polymer surface so that a reasonably uniform field could be generated in the gap between the grid and the polymer surface. At the same time there is no unnecessary restriction on the flow of ions from the corona point to the surface.

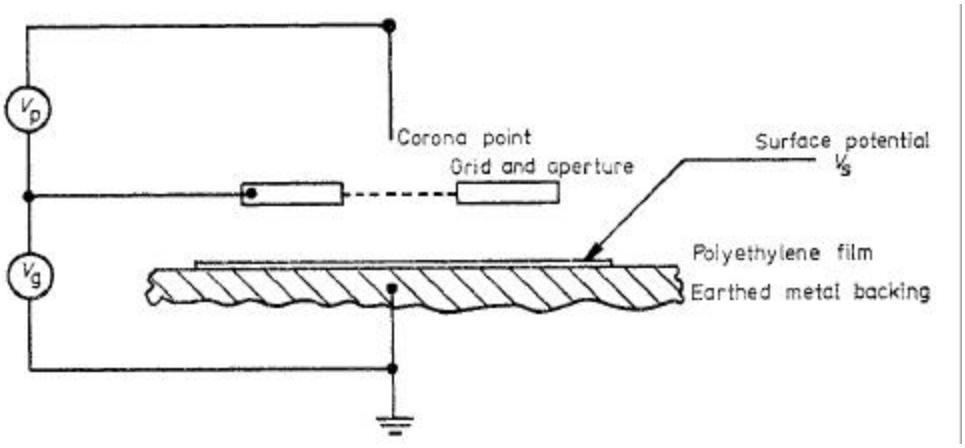

Fig. 1.5. Diagram for corona charging arrangement for a polyethylene film.

By selecting appropriate corona point and grid potentials V_p and V_g respectively, it was possible to charge the surface with ions of either sign and to a concentration limited by V_g. As the surface charges up and the surface potential V_s (fig. 1.5) rises, so the charging current will decline and it will tend to zero as V_s approached V_g. V_s is determined not only by surface charge but also by charge which has moved into the polymer bulk. If the latter charge is mobile, i.e. the film is sufficiently conductive, and then V_s may reach a limiting value less than V_g, whereby the influx of charge from the corona point balances charge leaking through the film to the backing electrode.

The most relevant experiment for the measurement of resistivity on spacecraft insulators was done by Levy *et al.* [17]. Though the ASTM standard for measurement of resistivity is good for normal applications, it may not be the most applicable for spacecraft insulators since the insulators are exposed to a different kind of environment in space and subject to different charging geometries. These differences were brought about in the earlier part of the chapter. Many properties that are significant for the charge exchange with the space environment and the charge exchange between outer coatings and satellite frame were identified. There was also an emphasis on the need for a database with resistivity values of insulators for the spacecraft applications. Hence a new method for the measurement of spacecraft insulators resistivity was introduced. It was called *surface voltage decreasing method*.

The approach for the method is as follows [17]:

a) The sample is fixed onto a holder: thermal control outer materials are generally metallized on their rear side. This metallization is grounded together with the sample holder.

b) The sample is first exposed to charging by means of an electron beam. No metallization is compulsory at the outer surface of the sample charged by the electron beam. Electrons penetrate into the sample a few microns below the exposed surface. The penetration depth is dependent on incident electron energy.

c) Sample irradiation is then interrupted and its surface voltage is continuously monitored with a surface voltage probe [18].

These measurements are made in a dedicated facility named "CEDRE" which is installed at the Centre d'Etudes et de Rescherches de Toulouse, Toulouse, France [17]. The simulation of the electron distribution of the space plasma was achieved by means of quasi-mono energetic electrons in the 2 to 30 keV energy range with fluxes 10 nA/cm^2. Two independent electron guns could be operated simultaneously and the two beams are scattered by aluminum thin foils and enlarged enough to irradiate a 200 x 200 mm^2 surface with good homogeneity. Simulation also required the possibility of illuminating the irradiated samples with ultraviolet light, performance of irradiation under vacuum at controlled temperature. The sample holder were made up of 4 plates (200 x 200 mm^2), one of which is temperature controlled between -180°C to -120°C. This holder is fixed onto a rotating shaft allowing the presentation of any of four plates in front of the electron gun. In normal condition, three faces could receive samples, the other being used as a Faraday cup holder and surface potential measurement calibration system. Three samples could be tested without opening the chamber so as to perform comparative tests on them. The surface potential induced on an irradiated sample was measured by a potential probe held by a mechanical scanner, facing the surface to be measured. A potentiometer system yielded the position of the probe and allows recording the surface potential profile on the

electrically charged sample on an X-Y plotter. The measurement yielded the following:

a) Surface potentials or surface potential profiles

b) Discharge transient currents

c) Radiated Electro-magnetic Interference on an in-situ antenna

d) Localization of discharge by optical sources

The most important observations from the measurements taken by Levy were as follows:

- The resistivity behavior of Kapton and cerium doped glass can be modeled using an analytical expression which expresses the resistivity as a function of applied potentials. This can be expressed as $? = ?_0 \exp -a (V_s^{1/2})$ where V_s is the surface potential proportional to surface charge and $?_0$ and a are dependent on the material on a semi log plot $\ln(? / ?_0) = - a V_s^{1/2}$.
- Dielectrics in space environment exhibit the well known radiation-induced resistivity phenomenon. Energetic trapped electrons of the geosynchronous orbit penetrate completely through the thin materials used. They create the radiation induced conductivity which adds to the dark conductivity.
- The radiation induced conductivity is measured for three dose rates of and values were found to be 5×10^{-15}, 5.2×10^{-15}, 4×10^{-15} $(O\text{-}m)^{-1}$ / $rad\text{-}s^{-1}$ respectively for dose rates of 2, 0.27, 0.07 $rad\text{-}s^{-1}$.

Coelho *et al.* [19] reported an electrostatic model of the voltage decay which deals with drift of carriers from the surface into the sample and also discussed the significance of surface voltage decay on charged insulators. The setup had the sample mounted on a conducting, grounded plate, and its floating surface was charged by contact, by rubbing

against a different material, or by exposure to a DC corona discharge or an electron beam. The potential of the free, charged surface was measured using a non-contacting probe of a vibrating type. The potential of the probe is monitored by feedback in such a way that it adjusts itself to the sample surface, so that the field between the sample and probe remains very small. The difference between the measurements of the potential decay from the sample surface using an electrode in contact and by charging the sample by an electron beam is brought out. For relatively conductive materials, the surface voltage decays as if the sample charges, $Q = CV$, leaked through the sample resistance R. The actual decay was never simply exponential, but by using a proper field-dependent resistivity the theoretical decay may be made to fit the observed decay fairly well. However, the model was unable to predict the 'crossover' of the decay curves often exhibited by a sample charged at different levels. Nor can it predict the 'return voltage' displayed by the sample which has been temporarily short circuited after charging.

The Coelho experiments with the electron beam were done in a chamber that was evacuated to 10^{-6} Torr on Kapton polyimide, which is used as protection material for satellites. These experiments were also carried on in the CEDRE facility mentioned in the work by Levy [17]. An electron beam of 20 keV energy and 0.5 nA intensity was used, simulating the space radiation. The samples used in the experiment were square sheets of 6 cm side length and 50 μm thickness. They were aluminum coated on one face, which was applied on the grounded substrate. A proper mechanism allowed automatic scanning of the sample, over a distance of about 10 cm comparable to the beam diameter on the target plane, by an electrostatic probe which measured the potential acquired by the irradiated surface, and its subsequent decay. A circular aluminum coating of 0.1 pm

thickness and 2 cm diameter was deposited on the side of the free sample face, and a 0.5 mm thick aluminum plate opaque to the incident electrons is fixed on the coating. This plate divided the Kapton sample into two distinct zones. The electrons hitting the unprotected area penetrated the polymer film and were trapped a few microns under its surface. In the protected area, they were absorbed in the aluminum plate, thereby raising its potential and consequently that of the polymer surface as if it were charged by contact with a high-voltage source in the manner similar to the classical ASTM method of measurement [8]. After the irradiation was stopped, the sample was scanned repeatedly with the probe along a diagonal, so that the potential of the protected and unprotected areas could be easily compared during the decay. Figure 1.6 represents the potential decay measured in both the protected and unprotected sample areas.

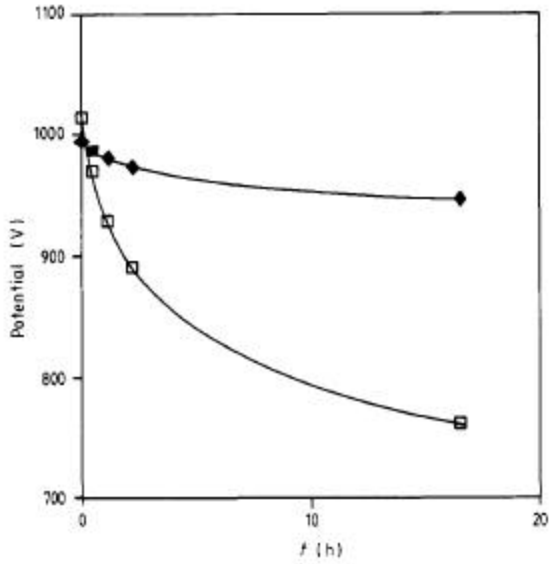

Fig. 1.6. Potential decay comparison when a Kapton is charged by direct electron beam [□] and by having an electrode in contact with the sample [◆]

The initial voltage in the unprotected area was 1115 V and that of the protected area was only 20 V lower. This small difference was ascribed to the order in which the two areas were scanned. The salient result is that the initial decay rate on the unprotected area, which is of the order of 0.028 V s^{-1}, was about 10 times faster than that measured on the protected area. The electrons which were directly injected into the polymer bulk without having to cross an interface barrier appear more "mobile" than those which are somehow retained by the barrier before they can move across the sample. The initial decay rate in the protected area was slower than the "bulk" decay rate related to the true effective mobility.

The importance of having slightly conducting insulators for spacecraft missions and that the electron beam was the best way to emulate space environment was emphasized by Frederickson [20]. The experiments were done by Frederickson at The Air Force Research Laboratory, Philips Research Site, Kirtland AFB, NM, USA on the dependence of charging of insulators upon the insulator thickness, electron energy spectra and material properties. The investigation was aimed at addressing the question, "as the electric fields build up, does the surface voltage continue to increase with time or were there some limiting phenomena which allow for the leakage of the current before the surface voltage rises too high." It was also felt that the handbook values for the insulator resistivity were misleading. The modeling of the study required consideration of various parameters which were extremely critical viz., dark conductivity, radiation induced conductivity, electron backscatter, secondary electron emission and field enhanced secondary electron emission. Radiation induced conductivity was assumed to be $1x10^{-13}$ sec/ O -m-rad and the dark conductivity to be $1x10^{-15}$ per O -m which could be the lowest

values possible for the insulators exposed for years to high vacuum in space. Whenever the samples are tested in vacuum chambers with electron beams the dark resistivity values have been often found to be at least two orders of magnitude higher than that suggested by the handbooks. The electron beam method measures the resistivity by monitoring the time rate of decay of a sample previously charged by brief exposure to the electron beam. It was felt that this is the best method for measurement of resistivity for space materials. Normal atmospheric tests use high electric fields with electrodes on the sample thereby produce enhanced conductivity by the method measurement itself. A computer program NUMIT [12], was used for the calculation of dose rate in rads per second, thereby giving an accurate value of the secondary electron current density. The experiments showed that small samples in a large satellite cavity might have fewer problems with surface charging due to conduction in the ionized ambient. The electron current density which is sufficient to cause charging usually depends on the dark conductivity of the thickest insulator but is not accurately known for spacecraft applications.

The thin film insulator used in the experiment was a thermal control paint used in the spacecraft. Experimentally it was found that the steady state voltage is held low only for very thin film insulators with the rear surface in good contact with the spacecraft frame. High surface voltages were not necessarily a problem by themselves. The problems occur when a small spontaneous discharge of plasma and gas neutrals is produced in the cavity. Once a discharge has begun, the high surface voltages acting on gas and plasma will cause a rapid avalanching of charge and current in the cavity. The resulting pulsed currents produce electromagnetic interference with the onboard

electronics and hence high surface voltages should be avoided. Insulating surfaces inside the closed spacecraft cavities would often charge to extremely high voltages when leakage is not provided. Insulator surfaces should be guarded from exposure to the environment of the spacecraft cavities.

Whittlesey *et al.* [21] collected relevant data from the CRRES IDM space experiment and proposed that the resistivity data values from the handbooks are not relevant to the spacecraft materials. The experiments were done on an onboard FR4 and PTFE samples. Modeling of the CRRES IDM found that these samples should never have produced pulses because the electric fields should not exceed 10^7 V/m. But this modeling was base on the resistivity values taken from the handbooks [8] that were much too low for predicting the sample charging times. Because the pulse rate and the amplitude depend on the electric field in the insulator, and because the electric field is controlled by the resistivity of the insulator it is vital to know the actual resistivity. The new method of measurement of resistivity for the spacecraft applications was called the *space charge decay method.* A comparison was also done between the classical method and the new charge decay method and the results were compared. The classical method gave a result of 0.37×10^{14} O -m for a sample which is of 51 μm thickness and exposed area of 16.6×10^{-4} m^2. The voltage applied at one of the electrodes is 64 V. In the new method, keV electrons in vacuum were applied directly to the exposed insulating surface of the samples instead of an electrode contact. After injecting the electrons, the samples were then monitored with a TreK^{TM} non-contacting probe [18] for the decay of the resulting surface voltages. The RC time constants of the decay indicated that the resistivities were in excess of 6×10^{16} O-m .Hence the new method was more indicative of the charge

leakage properties of the polyimides in space than the method using a conducting contact on the surface. The following relevant conclusions were drawn from the experiments performed on various samples using the space charge decay method:

1.) Applicable resistivity values of insulators in space may be much higher than tabulated from ground based testing that used metal electrodes on the material.

2.) Resistivity of the insulators in the space environment is altered by environmental effects and thereby patterns of pulsed discharging are changed.

Frederickson and Dennison [10] emphasized that the insulators used for the spacecraft applications need to have sufficient conducting electrons and holes to prevent the development of very large electric fields. A generic spacecraft insulator problem was simulated in a vacuum chamber is shown in fig. 1.7. A specific method of measurement of resistivity of spacecraft insulators is shown in the fig. 1.8.

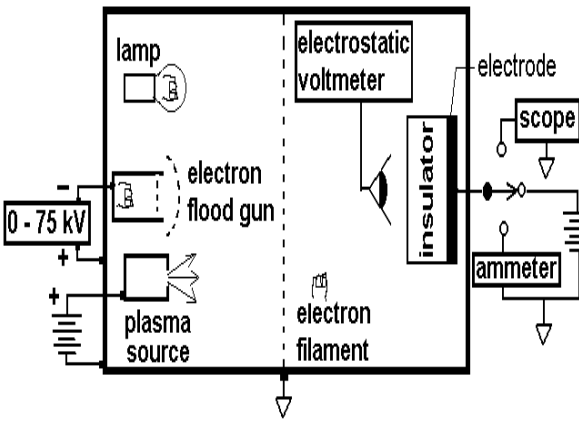

Fig. 1.7. Generic spacecraft insulator problem simulated in vacuum chamber.

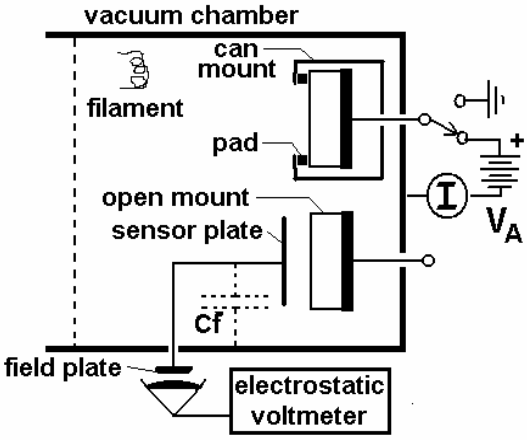

Fig. 1.8. Two sample mounts and floating voltmeter measuring the charge decay and resistivities.

The chamber had a flood gun from 0 to 75 keV, a plasma source with bias capability to a kilovolt, an electron emitting source, a light source, electrostatic voltmeter and temperature probes. There were two methods to determine whether or not the charge remains at the front surface, or leaks into the sample. It was suggested that a small amount of charge could be injected onto the surface of the sample and could be monitored by the voltage probe. If the charge was penetrating into the sample, then the incremental voltage would be reduced if the surface potential was measured for sufficient amount of time. Its capacitance could be determined from the slope of the curve at small charge Q. After charging the sample in the given arrangement, one could also measure the effect of light upon conduction through the insulator. In addition to this, one could also perform high energy electron beam tests and measure the sample leakage during and after application of the electron beam, thereby determining how conductive the insulators were. But the most important observation of the experiment was that most of the other measurements have the surface voltage probe in vacuum chamber. When the voltage probe was mounted directly inside the vacuum chamber facing the sample, extended electron beam exposure drove it off scale. So a sensor plate was used to transfer the surface voltage to the probe placed in air outside the chamber. Therefore the arrangement in the fig. 1.8 was preferred. Hence a new method was provided for the measurement of resistivity in practical insulator materials applicable for space environment. Also techniques that distinguish amongst various charging and conduction mechanisms were discussed so that better predictions can be made for spacecrafts.

Table II gives a summary of all the prior experimental work done related to the charge storage method. It gives an account of the techniques, experimental set up and the

samples used in each of the techniques.

TABLE II

SUMMARY OF EXPERIMENTAL INVESTIGATIONS ON MEASUREMENT OF RESISTIVITY AND SURFACE CHARGE DECAY

Researchers	Experimental Details	Pertinent observations
Sonnonstine *et al* 1975	***Objective*:** Measuring the surface potential decay characteristics of corona charged insulators. ***Set-up*:** Sample is on a plane – parallel geometry equipped with a grounded electrode on one surface, while the free surface is corona charged and the surface potential is monitored as a function of time with a surface potential probe. ***Sample used* :** Polyethylene	At the highest initial surface potentials all the surface charge injected is into the insulator in a time small compared to time of scale of measurement. The injected charge drifts under its own self field to the collecting electrode by means of a field dependent transport process. At lowest initial surface potentials little or no charge is injected and the surface potential is constant in time. Intermediate charge injection is both time and field dependent.
Baum *et al* 1977	***Objective:*** Identifying the decay of the surface potential. The samples are corona charged by exposing them to a corona point in a well defined circular region. ***Set-up*:** The free surface to a corona point which is a mesh grid about 5mm above the sample surface and the surface potential is measured by metal induction probe. ***Sample used:*** Polyethylene	Light with photon energies of several eV is found to play an important role in facilitating the subsequent decay of the negative charge which means that the light causes photo-injection of electrons from the states in the insulator surface into the bulk where they become mobile in the total space charge field.

TABLE II CONTINUED

Researchers	Experimental Details	Pertinent observations
Levy *et al* 1985	***Objective*:** Developing methods and laboratory experiments for the evaluation of resistivity and secondary electron emission of dielectrics. ***Set-up*:** A new method called surface voltage decreasing method, which allows precise measurements of insulator resistivities as low as 10^{15} O-m with the vacuum chamber evacuated at 10^{-5} Torr. Samples metallized on the rear side are placed on a holder and charged by means of an electron beam. The surface voltage is continuously monitored by a TreK^{TM} voltage probe. ***Samples used***: Kapton Cerium doped glass	The radiation induced conductivity is measured for three dose rates of and values were found to be $5x10^{-15}$,$5.2x\ 10^{-15}$,$4x10^{-15}$ $(O\text{-}m)^{-1}$ / $rad.s^{-1}$ respectively for dose rates of 2, 0.27, 0.07 rad/s. The resistivity behavior of the samples can be modeled using an analytical expression which expresses the resistivity as a function of applied potentials which is $? = ?_0 \exp -a\ (V_s^{1/2})$ where V_s is the surface potential and $?_0$ and a is dependent on the material. Dielectrics in space environment exhibit the well known radiation induced conductivity phenomenon. Energetic trapped electrons of the geosynchronous orbit penetrate completely the rather thin used materials. They create the radiation induced conductivity which adds to the dark conductivity.
Coelho *et al* 1989	***Objective*:** To develop an electrostatic model for voltage decay which deals with the drift of carriers from the surface into sample. ***Set-up*:** The sample rests on a conducting, grounded plate and its floating interface is charged an electron beam of 20 keV energy and 0.5 nA intensity under a vacuum of 10^{-6} Torr simulating the space environment. Potential of the surface is monitored by using non-contacting probe. ***Samples used:*** Kapton	Surface voltage decays as if the sample charge $Q=CV$ leaks through the sample resistance R. Decay for deeply injected high energy electrons is controlled by their bulk mobility that for charges deposited on the surface is limited by the injection at the barrier.

TABLE II CONTINUED

Researchers	Experimental Details	Pertinent observations
Fredrickson 1993	***Objective*:** Investigation of the dependence of charging upon insulator thickness, electron energy spectra and material properties. ***Set up*:** The arrangement is in such a way that the sample is exposed to the electron beam much in the same way as it is in the space environment with one surface of the insulator exposed to the electron beams and the other surface fixed to a grounded electrode. ***Sample used*:** Kapton	The best way to find the resistivities of spacecraft insulators is to check in the space environment. The electron beam tests measure the resistivity by monitoring the time rate of decay of a specimen previously charged by brief exposure to the electron beam. The resistivity values for Kapton show an increase of at least 2 orders of magnitude when compared to handbook values. Electrically leaky insulators should be chosen for spacecraft insulation and they should be made as thin and small as possible.
Whittlesey *et al* 2001	***Objective*:** Comparison of the data from the CRRES Internal Discharge Monitor to the ground experiments performed on the space craft insulators. ***Set-up*:** In the ground based tests, keV electrons in vacuum were applied directly to the exposed insulating surfaces of the samples. After the electrons were injected the surface was monitored continuously by using a non-contacting probe for decay of the resulting surface voltages. ***Samples used*:** Kapton, LaRC-SI,PTFE Teflon,FR4 Circuit Board	Measurement was more indicative of the charge leakage properties of spacecraft polyimides than the classical resistivity method. By the prediction of electric fields in CRRES using classical method the samples should not have pulsed. But in comparison, by using the electron beam way of charging the samples the resistivity values were found to be very high.

TABLE II CONTINUED

Researchers	Experimental Details	Pertinent observations
Frederickson *et al* 2003	***Objective*:** Discussion of a new experimental method for the measurement of resistivity and electric fields in insulating spacecraft material intended for space radiation and plasma environments. ***Set-up*:** Most of the earlier measurements for measuring surface voltage had the surface voltage probe inside the vacuum chamber and the probe was sent off scale by the electron beam. But this method has a sensor metal plate inside the vacuum and the surface voltage was transferred to the probe outside in air so,not only is the probe safe from electron beams but can also be repaired without breaking the vacuum. ***Samples used*:** Kapton, LaRC-SI	Measurements of resistivity are up to four orders of magnitude smaller than those determined by existing smaller methods. Resistivity is altered as radiation accumulates and trapping states fill with electrons. With electron irradiation electrons are continually emitted for hours even after the irradiation ceases. Charging by electron irradiation is modified by the electron hole pairs and on electrons in shallow traps to provide extended conductivity.

E. Overview of the Thesis

Details are provided in the different sections of the thesis about the instrumentation to measure surface charge and current. The thesis is laid out in the following manner. Chapter 2 discusses the salient features of the instrumentation and how the system is automated. Details about the environment in which the samples are tested and the sample charging techniques are also outlined in this chapter. The methods for measuring the

surface voltage on the samples and how the measurements would vary according to the changes in the environment are listed in Chapter 3. The system performance and evaluation of the system is explained in Chapter 4. Chapter 5 contains the sections on results obtained from the system, proposed future work with the system developed and conclusions. Appendix I contains LabVIEW panels used for the automation of the charge storage system and Appendix II describes about the Charge Storage Chamber set up at JPL.

CHAPTER II

INSTRUMENTATION AND AUTOMATION

This chapter provides an extensive description of the instrumentation developed for the project. It explains the necessity of automation of the system for the measurement of the charge stored in an insulator and the subsequent leakage of the same. Before various instruments are discussed it is imperative to note the performance requirements of the charge storage chamber used [2]. Table III [2] below gives the performance requirements of the test chamber.

TABLE III

LIST OF PERFORMANCE REQUIREMENTS FOR CHARGE STORAGE DECAY TEST APPARATUS

1. *Sample Quantity*--Multiple samples in the chamber to enable high sample throughput
2. *Sample Monitoring*
    a. Monitor one sample at a time
    b. Isolate samples from one another during all treatments and monitoring
    c. Measure the current that charged the sample
    d. Require about 1-volt resolution for the charge probe
3. *Sample Treatment*--Apply special treatment to each sample
    a. Charge one sample at a time
    b. Charge the sample surface uniformly
    c. Charge samples using slow electrons and sample bias
    d. Charge or discharge samples using sample bias and plasma source
    e. Charge or discharge samples using fast electron beam
    f. Discharge samples using light for amenable samples
4. *Sample Environment*
    a. Avoid placing objects in the chamber (other than samples) that might accidentally charge up
    b. Maintain vacuum and instrument functions for at least one month
    c. Temperature control of sample over life of experiments

The design at USU is a stand alone system that provides a low cost method for performing the charge storage and resistivity measurements where one needs to build both a vacuum system and experimental sample handling capability. The system has evolved from the performance requirements mentioned in Table III. The enumeration of the performance requirements indicate how precise and elaborate the instrumentation for the chamber needs to be. Since the experiments are all made in vacuum and tend to take a period of one month for completing one set of data, one cannot afford to break vacuum whenever we want to do the same measurement for another sample. Thus it is prudent to have multiple samples and do the same measurements simultaneously. *Sample monitoring* in Table III points to the importance of having the capability of monitoring the charge deposited and charge decay for each of the samples accurately. Also it is imperative that we isolate samples from one another for all measurements and treatments.

Since we are dealing with charge deposition there is a very good chance that charge deposited on one sample will influence the measurement taken in the other, if proper isolation is not carried out. One needs to have accurate monitoring systems to measure the charge on the sample and the leakage of the same through the sample. Resistivity in charge storage method is based on this leakage and no compromise on accuracy can be made in this measurement. The requirements, as far as treating the samples are concerned, are given in *Sample Treatment* of Table III. As mentioned earlier, the chamber has to have the capability of charging one sample at a time. Care has to be taken to make sure that the charge is uniformly distributed so that the leakage through the samples can be accurately characterized. Sample charging has to be done using an electron beam as that is how the insulators are charged in the space environment. The

system also has to have the capability to discharge the sample using light. *Sample environment* in Table III is extremely important to make sure we emulate the space environment in the correct manner. It is necessary to have the system equipped with good temperature control so that we can monitor the changes in the behavior of the sample with changes in the temperature. One has to be extra careful in designing the vacuum and the temperature controls since the experiments need to go on for a period of one month or so. Because of the long data collection period, it is essential that the controls are made fool-proof. Also it must be made sure that the only objects in the chamber that are charged are the samples, otherwise the accuracy of the measurements will be affected.

A. Charge Storage Decay Chamber

This section describes the construction of the decay chamber in which the experiments are performed. Figures 2.1 and 2.2 show the charge storage chamber and the instrumentation used for the measurement of resistivity and the decay time. Figure 2.3 shows a photograph of the chamber, equipment rack and the data acquisition computer. The charge storage chamber rack with its electrical and mechanical accessories provides mounting for the instrumentation, the control computer, vacuum system and the rotary feed through assembly. It also provides distribution of filtered AC power and common ground connections. The instrumentation of the chamber can be classified into five main categories viz.,

- Vacuum chamber, pumps, gauges, and control
- Sample mounting and motion
- Temperature Control

- Electron & Optic Sources, Sensing Control, and IV circuit
- Computer Control

These instrumentation categories are dealt with in detail in the Sections A-D. The electrical connections of the system are shown in the fig. 2.3.The figure shows various instrumentation sub-systems as blocks. The vacuum chamber itself is marked in dark blue in fig. 2.4 so that the inlets and outlet connections can be easily identified. The vacuum sub-system and its connections are represented in fig. 2.4 with the section colored red. The details of the sample holder design and how the samples are placed in the holders are found in the Section A.4. The temperature control for the system is depicted by the section in green. The electron gun and the I-V circuit associated with it is identified by the brown color in fig. 2.4. The chamber is connected to the computer controls for the purpose of data acquisition. The computer controls are marked blue in fig. 2.4 and are described further in the section D. A data acquisition (DAQ) card helps in data collection from various portions of the chamber. This section also includes a description of current measurement instrumentation, design details of the TReK^{TM} capacitance probe apparatus and details of the charge storage measurement calibration.

1) Chamber Overview: The chamber is designed so as to allow simultaneous testing of multiple samples. The approximate size of the samples and the number of samples to be tested are crucial for the chamber design. The sample carousel has all the samples at a single height on the circumference of a sample carousel that can be rotated in front of various ports with electron or photon sources, the TReK^{TM} probe, etc.

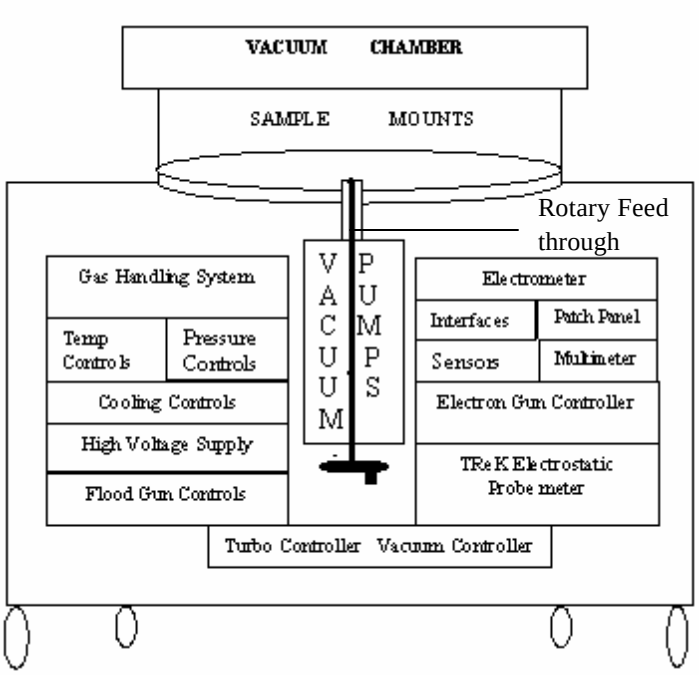

Fig. 2.1. Schematic representation of the vacuum chamber and its instrumentation.

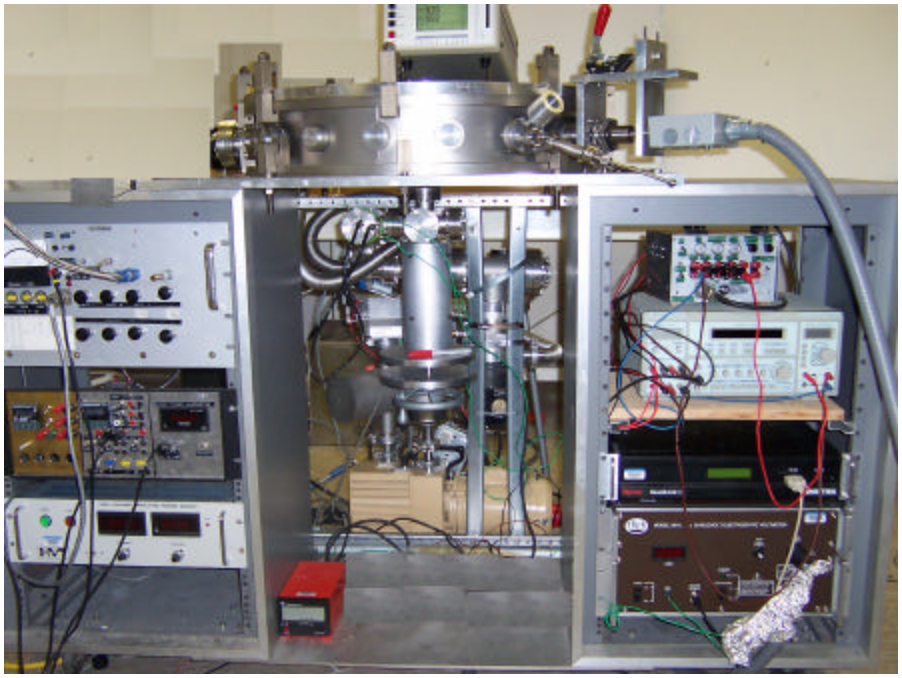

Fig. 2.2. The chamber with different measurement equipments.

The vacuum chamber is a 60 cm inner diameter stainless steel bell jar collar with ten ultra high vacuum (UHV) metal-gasket sealed 7 cm Conflat^{TM} flange ports and six o-ring sealed 2.5 cm base plate hole ports [2]. Aluminum plates, 12 cm thick, are placed above and below the collar. The bell jar vacuum chamber assembly is shown in detail in fig. 2.6. Figure 2.5 shows the assembly of the rotating sample carousel. Figure 2.5 (d) shows a clear view of the arrangement of the sample holders inside the chamber. Several ports in the vacuum chamber are dedicated to different diagnostic sensors. The ports in the vacuum chamber are dedicated to the TReK^{TM} probe, sample holder manipulator, ion gauges, a residual gas analyzer, a couple of view ports, a humidity sensor, etc., These positions are accessed by a custom rotary feedthrough design which is attached to the carousel.

Fig. 2.3. The charge storage chamber and integral equipment rack with computer control.

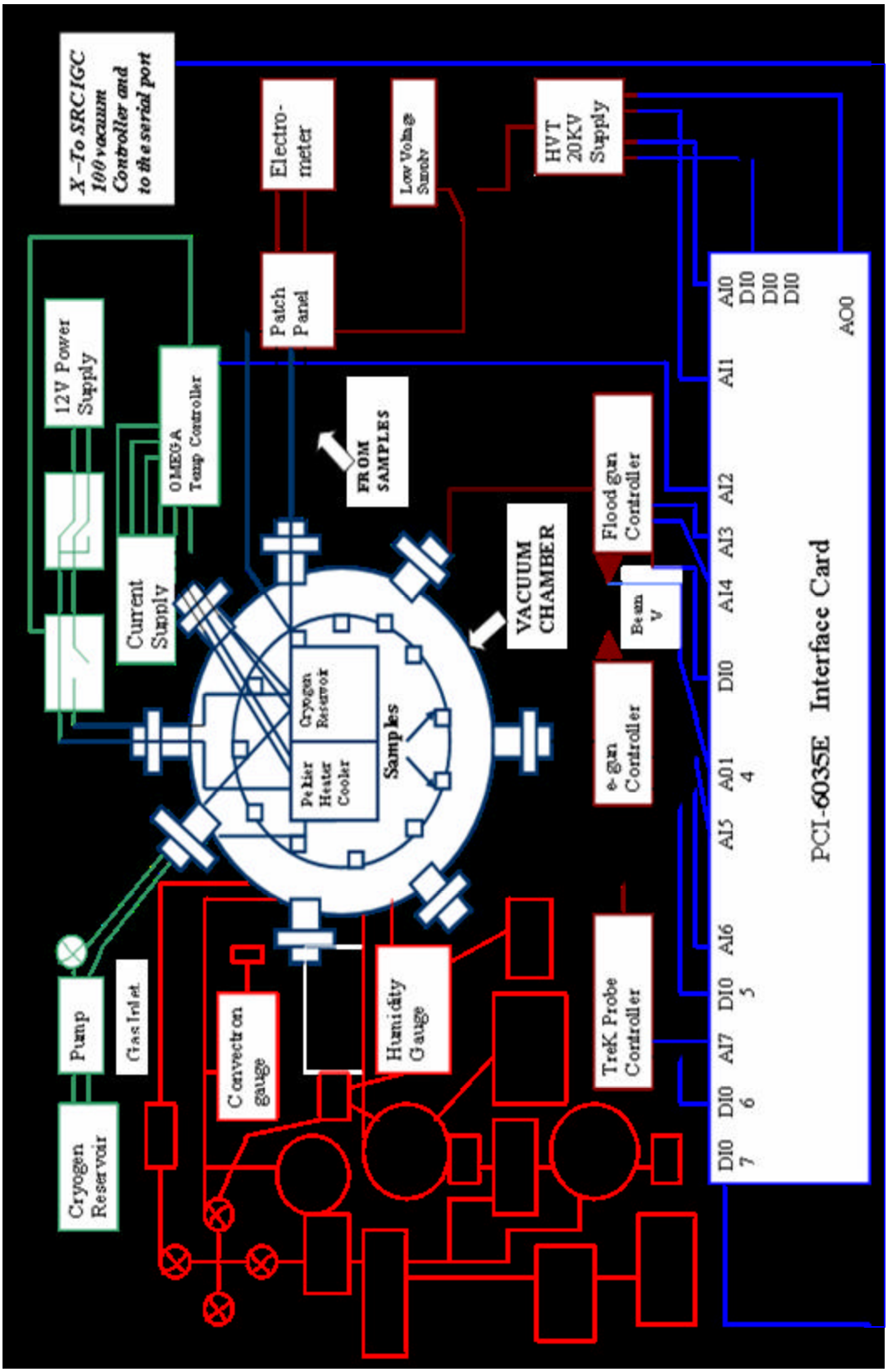

Fig. 2.4. Schematic diagram of the charge storage chamber with electrical controls.

The details of the feedthrough are described in Section A.3. As far as the sample positions inside the chamber are concerned, one of them has a flat metal sample coated with micro-crystalline graphite (Acquadag^{TM}) which acts as a field probe calibrator and as the zero set sample. The graphite coating serves to minimize stray electrons, since graphite has a low slow electron yield.

2) Sample Carousel Design: The 32 sample holders form a 58 cm diameter, 32-sided right cylinder approximately 8 cm high [2]. Figure 2.6 (b) shows a closer view of the sample holders in the chamber. Attached top and bottom Al plates provide a light-tight conducting seal for the sample carousel enclosure to minimize electrical charging (see fig. 2.6 (c)). Feedthroughs for electrical connections and cryogenic fluids are coaxial with the rotary drive. Two 20-pin electrical feedthroughs, mounted on a 7 cm Conflat^{TM} flanged tee attached to the 7 cm Conflat^{TM} flanged 6-way cross, provide access for the coaxial leads to each sample electrode (see fig. 2.7 (c)). A four-lead miniature high voltage (MHV) electrical connector is attached to another port of the 6-way cross; lead connections are made to diagnostics on the sample carousel. A high current 10-pin electrical feedthrough is also attached to the 6-way cross to provide power to the temperature control elements. A solenoid vacuum valve is connected to the six-way cross, which is shown in fig. 2.9; this provides a connection from the turbo pump vacuum system to the charge storage chamber. A cryogen feedthrough for thermal control fluids is also attached to the 6-way cross. All electrical connections are made inside the sample carousel enclosure to minimize electrical noise and to prevent extraneous sample charging [2].

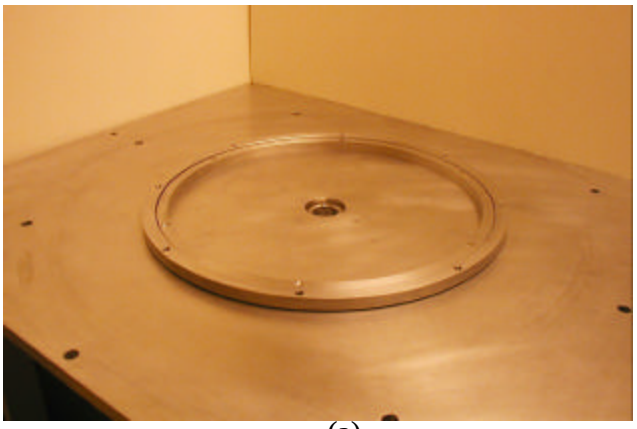

(a)

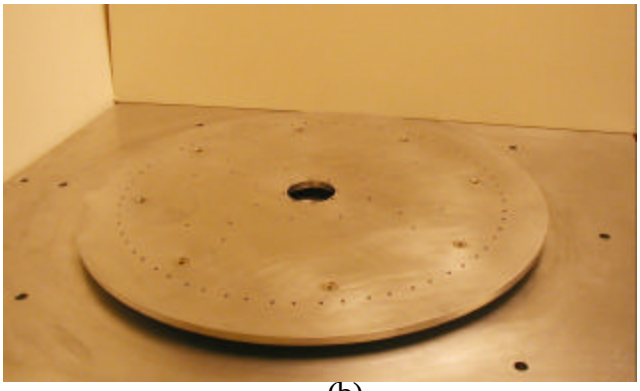

(b)

(c)

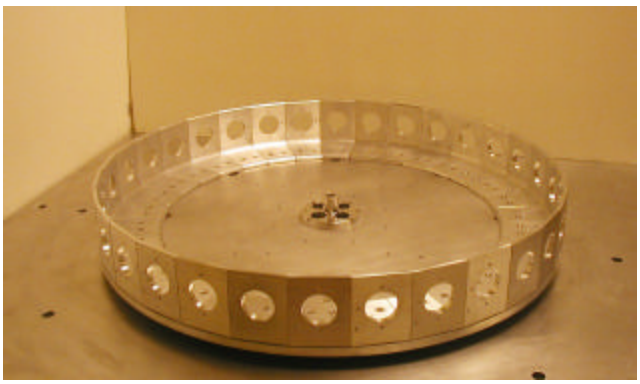

(d)

Fig. 2.5. Assembly of sample carousel.

(a) 43 cm diameter aluminum alloy lazy Susan bearing (Rocker Model 12451) attached to the bottom plate of the charge storage chamber.

(b) 58 cm diameter sample carousel base plate attached to the lazy Susan bearing.

(c) Side view of the sample carousel base plate attached to the lazy Susan bearing on top of the bottom plate of the charge storage chamber. The central region below the base plate houses the rotary motion assembly and the vacuum system as shown in fig. 2.10. Equipment racks are visible at the sides below the bottom plate.

(d) Sample holders mounted on the sample carousel base plate. The 32 sample holders form a 58 cm diameter, 32-sided right cylinder (~8 cm high).The sample/electrode/ polycarbonate sample mount assemblies are not attached to the sample mounts in this photograph. Also note the rotary shaft flange attached to the center of the sample carousel base plate; this couples the base plate to the rotary feed through shaft. The four holes visible in the rotary shaft flange provide access for electrical cables and cryogen lines from the feedthroughs below into the sample carousel enclosure.

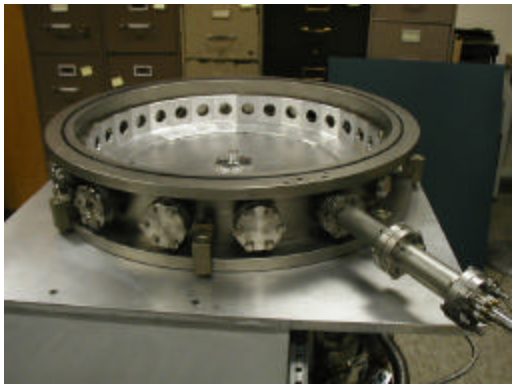

(a)

(b)

(c)

(d)

Fig. 2.6. Assembly of vacuum chamber and bell jar collar.

(a) The vacuum chamber with a 60 cm ID stainless steel bell jar collar resting on the Al bottom plate of the charge storage chamber. The upper vacuum O-ring is visible on the top of the bell jar collar.
(b) The chamber inner diameter is 60 cm, providing 1.3 cm clearance between the carousel and the chamber walls.
(c) An Al plate is attached to the top of the sample carousel. The attached top plate and bottom sample carousel base plate provide a light-tight, conducting seal to minimize electrical charging. All electrical connections are made inside the sample carousel cylinder to minimize electrical noise and to prevent extraneous sample charging.
(d) The steel bell jar collar has ten UHV metal-gasket sealed 7 cm Conflat™ flange ports and six o-ring sealed 2.5 cm baseplate hole ports. 2 cm thick aluminum plates are placed above and below the collar.

3) Rotary Feedthrough Design: The sample carousel can be rotated to move each sample in front of stationary electron, ion or photon sources, charge probes, or the sample cover manipulator to allow sample manipulation and inspection, charge deposition, sample treatments, or measurements. The carousel is mounted on a 43 cm diameter aluminum alloy lazy Susan bearing (Rocker Model 12451) [2] as shown in fig. 2.5 (a). Paint and lubricant were cleaned from the bearing to make the unit vacuum compatible; light turbo pump oil was then added to re-lubricate the bearing with a high vacuum compatible lubricant. The chamber inner diameter is 61 cm, providing 1.2 cm clearance between the carousel and the chamber walls. Each sample can be positioned in front of a field probe using a rotary feedthrough to facilitate the very large number of precise field measurements required in the long-term studies [2]. The rotary feedthrough was custom designed at USU for the purpose of rotation of the sample carousel. Figure 2.7 (a) shows the rotary feedthrough assembly. A schematic showing various parts of the feedthrough assembly is shown in fig. 2.7 (b). The rotary feedthrough has a long shaft (A in fig. 2.7 (b)) that connects it to the carousel (see fig. 2.9 (d)). The shaft and the handle (E in fig. 2.7 (b)) are attached to a base plate (B in fig. 2.7 (b)) which has 32 holes in it corresponding to the 32 samples. Each of the sample holders and sample cover plates is marked with a number so that user knows the exact sample on which the experiments are performed. The base plate is attached to another plate which is stationary (C in fig. 2.7(b)) and held in place by a cylindrical structure (D in fig. 2.7 (b)). The angular position of the sample carousel is set by fitting a pin (F in fig. 2.9 (b)) on an alignment arm attached to the fixed 7 cm Conflat^{TM} flanges at the top of the rotary feedthrough into one of 32 holes on a rotary motion positioning plate attached to the rotating exterior of the

rotary feedthrough. The number of sample-hole positions, the rotating plate has to be moved to be aligned with either the electron gun or charge probe has to be calculated before hand. The number marked on the rotating plate corresponds to the sample position in front of the charge probe. Four holes from that charge probe position will have the sample in front of the charge probe. This can be changed according to convenience. The rotating plate is held in its position by an alignment arm. The alignment arm is released so that the knob fits in the hole corresponding to the sample. With just minor adjustments one can get precise alignment of the source or probe with each sample center. There is a view port with the sample cover manipulator set up (A in fig. 2.9 (b)), which allows us to make sure that only the sample to be charged is open and the rest closed. There are four holes in the rotary shaft flange which provides access for electrical cables and cryogen lines from the feedthroughs below into the sample carousel enclosure.

4) Sample Holder Design: The design of the sample mount assembly and the sample carousel are intended to avoid things that will charge up and try to provide electrical shielding for the probes and current sources and as well as each sample. The sample carousel configuration shows how the electrons are prevented from reaching adjacent samples or the back of the irradiated sample through use of extensive grounded shielding. Figure 2.8 shows views of the fully assembled sample holder. Figure 2.8 (d) shows the view of a sample and copper back electrode as viewed through a quartz window from the outside of the charge storage chamber. Figure 2.9 shows partially assembled views of the sample holder. A key design goal is to make sure that charge does not get to the rear sample electrode at all. There should be no insulating surfaces visible by line-of-sight from the sample surface that can accumulate charge and produce

perturbing electric fields. Charge accumulation on the sample electrode can create a tangential field adjacent to the front insulator surface. Tangential fields on the sample make it hard to characterize the surface voltage [5]. Stray charge accumulation on the sample electrode also removes the ability to measure how much current is landing on the front of the sample surface during sample charging [2].

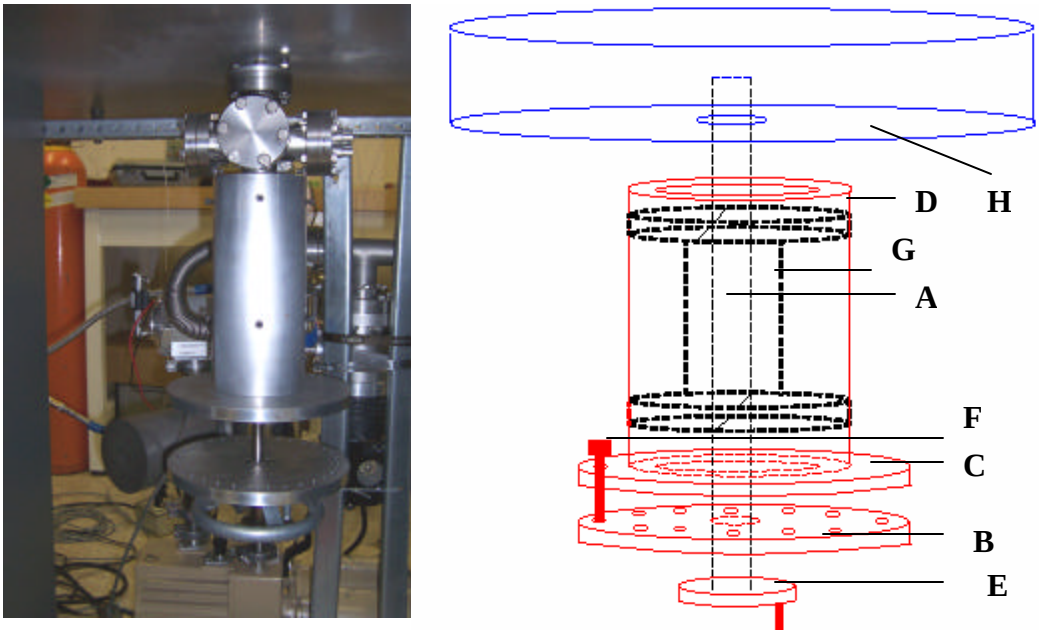

(a) (b)

Fig. 2.7. Rotary feedthrough design.
(a) Photograph showing the rotary feedthrough assembly.
(b) Schematic of the rotary feedthrough showing the different parts that make the set-up. The parts of the rotary feedthrough are shown in red. (A) Shaft that attaches the sample carousel to the handle outside the chamber for rotating the carousel. (B) Rotary base plate that rotates with the shaft. This plate has 32 holes on it corresponding to each of the samples on the carousel. (C) Stationary plate that attaches to a stationary cylindrical vacuum structure. This has a hole on it with a pin. This enables the rotary base plate to be locked depending on which sample is selected. (D) Cylindrical vacuum structure that is tightened onto a 7 cm Conflat nipple. This structure holds the carousel in place. (E) Handle attached to the shaft which enables the user to rotate (F) A pin which can be lifted up and down that locks the stationary plate onto the rotary base plate. (G) 7 cm Conflat nipple. (H) Sample carousel.

Furthermore, even a small hole in the insulator sample that exposes the rear electrode to the charging electron flux will cause a very strange process of electrons hopping along the surface to produce tangential fields of large magnitude. In addition, there should be no sources of light visible from the sample surface that could charge or discharge the sample surface; this requires a nearly light tight seal for each sample. Finally, RF signals emanating from the sample surface should get to the outside world only by coupling to the wire leading to the back of the sample [2]. That is, with the sample electrode connected to ground by a very short wire, there should be no path for RF signals generated on the sample surface to get through the polycarbonate sample mount to outside the sample enclosure. If such a path exists, then the DC bias on the sample during its charging will also cause charging on the polycarbonate and distort the later field measurements.

Particular attention is paid to the design and assembly of the sample mount. Figure 2.9 (a-c) shows the pictures of the sample holder assembly. The sample mounts are made of ~0.6 cm thick Al angle stock, ~8 cm high, 5.9 cm wide at the front and 4.8 cm wide at the back, with a distance of 6.4 cm front to back (see fig. 2.8 (a)). Access to the front surface of the sample is provided through a 3.2 cm hole in the Al sample holder. A 0.1 cm thick 316 stainless steel sheet metal cover disk normally covers this opening (see fig. 2.7 (b)), but can be rotated out of the way with a wobble stick to expose the sample for charge deposition, sample treatments, or measurements (see fig. 2.8 (c)). The sample cover manipulator set up is mounted on one of the ports of the vacuum chamber. The setup has three inclined 3.8 cm ports which fit into a 7 cm Conflat flange. A wobble stick is attached to a standard bellows (Motion Industries Model # C05-10) that allows

extended motion manipulation of the stick. A rod with a ball driver Allen wrench is mounted on the end through a compression port with O-ring seal that allows linear translation. The other two ports are dedicated to a view port and to serve as a flashlight holder to make the sample cover visible during measurements.

Figure 2.8(e) shows the photograph of the sample manipulator setup. Two 8-18 stainless steel set screws extend out the front surface of the sample mounts; these act as positive stops for the cover disk in the fully open and fully closed positions (see fig. 2.8 (a) and fig. 2.8 (b) respectively). The back of the sample/electrode/PC sample mount assembly is enclosed in a solid Al can, to provide complete electrical and light shielding (see fig. 2.7 (c)). UHV compatible Kapton^{TM} insulated lead wires (MDC Vacuum Model KAP50-5) from the electrodes are coaxially shielded with metal braid before leaving the tight metal cover. The wire is rated at 1.5 A and 2kV. A Be-Cu tension relief clamp visible on the bottom of the sample holder (see fig. 2.7 (c)) provides strain relief for the coaxial cable.

Each insulating sample is mounted with glue or tape on its own polycarbonate sample mount (~5 cm dia., 0.6 cm thick) [2]. A thin back electrode made of ~0.012 cm thick Cu foil, ~3.8 cm in diameter, with no guard electrode, is glued to the polycarbonate (PC) sample mount (see fig. 2.9 (b)). An electrical connection to the back electrode is made via a phosphor bronze spring held in place with a Be-Cu clip and 2-56 screw on the PC sample mount; the connection leading out the back is made using a coaxial ground-shielded cable (see fig. 2.9 (a)). The sample/electrode/PC sample mount assembly is then mounted (using two nylon 4-40 screws) to one of the 32 sample holders on the sample carousel.

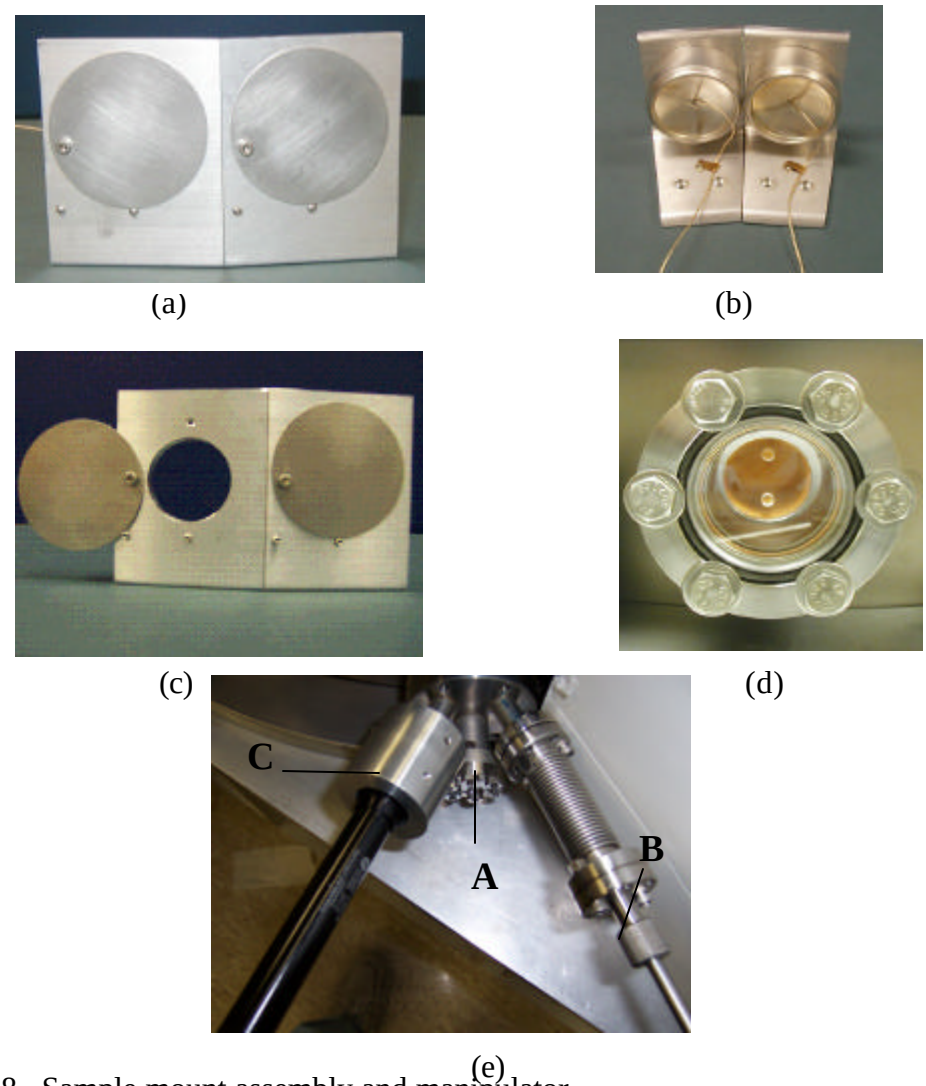

Fig. 2.8. Sample mount assembly and manipulator.
a) Front view of assembled sample mount with shutters open. A sheet metal cover disk or shutter, can be rotated out of the way with a wobble stick to expose the sample. Access to the front surface of the sample is provided through a 1.25" hole in the Al sample holder. (b) Rear view of assembled sample mounts. The back of the sample/electrode/PC sample mount assembly is enclosed in a solid Al shield can to provide complete electrical and light shielding. Leads from the electrodes are coaxially shielded before leaving the tight metal cover. A tension relief clamp visible on the bottom of the sample holder provides strain relief for the coaxial cable. (c) Front view of assembled sample mount with one shutter open and the other closed. The sample mount is made of ~1/4" thick Al angle stock,~3" high, ~2.325" wide at the front and 1.875" wide at the back, with a distance of ~2.5" front to back. (d) View of a sample and copper back electrode as viewed through a UV sapphire window from the outside of the charge storage chamber.(e) A view of the sample manipulator set up which is represented by a view port (A), motion manipulator bellows (B) and flashlight holder (C).

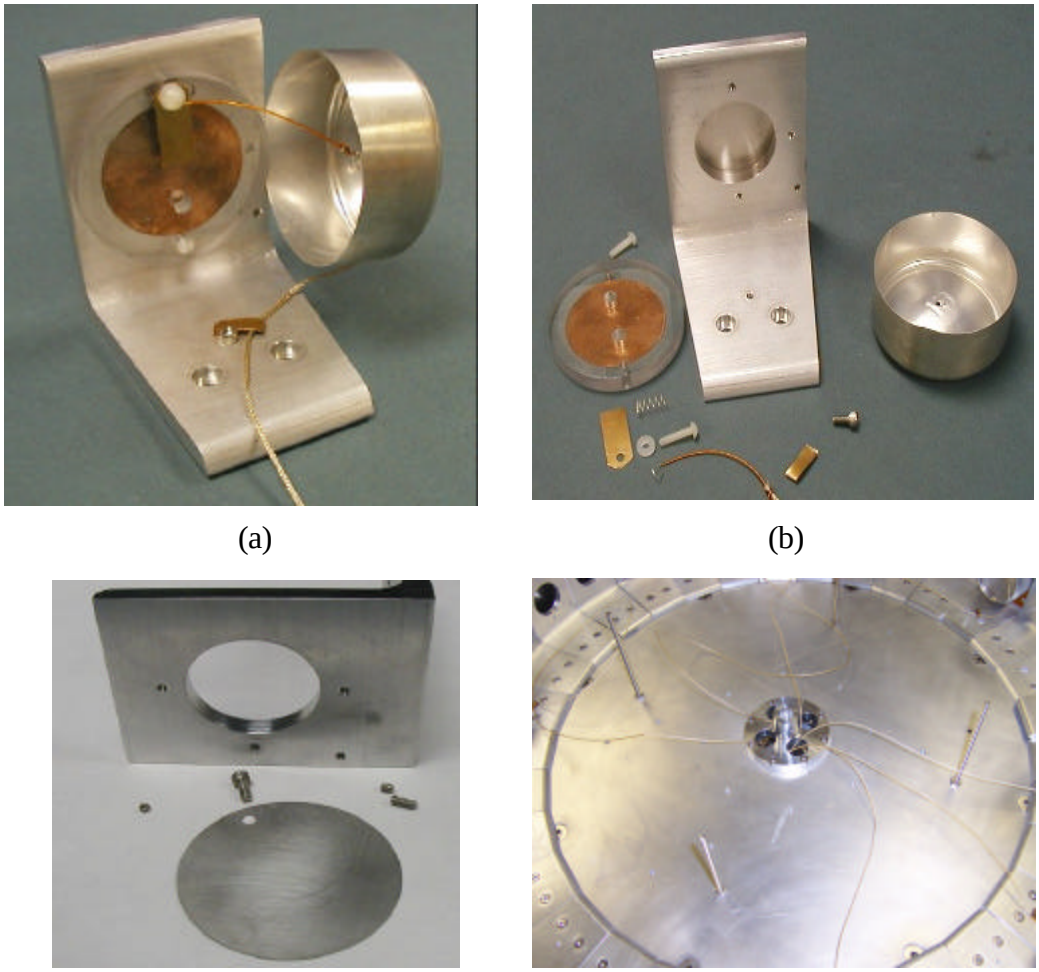

(a) (b)

(c) (d)

Fig. 2.9.Views of the disassembled sample mount assembly and connections.

(a) Rear view of assembled sample mount with shield can removed. Each insulating sample is mounted on its own polycarbonate sample mount (~6.5 cm dia., 0.6 cm thick) with a thin back electrode (made of 0.012 cm thick Cu foil, ~3.8 cm in diameter), with no guard electrode, glued to the polycarbonate sample mount, and with electrical connections via a phosphor bronze spring held in place with a Be-Cu clip and 4-40 nylon screw and washer on the PC sample mount leading out the back using a coaxial ground-shielded cable). The sample/electrode/PC sample mount assembly is mounted (using two 4-40 nylon screws) to the sample holder.

(b) Disassembled sample holder shown from the front. The sample/electrode/PC sample mount assembly and the coaxial cable tension relief clamp are shown disassembled.

(c) Disassembled sample holder shown from the rear. The shutter assemble has been disassembled.

(d) Top view of the chamber with the wires from the sample holders exiting through the rotary motion feedthrough.

Stainless steel set screws are inserted into the front of the two through-tapped holes to prevent the insulating surface of these nylon screws from being visible to incident electrons (see fig. 2.9 (b)) [2].

Preparation and mounting of the samples in the sample holder requires careful attention, especially in making sure that proper connection exists between the sample and the back electrode. Samples of certain thicknesses with metal vapor deposited on the back of the sample (manufactured by Sheldahl (http://www.sheldahl.com)) [2] are used for the experiments. The contact between the back metal of the sample and the electrode is done using an adhesive conducting liquid with is made by a combination of High Vacuum Leak Sealant (VACSEAL), silver powder and methanol which is mixed approximately in the ratio of 1:1:3. This combination is mixed thoroughly to have the silver particles suspended in the adhesive to aid conduction. An extremely thin layer of the conductive adhesive is applied on the top of circular copper electrode first. The sample is cut to the same size as the copper electrode and the sample is placed over the electrode and the set up is allowed to dry with the adhesive for about 5-7 minutes. Care should be taken to make sure that there are no lumps of adhesive which may cause ripples in the sample. The vacuum sealant is then applied onto the polycarbonate sample holder and the copper electrode is then stuck on the sample holder. It is possible to use a commercially available copper tape (3M^{TM} electrical tape) with conductive adhesive on both sides. This tape can be used to have the copper electrode stuck onto the PC holder and also the insulating sample on the copper electrode.

It was determined that sample thickness should range from 0.1 mil to 20 mils while using voltages from 100 volts to 10^4 volts. Alternate high voltage cables are

required for voltages above 2kV. Such combinations allow us to test the charge storage and resistivity under electric field strengths of order 10^7 V/m, which is a typical value for testing since insulator problems occur only occasionally. Insulator discharge pulsing begins to occur when the field strength in insulators exceeds 10^7 V/m. At larger field strengths, carrier motion is field dependent, difficult to model, and may further assist in producing electrical breakdown. At low field strengths the insulator rarely causes problems from the spacecraft charging perspective. Therefore, in order to reliably prevent spacecraft charging problems, one needs to demonstrate sufficient conducting particle motions at fields less than 10^7 V/m [10]. When measuring conduction currents in insulators, knowledge of the electric fields developed in the insulators is needed. Given enough time in the absence of conduction, the accumulation of high-energy charged particles stopped in the insulators will ultimately produce pulsed discharges, no matter how well shielded. To prevent the occurrence of pulsed discharges the conduction currents must remove charge as fast as it is deposited by the radiation while holding electric field strength below 10^7 V/m [5].

B. Sample Treatment

The experiment requires complete control of the environment in which the samples are placed. To understand the process of charge decay in insulators used in spacecraft, emulation of the space environment becomes mandatory. To achieve this, consistent high vacuum has to be provided and the behavior of the samples depending on the temperature variations needs to be monitored. Details about the instrumentation and monitoring of the vacuum system and the temperature control of the system are provided below.

1) Vacuum System: In order to measure long charge decay time constants, one must provide continuous high vacuum testing, without exposure to even partial vacuum, with approximately one measurement per sample per day for nearly a month. Hence it is imperative to design a reliable vacuum system that will be stable for long periods. Gas conduction activated by background radiation is a limitation for our methods. It will slowly discharge samples, or bring charge from one sample to another [2]. Thus, the less gas the better. On the other hand, use of ultra high vacuum techniques to attain pressures of less than 10^{-8} Torr requires much more sophisticated vacuum seals, limits available materials that can be used, and increases cost. An operating pressure of ~10^{-7} Torr has been identified as a compromise for these issues.

A turbo pump was chosen for evacuating the sample chamber after considering various possibilities. Diffusion pumps are probably not clean enough to avoid serious contamination over a month unless continuous $l N_2$ cold trapping is done; this is too costly and time consuming for a production chamber. Ion pumps are not acceptable because of the potential of sample charging from the pump plasma, although this may be minimized by eliminating line of sight of the ion pump plasma from the samples and by providing electrostatic screening [2]. Both cryo-pumps and ion pumps require something like a turbo pump to get to low vacuum anyway. However, the turbo-pump is susceptible to power failure. To minimize this concern, the computer controlling the vacuum system is run on an uninterruptible power supply. We will use an ion gauge and Convectron™ gauges for pressure monitoring; careful pressure measurements can be made without disturbing charged samples. Specifics of the design follow.

Aluminum plates that are 1.9 cm thick are placed above and below the collar.

Various parts of the vacuum system are shown in fig. 2.10 and the labels in brackets in the following section indicate the respective parts in the figure. The charge storage vacuum chamber is pumped using a turbo molecular pump(Leybold Model CF63 55 liter/sec[K] and Model NT50 turbo pump controller [A]) backed by a ~150 liter/s, two-stage, direct-drive, rotary-vane mechanical vacuum pump (Leybold Model Maxima D4A) [I]. Ultimate pressure of the system is estimated to be 10^{-7} Torr, limited by the pumping speed and o-ring seals. Vacuum connections between the pump and chamber are made using standard NW40 Quick Connect and CFF fittings. A standard bakeable molecular sieve trap (MDC Model KMST-152) [F] is mounted between the mechanical pump and turbo pump to minimize contamination due to back streaming. Pressure is measured by a low-pressure nude UHV ion gauge (Varian Model 275) [B] in the 10^{-5} to 10^{-10} Torr range, an intermediate pressure Convectron gauge (Granville-Phillips Model 275) [L] in the range of 10^{-4} to 10^{+3} Torr, and a high pressure Si strain gauge transducer (Omega Model PX 120-050GV) [J] in the range of 10^{0} to 10^{+6} Torr (50 atm). Relative humidity is monitored over a 0% to 100% range with a 2% accuracy using a standard gauge (Honeywell Model HIH-3610-001) which is not indicated in the figure. All vacuum gauges and vacuum process controls are monitored by a vacuum gauge controller (Stanford Research Systems Model IGC100)[H] that is fully interfaced with the control computer via a GPIB interface under the LabVIEW control (see Appendix I for further details on interfacing and the LabVIEW controls of the same). In the event of a vacuum interrupt, a solenoid-controlled value (Varian Direct-acting Electromagnetic Block Valve Model L9942602/NW25) [C] between the turbo pump manifold and the charge storage vacuum chamber closes to prevent venting of the chamber, an automatic solenoid turbo

vent value (Skinner Model V52RKM2050) [D] opens to prevent backstreaming, and a solenoid value (MKS Vacuum Model Vacuum Sentry Valve) isolates the mechanical pump from the vented vacuum line.

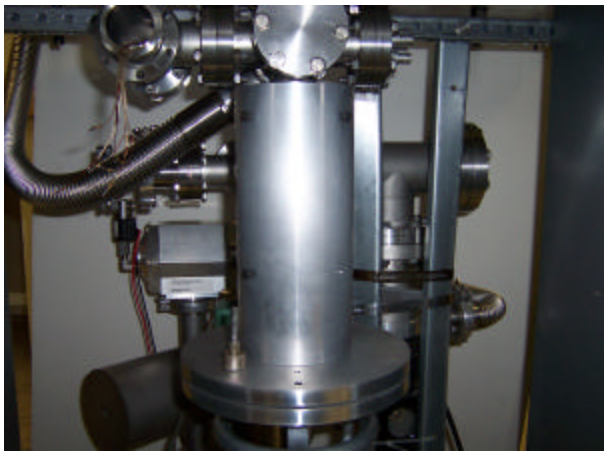

(a)

(b)

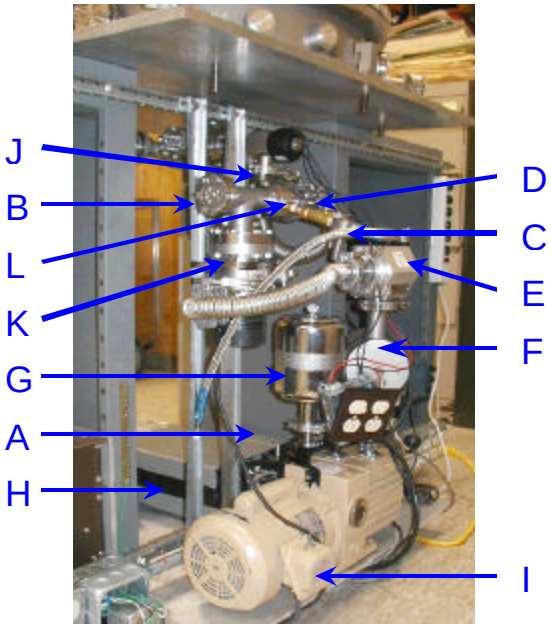

(c)

Fig. 2.10. Description of the vacuum system.
(a)Front view of the Vacuum system with the rotary feedthrough
(b)Rear view of the vacuum system
(c)Indicates various parts of the vacuum system :

(A) turbo pump controller
(B) Nude UHV ion gauge
(C) Automatic solenoid valve
(D)Gas handling system valve
(E) Solenoid valve
(F) Bakeable molecular sieve trap
(G) Exhaust mist filter
(H) Vacuum gauge controller
(I) ~150 litre/s mechanical vacuum pump
(J) High pressure Si transducer
(K) Turbo molecular pump
(L) Convectron gauge.

Power to the vacuum controller, computer, valves and turbo pump controller are provided by a computer-interfaced uninterruptible power supply (Cyber Power Model 900 AVR) in the event of a power failure or surges. The vacuum controller regulates the correct order of valve operation and pump restart in the event of a power failure or vacuum interrupt.

2) Temperature Control: The project requires temperature control of the samples over the lifetime of the experiments, on the order of a month. The samples are expected to demonstrate their worst charging behavior at low temperatures. Typical experiments to compare temperature dependence with theory for polymer insulator resistivity require approximately ±50°C about room temperature, although even ±30°C would be sufficient for our measurements. The description of the temperature control instrumentation is given in the section below.

The arrangement of the temperature system is made in such a way that temperature of the entire sample carousel is controlled. This is accomplished with a combination of Peltier cooling, resistive heating and liquid cryogen reservoirs in contact with the sample carousel. Figure 2.11 shows the Temperature Control Unit used to control temperature of the charge storage chamber sample carousel in the left and center of the photograph. Temperature control of the entire sample carousel is provided by two heat reservoirs attached to the carousel base plate.

The unit is designed to control the temperature of the samples and entire sample carousel to approximately ±5 °C using a standard Proportional-Integral-Derivative (PID) temperature controller (Omega Model CN9300).

Temperature is measured with four platinum Resistance Temperature Detectors (RTDs) mounted on the carousel, field probe calibrator module, and heat reservoirs [2]. Thermal isolation of the sample carousel from the rest of the chamber results from the weak thermal link across the lazy Susan bearing. The heat reservoirs can be filled with cooled or heated water from a closed loop system in contact with an external temperature bath, or can be filled with liquid nitrogen or other cryogens. The heat reservoirs can also be heated with resistance heaters. Alternately, the heat reservoirs can act as thermal reservoirs to dissipate excess heat from four 12 V 70 W thermoelectric Peltier cooling units in thermal contact with the carousel base plate and below the heat reservoirs. In cooling mode, the Peltier coolers are designed to cool the sample to –100 °C and exhaust excess heat to the heat reservoirs where it is transferred via the liquid cryogen to an external heat bath. In heating mode the Peltier coolers are run with reverse voltage, drawing heat from the external heat bath.

Fig. 2.11. Left and center portions of the photograph showing the temperature controls units.

In this mode, the unit is designed to heat the electrodes up to +100 °C. The cryogens will be transferred from the external heat bath through the vacuum wall using a standard liquid feedthrough (Insulator Seals Model 9812102) via a closed loop of stainless steel tubing coiled to allow rotation of the sample carousel and sealed internally with VCR fittings [2].

3) Electron Source and Sensing Control: In order to measure the resistivity of samples, by charge storage method, the amount of charge deposited and leakage through the sample is measured. Uniform surface charge is deposited on the sample and for this purpose a custom electron flood gun was designed, built and tested at USU. The details about the construction and the features of the electron gun are given below.

Details of the gun assembly are shown in fig. 2.12 (a) in which the conducting parts are shown in blue and the insulators are shown in red. The gun will be mounted on an available 7 cm Conflat ^{TM} flange (D in fig. 2.12 (b)) for use in the charge storage chamber. The electron gun was constructed at relatively low cost. The custom-design electron gun was machined at the Space Dynamics Laboratory Machine Shop. The gun is comprised of a Tungsten hairpin light bulb filament, a mesh grid for the acceleration and distribution of the electrons evenly on the sample surface. The design of the gun consists of four main parts. First is a Teflon^{TM} cylindrical standoff (C in fig. 2.12 (d)), which insulates the electron gun from the 7cm Conflat ^{TM} flange. An aluminum can (B in fig. 2.12 (d)) is placed above this insulation. This Al can, holds the filament (Maylight, rated at 2.5 V and 800mA) as shown in fig. 2.12 (a). The use of a commercial flashlight filament and associated filament holder facilitates filament replacement and greatly reduces the cost. A custom-built 3.2 cm diameter hemispherical stainless steel mesh grid

is mounted above the Al can and this structure is totally insulated from the filament by Al_2O_3 (Kimball Physics EV parts) tubing and spacers. All the structures have a base diameter of 3.2 cm to fit in the in the 3.4 cm inner diameter of a vacuum port tubing. A second flat stainless steel wire mesh is placed at the end of the grounded vacuum port tubing at the entrance of the bell-jar collar. This screen prohibits electric fields from the gun penetrating into the bell jar near the samples and also provides mechanical protection to the electron gun. The wiring from the mesh grid and the filament is attached to a standard 4 pin UHV vacuum feedthrough mounted on a 3.3 cm Conflat ^{TM} flange. The UHV feedthrough is shown as a view from inside and outside in fig. 2.12 (f). The feedthrough is mounted on a 7cm Conflat ^{TM} flange to a 3.2 cm Conflat ^{TM} flange adapter. The schematics of the pin diagrams of the feed through are shown in figs. 2.12 (g) and (h).

A custom electron flood gun controller was designed and constructed at USU to control the power supplies and to switch between the emission and suppression modes of the gun. The power supplies, TTL, Function generator and a multimeter are from a commercial unit, (Bel MERIT Model MT-100 *"All-in-one"*), which is shown in fig. 2.12 (f), are used as sources that drive the filament and the mesh-grid. The commercial variable power supply provides a maximum of 53 V at 10 mA for the beam voltage. Current to the filament, which controls the filament emission is controlled by another 5 V DC power supply from the commercial unit. As shown in the electron gun controller, the filament is can be floated to a maximum of -53 V by the beam voltage (anode supply). The voltages of the filament, the mesh grid and anode are controlled using standard 500 ohms 10 turn, wire wound potentiometers (Beckman Instruments, Inc.) rated at 5 W. The

electrons emitted by the filament can either be made to emit or be suppressed by controlling the grid voltage. The suppression or the emission mode is chosen by switching between the two voltages, approximately 5-10 V more negative than the anode voltage by controlling the potentiometer for suppression. This switching is achieved using a CMOS TTL controlled relay, (Maxim Integrated Products Part # DG 303 A) [22].The commercial unit also contains a DMM which helps in measuring current and voltages supplied to various parts of the electron gun. The controller has a 3P-4 position rotary switch (ITT Industries, Cannon) which is connected to the DMM voltage inputs in such a way that it can be used to measure the filament voltage, mesh grid voltage, the emission and the suppression voltage. The controller also is routed in such a way that the emission, filament and the grid currents can be measured as shown in fig. 2.14.In order to measure the currents the rotary switch is set to the suppression voltage position, the DMM is switched to current mode and the front panel jumpers are replaced with ammeter leads. The capability exists also to monitor these voltages with the computer under LabVIEW control using DAC analog voltage inputs. Figure 2.13 shows photographs of the flood gun controller with the power supply. The beam voltage can be transferred to the computer by attaching the output voltage from the ± 60 V DC GPIB controlled Agilent (Model E3647A) power supply, the ± 100 V DC GPIB controlled Keithley 237 power supply or the ± 1000 V Bertan (Model 230-01R) power supply to the input connector normally attached to the BEL Merit 0-53 V DC power supply. Computer monitoring of the electron flood gun power supply voltages could be easily added by making connections from the pins of the rotary switch to analog input ports of the DAC card.

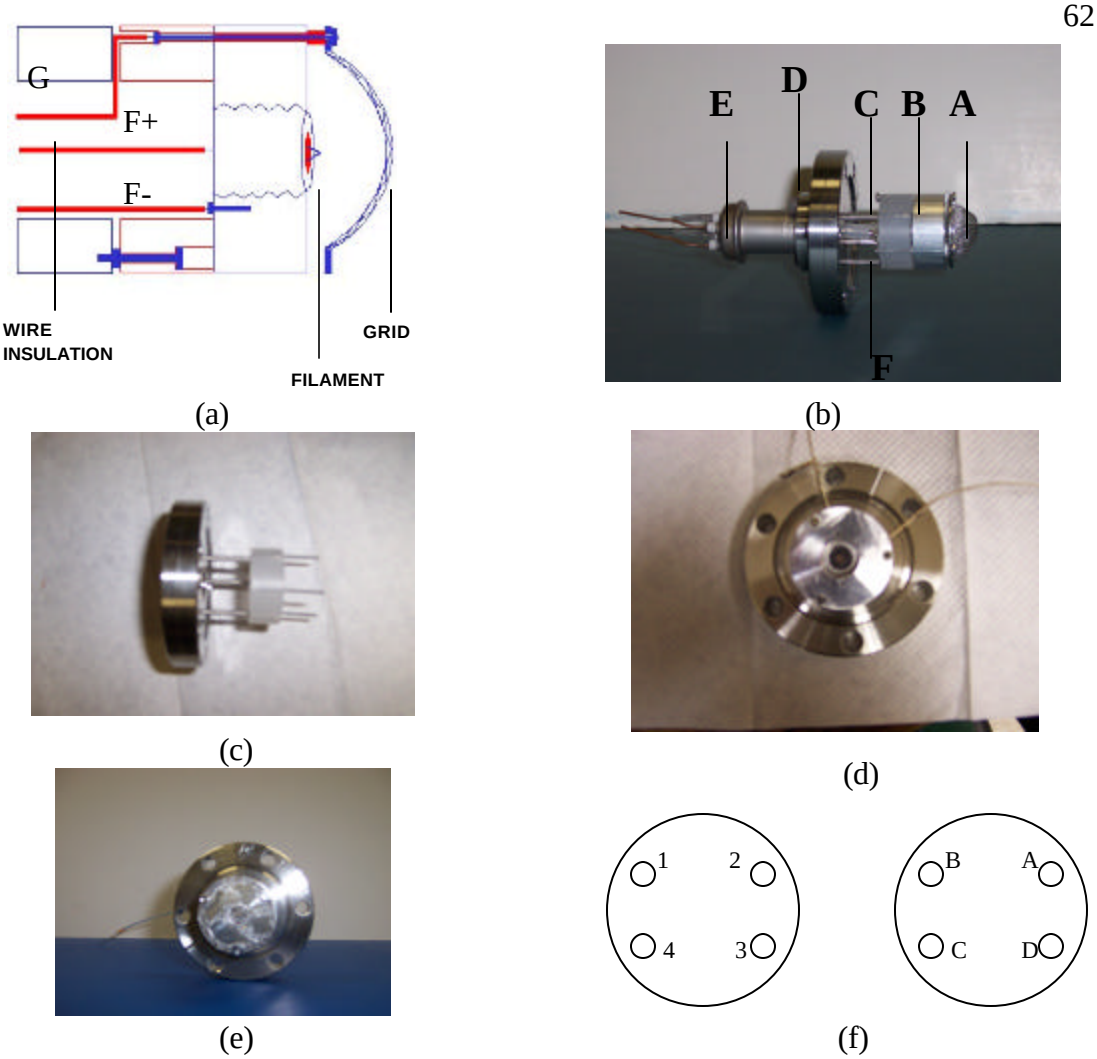

Fig. 2.12. Assembly of the electron gun.
(a) Schematic of the electron flood gun mounted on a Conflat™ flange. Insulating ceramic parts and the wire insulation are identified in red and conducting parts are indicated in blue. The labels indicate the positive (F+) and negative (F-) leads and the grid (G) (b) Fully assembled electron gun mounted on the 7 cm Conflat™ flange attached to a 3.6 cm Conflat™ which is represented by (A) Mesh grid; (B) Al can for mounting the filament holder; (C) Teflon™ stand-off to provide insulation (D) 2 ¾'' CFF (E) 1 ½'' CFF (F) Wiring for the electron gun. (c-e) show the assembly of the electron gun in steps,(c) Side view after mounting of the Teflon standoff to the 7cm Conflat™ flange (d) Top view after the Al can is placed over Teflon standoff with the filament (e) After mounting the mesh-grid in place. (f) The four lead UHV electrical feedthrough, which is mounted on a 3.6 cm Conflat™ flange. Left schematic indicates the view from outside the feedthrough where the representation is as follows: 1- Ni+ – Filament +, 2- Cu – Mesh grid, 3-Ni- – Filament-, 4–Cu+ NC. The schematic to the right shows the feedthrough from inside with the representation as A – Filament +, B – Mesh Grid, C– Filament, D – No Connection.

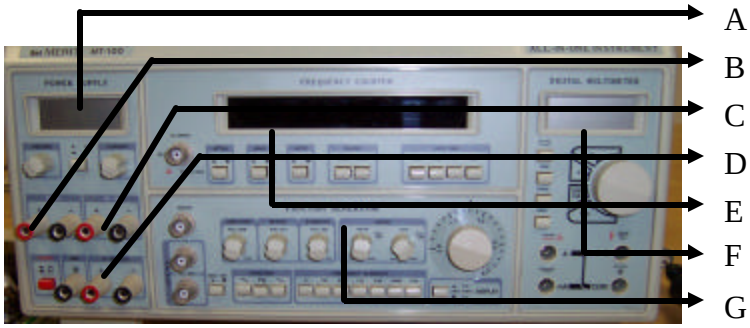

(b)

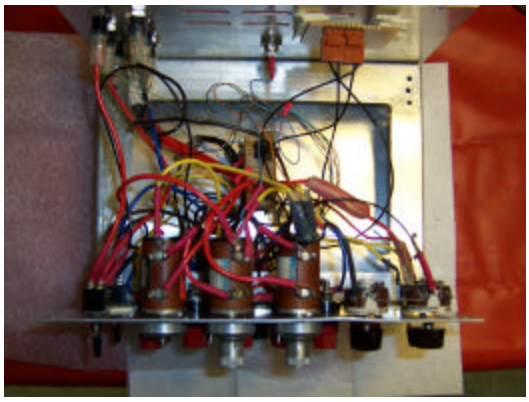

(c)

Fig. 2.13. Flood gun controller assembly.
(a) Bel MERIT MT-100 *"All-in-one"* which supplies power and provides the TTL pulse for the relay(DG303A)for switching between emission and suppression mode of the electron gun and this includes (A) Power supply meter (B) 5V DC,2A power supply; (C) 15 V DC 1A power supply; (D) ± 53 V DC 0.5 A power supply (E) Frequency meter (F) Pulse generator (G) Digital Multimeter. (b-c) Photographs showing the outer and inner view of the flood gun power supply.

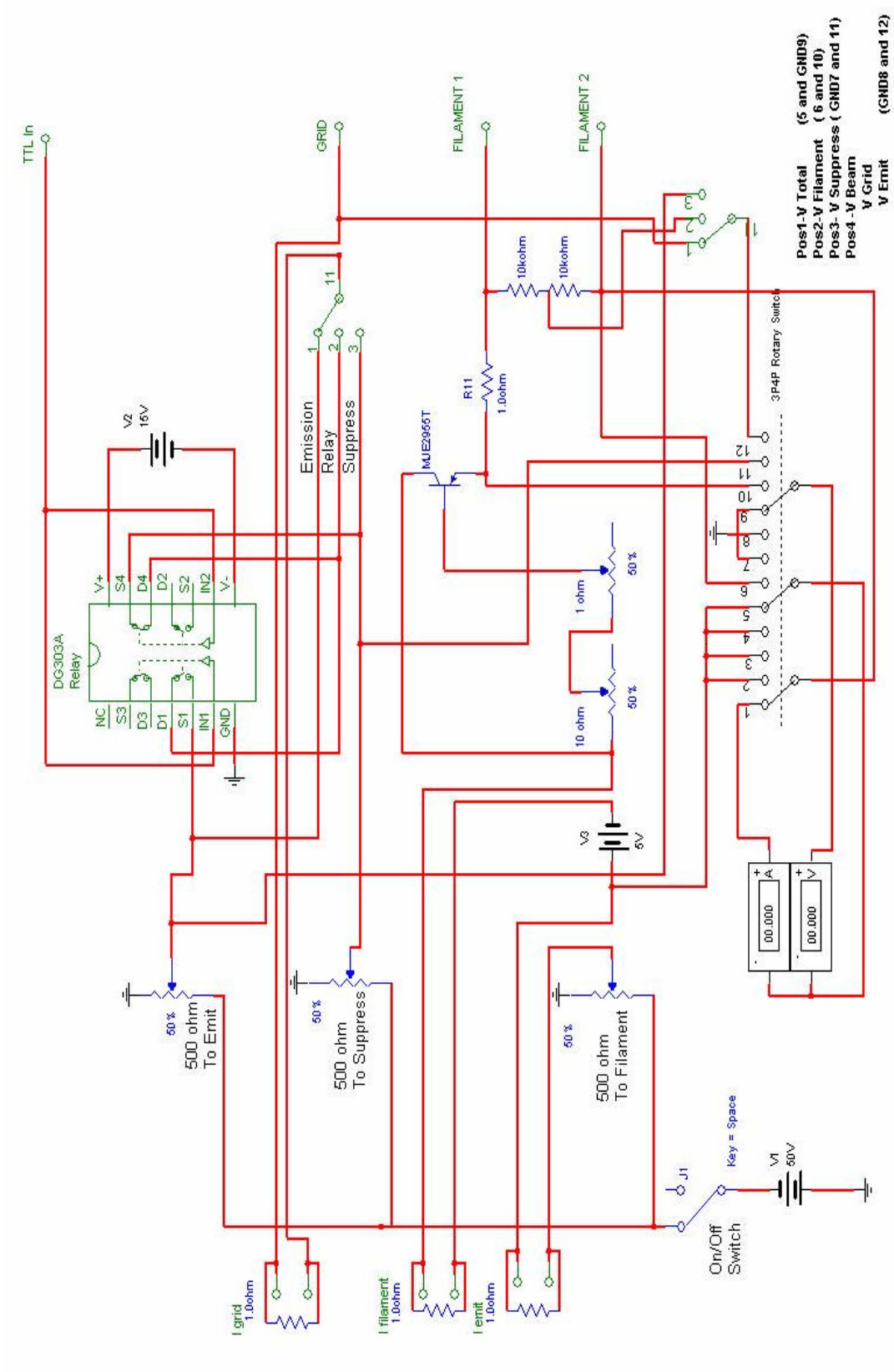

Fig. 2.14. Schematic of electron flood gun control power supply drawn in MultiSIM

The chamber also has an integral plasma source with bias capabilities, plus W-filament and UV light sources. This plasma source is required to charge or discharge of samples using sample bias with the sample electrode and a plasma source. Charging with electrons from the plasma can, in general, be accomplished more effectively with the low energy flood gun described above. But charging with positive ions is best accomplished with a plasma source. The plasma source is used while rear sample electrode is biased negative in order to get ions onto the surface. This is useful, for example, to see if ions chemically diffuse and produce conduction in insulating polymers when electrons do not, or to study about atomic diffusion in dielectrics. A medium energy electron flood gun will be installed for uniform, stable charge deposition at energies in the few keV regimes near the second crossover energy, which is the energy above which the secondary electron emission is less than the incident particle flux, for the insulators to be studied. The gun will be mounted on an available Conflat^{TM} flange on the vacuum chamber to allow charging of one sample at a time. Beam currents and beam profiles will be monitored with a standard Faraday cup mounted on the sample carousel.

4) Optical Sources: To provide optical access to the samples to treat samples with UV/VIS light and to discharge samples using light, a standard UV-grade sapphire view port mounted on a 7 cm Conflat^{TM} flange is attached to the chamber bell jar collar like one shown in fig.2.7 (d). Broadband W-filament and Deuterium or Hg discharge sources and IR/VIS/UV quasi-monochromatic LED external light sources can be mounted on the viewport flange as required. In particular, two intermediate intensity LED light sources have been developed [23].The sources use commercial LED lamps with high intensity LEDs per source and a parabolic reflector. An additional quartz view port is available for

visual inspection of the samples. Both view ports are equipped with external covers to prohibit light from entering the chamber, except when desired since light might result in sample charging through the photoelectric effect [2].

C. Charge Measurement

1) Charge Deposition Methods: A flood gun will be used to provide uniform surface charge. A positive bias is applied to the rear sample electrode. A filament source is used to inject electrons into the vacuum; slowly raising the sample electrode voltage to, say, 1 kV, develops 1 kV across the sample [5].The filament source is then turned off, the rear sample electrode grounded, and a 1 kV voltage is measured on the front surface of the insulator sample with the TReK^{TM} probe. This method places the electrons gently onto the front surface, not deeper into the bulk of the insulator. The field in the sample is therefore ideal for our measurements. Measurement of total current flow with an electrometer (Keithley Model 619) as the sample electrode is changed from 1 kV to ground, as well as the sample electrode voltage (Keithley DMM Model 196), can be used to determine the current required to charge the sample and to estimate the sample dielectric constant.

2) Current and Voltage Measurements: The sample electrode can be attached to an oscilloscope, a current monitor, a voltage source or a voltmeter. One sample position on the sample carousel has a flat metal sample to serve as both field probe calibrator and as the zero-set sample. Other positions will have a Faraday cup and UV sensitive photodiode to calibrate the flux of the charged particle and photon radiation, respectively

3) Surface Voltage Measurement Instrumentation: An electrostatic voltmeter (TReK^{TM}) is used to sense surface voltages from –20 kV to +20 kV relative to local

"ground," and from this infer local surface charge distributions [18]. The TReK™ voltmeter is actually composed of an electric field sensor and an adjustable voltage source (TReK™ Model 0341A). An internal sensor monitors the electric field that penetrates into the hole in the face of the TReK™ probe's metal housing (see fig. 2.15 (b)). The circuits adjust the potential of the metal housing until it attains nearly the potential of the nearby high voltage (HV) surface, at which condition there is zero field penetrating into the small hole. A standard voltmeter is used to measure the potential of the box, and the sample surface potential is proportional to the metal housing potential. No electrical contact is made to the nearby HV surface. In addition, as the metal housing voltage approaches the nearby HV surface voltage, the effective capacitance of the box to that surface approaches zero. The electron beam, low-energy electron treatments, light photon treatments, thermal treatments, or other treatments of the samples have been carefully designed to make sure not to affect the capacitor sensing circuit that brings the sample surface voltages out of the vacuum chamber [2].

At USU a custom capacitance transfer probe was constructed to make electric field measurements at sample surfaces *in situ* in the vacuum chamber, using a TReK™ probe external to the chamber; this isolates the sensitive TReK™ probe from the sample treatments. The design at USU is largely based on the design proposed by Frederickson at JPL [2, 5].When the probe was mounted directly inside the vacuum chamber facing the sample, extended electron beam exposure drove it off scale [10].Hence, the external mounting shown in the fig. 1.8 is preferred.

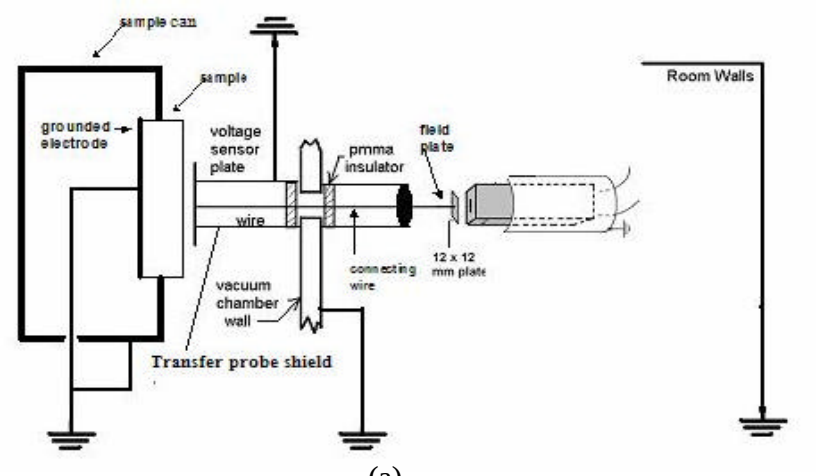

(a)

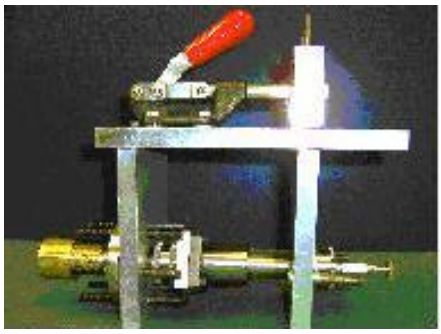

(b)

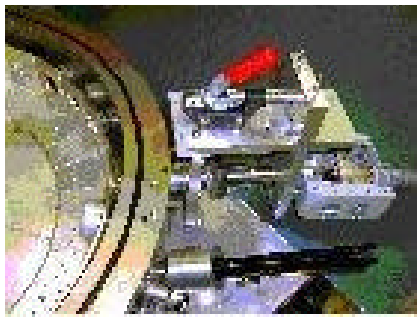

(c)

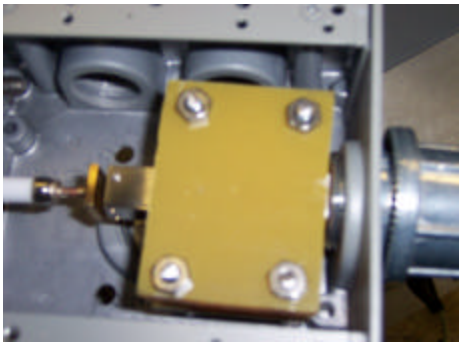

(d)

Fig. 2.15. Charge transfer probe assembly.
(a) Schematic of charge probe assembly at USU showing the TreK^{TM} probe and grounded copper guard tube (right), capacitance transfer probe–consisting of field plate, connecting wire and voltage sensor plate (center), and sample and grounded sample electrode (left) (b) Photograph of the USU TreK^{TM} probe assembly with translation mechanism. (c) Translation mechanism mounted on the vacuum chamber with the sample electrode and the TreK^{TM} probe box attached. (d) Arrangement of the probe in alignment with the gold coated plate which transfers the surface potential of the sample from inside the vacuum chamber. The probe is aligned and insulated by to printed circuit board clampings.

Here a copper plate, on which gold is electro-coated to minimize the stray fields from the formation of metal oxides, is remotely moved adjacent to the charged sample surface and connects to another plate outside the chamber through a copper tube. A small hole is drilled into the copper tube to prevent any air pockets since those would produce virtual vacuum leaks. The electrostatic voltmeter, in air outside the chamber, senses the voltage developed on the field plate (see fig. 2.15 (e)) and hence indirectly on the sensor plate and the sample. This arrangement for measuring surface voltage of sample presents a few distinct advantages [10]:

1. The probe will not be affected by the electron beam.

2. This arrangement enables us to repair the probe, if it breaks, without having to open the vacuum chamber, thus preventing the loss of data in prolonged runs.

3. A time dependent increase in the voltage on the sensor plate is a sensitive indicator of charge emitted by the sample, a valuable added benefit to the existing measurement.

Key aspects of our design are the geometry, construction and materials of the field probe, voltage sensor plate, connecting wire, and wire vacuum feedthrough. In addition, the coupling of the charge probe assembly—particularly the voltage sensor plate—to the sample and sample electrode are important. Both the mountings and the samples themselves must be coordinated so that the measurement technique corresponds to the physical and mathematical modeling. The spacing between the biased field-generating plate and the field probe needs to be much smaller than the extent of the probe. In this case, the electric field plane between the flat surface of the probe and the flat plate the electric field is plane-parallel. Note that surfaces at other voltages must be relatively far

from the flat plate so as not to alter the field between the plate and the probe. It was determined by Frederickson that a 12 mm x 12 mm flat plate spaced 3 mm from the probe satisfied this condition, even with most of the probe surrounded with grounded protective copper pipe [2]. Figure 2.15(a) illustrates the basic components of this capacitance transfer probe assembly used by Frederickson, including the field plate and adjacent grounded copper guard tube and TReK^{TM} probe (at right), the connecting wire and associated insulation and vacuum feedthroughs (center), and, the voltage sensor plate and interface to the sample and sample electrode (at left). The capacitance transfer probe uses a voltage sensor plate that truly integrates over the sample surface to obtain some measure of the average potential of its surface. The USU voltage sensor plate (see fig. 2.15 (b)) is made of OFHC Cu with Au plating to minimize stray electric fields and charging that would be a result of oxidation of the plates [2].

The capacitance transfer probe and the TReK^{TM} mounted on a UHV manipulator (see fig. 2.15 (c)) to allow measurements to be compatible with the USU sample carousel. A ~2.5 cm diameter voltage sensor plate is housed in a grounded Au plated metal housing (see fig. 2.15 (d)). With the sample cover disk fully opened on a sample holder, the voltage sensor plate housing will fit snuggly into the 3.5 cm diameter hole in the sample holder to provide reproducible positioning relative to the sample surface and tight shielding during charge measurements. Precise positioning of the voltage sensor plate approximately 2 mm above the sample results from alignment of a chamfer in the voltage sensor plate housing with the outer surface of the sample holder. When the housing is retracted, the sample carousel can be rotated to align another sample with the housing. The TReK^{TM} probe and field plate are mounted in a probe box (see figs. 2.15 (c) and 2.15

(e)), that moves with the voltage sensor plate maintaining the precise 3 mm gap between the TReK^{TM} probe and field plate. The probe is held in its place by two 0.6cm thick FR4 printed circuit boards (see fig. 2.15 (d)).The FR4 material is a somewhat leaky dielectric that was chosen so that clamps would not charge appreciably due to the voltage on the metal housing of the TReK^{TM} probe.

D. Computer Interfacing and Control

1) Hardware: To maintain vacuum and instrument functions for the life of the experiments (on the order of one month), it is obviously impossible for one to manually take data. Hence for the purpose of data acquisition and control a PC computer has been assembled with extensive hardware and software interface capabilities. Figure 2.4 shows much more detailed schematics of the interface controls and wiring circuitry. As much of the data collection, instrument control and sample manipulation as is practical has been automated under LabVIEW control, so as to facilitate rapid surface charge measurements thereby minimizing the likelihood of disturbing charge on the samples. The computer has a 1.4 GHz MHz processor (AMD Model K-7), with 256 MB of RAM, a 15" SVGA monitor (DELL 1024 X 720 M781P), with high speed internet and LAN connections. There are a 43 Gbyte hard drive, CD-RW drive, 100 Mbyte Zip drive, and 1.44 Mbyte floppy drive for data storage. Additional storage is available on file servers accessed via LAN. A color inkjet printer (HP Model 920C DeskJet) is attached and access is provided to a high speed laser printer (HP Model 4000 Laser-jet) via the internet. Instrumentation interfaces are provided by two serial ports, four USB 2.0 ports, and two DAC cards (National Instruments Model PCI 6014). In addition, a standard GPIB interface card (Axiom Model AS50999) is used to control a number of instruments including an 60

VDC power supply (Agilent Model 3647A), a ±100 VDC power supply (Keithley Model 237), a 6-digit multimeter (Keithley Model 196), an electrometer (Keithley Models 619), a ±1kV DC power supply (Bertan Model 230-01R), a ±50 kV DC power supply (HVT Model LS50-1 2R2-43/3) and a UV/VIS spectrometer (Ocean Optics Model SB1000).Connections between the control computer and peripheral devices are shown in fig. 2.16.

The standard data acquisition card (DAC) used are 12-bit resolution, and the PCI-based DAC is configured with eight ~100 kHz analog differential input channels, two analog output channels and numerous digital I/O channels. One DAC card is dedicated primarily to the charge storage chamber and the other to the capacitance resistance apparatus. Connections to the two DAC cards are made through advanced terminal blocks (NI Model BNC 2120). Analog inputs on the DAC card are used to monitor various voltage signals including: the output voltages from the sample voltage supplies (including the ±1kV DC power supply (Bertan Model 230-01R), ±50 kV DC power supply (HVT Model LS50-1 2R2-43/3)); voltages from the electron flood gun and medium energy electron gun supplies; the temperature voltage signal from the temperature controller and the electrostatic field strength from the TReK^{TM} probe controller. Analog outputs from the DAC card are used to control the output voltage of the Bertan 1kV and the HVT ±50 kV DC power supplies. Digital outputs from the DAC card are used to enable the output of the low voltage and high voltage power supplies, and to trigger a reading of the TReK^{TM} probe controller, and to provide beam blanking signals to the electron flood gun and medium energy electron gun controllers.

A serial port-interfaced vacuum gauge controller (Stanford Research Systems Model IGC100, H in fig. 2.9) is used monitor and control all vacuum gauges and vacuum processes. The vacuum gauge controller reads signals from two UHV nude ion gauges (Varian Model 275, B in fig. 2.10 (c)), two low vacuum Convectron gauges (Granville-Phillips Model 275, L in fig. 2.10), a low vacuum thermocouple gauge (Varian Model 531TC gauge tube and MDC Vacuum Model 801 gauge controller), an intermediate pressure capacitance manometer (MKS Baratron Model L22AA-00100AD 100 Torr head and Model PDR-D-1 control unit), a high pressure Si strain gauge (Omega Model PX 120-050GV, J in fig. 2.9), and a relative humidity gauge (Honeywell HIH-3610-001 environment condition sensor). This allows monitoring the pressure of the charge storage chamber, the capacitance resistance apparatus, the gas handling system, and the turbo pumped vacuum system. The vacuum gauge controller also monitors digital input from the turbo pump controller and sentry valve and uses internal relays to open and close the Varian solenoid-controlled valve, the turbo vent valve, and small solenoid valves to the capacitance resistance apparatus and the gas handling system. Power to the vacuum controller, computer, valves and turbo pump controller are provided by a computer-interfaced uninterruptible power supply (Cyber Power Model 900 AVR) in the event of a power failure or surges.

2) Software: Instrumentation control is being implemented using the graphical user interfaced data acquisition and control program LabVIEW. The LabVIEW control program was developed by Mr. Alec Sim, a graduate student in the Department of Physics. LabVIEW program would enable the complete automation of the system both in terms of fast data acquisition and monitoring of the system. The program has the

capability to give out warnings in case of any foreseeable eventuality. These features are extremely important considering that the duration of the experiments. A description of the program and the panels used for monitoring and data acquisition is provided in Appendix I.

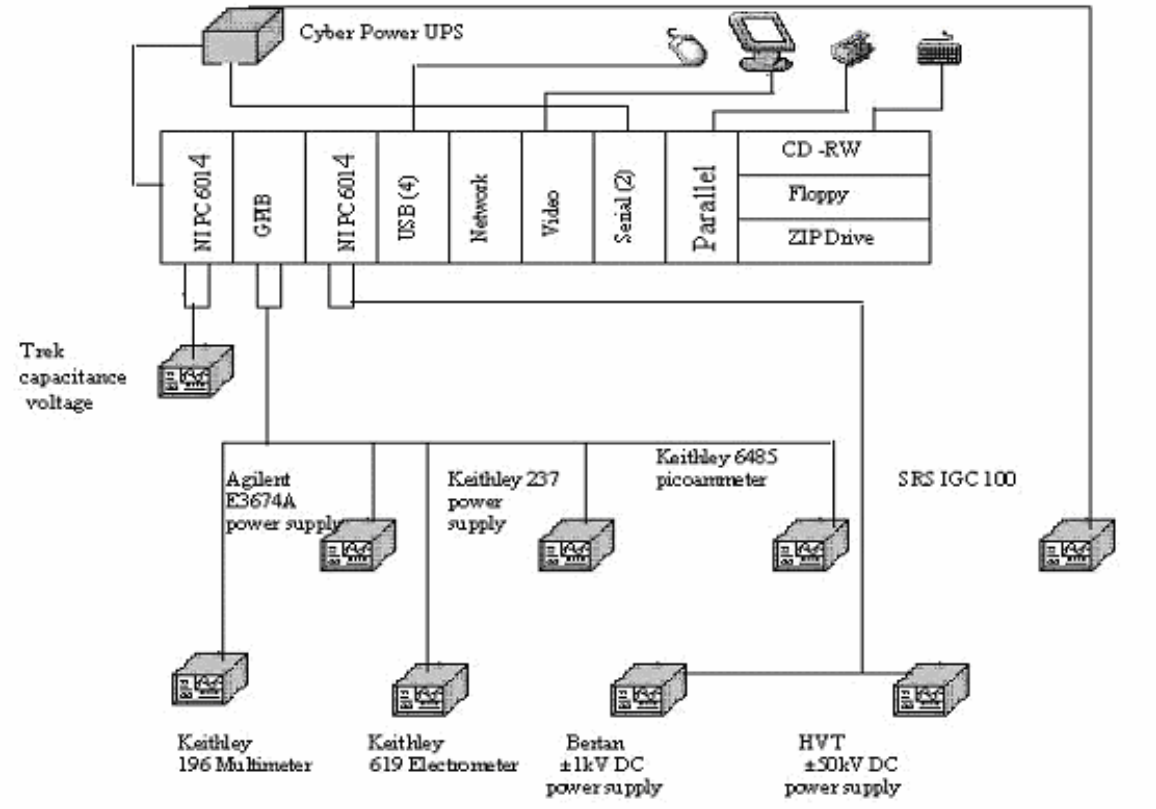

Fig. 2.16. Schematic of computer controls and various instruments controlled by the computer.

CHAPTER III

EXPERIMENTATION

The system design and instrumentation that is used for the measurement of charge storage for thin film insulators, were discussed the earlier chapters. This chapter explains the experimental methodology and the measurement of the surface voltage through the TReK^{TM} probe. The surface voltage measurement and the transfer of the measurement from the chamber to the outside world are also discussed here. Attempts have been made to measure the surface charge [17, 19] on the samples by having the TReK^{TM} probe directly inside the vacuum chamber and in front of the sample. But when this was done the extended electron beam exposure drove the probe off scale. Hence the external mounting arrangement as was shown in fig. 1.6 is generally preferred since, first it would prevent the electron beam from affecting the measurement. Second, in case any repairs need to be made to the probe it can be done without breaking the vacuum. This is especially vital since the experiments that are performed on the samples could go on for a period of one month and breaking vacuum would cost a lot of time and loss of data for the samples. Third, a time dependent increase in the voltage on the sensor plate is a sensitive indicator of the charge emitted by the sample, a valuable added benefit. This measurement procedure was first employed by Frederickson at JPL [10]. The same set up was adopted at USU. In order to accurately measure the surface voltage of the sample, the transfer probe needs to be calculated well. The following sections contain descriptions of the characterization of the probe, calculation of conversion factor of the transfer probe, the gas handling system, which gives control over the samples are

exposed to and lastly a list of samples that might be placed in the vacuum chamber for future testing. It also contains an overview of classical method of resistivity calculation and the results obtained from that method at USU.

A. Calibration of the TReK™ Probe

An electrostatic voltmeter (TReK™ model 341A) [18] is used at USU for sensing the surface voltages from -20kV to +20kV relative to the ground and from this, inferring local surface charge distributions. The electrostatic voltmeter must be empirically calibrated for each sample. Several problems relevant to the performance requirements mentioned in Table III occur with the probe of this voltmeter in our specific applications:

1. Although the probe works in high vacuum at pressures below 10^{-5} Torr, the introduction of electrons, ions or high-energy radiation into the same vacuum causes the probe sensor to drift, sometimes completely off scale. The probe then remains off-scale for weeks in vacuum, even after the electrons, ions or radiations are no longer present. The probe can be re-zeroed and stabilized by placing it in a warm (up to 50 °C), humid atmosphere for a few hours. We therefore wish to keep the probe away from free electrons or plasma.

2. The probe is “large” and is mounted to the end of its cabling. The entire probe body must float to the voltage of the surface being measured. Therefore, the probe and its cabling must be insulated from ground for 20 kV over its full length. This presents complex insulation mounting problems that need to be overcome in a vacuum chamber.

3. The probe cabling is encased in a thick electrical insulation tube (AFC (K) 1.8 cm) in order to insulate it for 20 kV. Physical movement or radiation can charge

the insulator surface, when in vacuum, to high voltage (HV). The placement of any charged insulation, including the polyethylene tube, in proximity to the samples under test can severely alter the electrostatic field and thereby change the voltmeter reading. Therefore, the polyethylene tube must be shielded by a flexible metal covering if it is placed in vacuum.

4. The probe is "large" and is mounted to the end of its cabling. If one is to measure many samples using a single probe, then one must either move the probe or move the samples. Thus, it is possible to measure many samples with one probe strategically placed in the vacuum chamber and with shielding on its cable runs. This design requires using one probe continuously in each vacuum chamber.

5. Probes are not highly reliable. One arc in the chamber can take out a probe that is mounted in the chamber. With highly charged samples in the vacuum it is probable that probes will fail during the test. In order to repair the probe one must open the vacuum to atmosphere and thereby discharge all of the charged samples in the chamber. If this happens significant data will be lost [10].

It is therefore advantageous, for reasons cited above, to leave the probe outside the vacuum chamber if one can bring the high voltage signal outside the chamber. This allows the TReK^{TM} probe to remain outside the vacuum chamber where it can be repaired or replaced without losing data.

1) Transfer of Charged-Sample HV Signal to TReK^{TM} Sensor Outside the Chamber: Contrary to common engineering practice, a direct current (DC) electrostatic potential can be coupled to measuring circuits using a capacitor. But the measuring

circuit must have very large resistance to ground, and the capacitor works best if one of its electrodes can be moved or switched.

For example, because of their 10^7 ohm input impedance, typical voltmeters cannot measure DC volts through a typical capacitor when used in the normal fashion, but it can be done. Consider the circuit in fig. 3.1 where the charged sample has capacitance C_1 with charge Q and voltage $V_1 = Q/C_1$ on it. The capacitance of the input circuit of the voltmeter to ground is C_3 and its input impedance is R. When the switch is thrown, a portion Q' of Q is transferred to C_2 and a voltage V_{m0} appears instantaneously at the voltmeter. The charge Q is now shared on all three capacitors so that the instantaneous voltage across C_1 is now,

$$V_1 = \frac{Q}{C_1 + \frac{C_2 C_3}{C_2 + C_3}} \tag{3.1}$$

For the purpose of simplifying the demonstration, let $C_3 << C_2$. Then

$$V_1 = \frac{Q}{C_1 + C_3} \tag{3.2}$$

In this case the instantaneous voltage on the voltmeter becomes $V_{m0} = Q'/C_3$ where

$$Q' = V_1 \frac{C_2 C_3}{C_2 + C_3} \tag{3.3}$$

and therefore ,

$$V_{m0} = \frac{QC_2}{(C_2 + C_3)(C_1 + C_3)} \tag{3.4}$$

Let $C_3 << C_1$ and $C_3 << C_2$, then

$$V_{m0} = \frac{QC_2}{C_2 C_1} = \frac{Q}{C_1} \tag{3.5}$$

Thus, a meter with small input capacitance and small lead capacitance will instantaneously achieve a reading of the voltage V_1 on the sample, C_1.

The reading will decay to 1/e of its value V_1 in a time $t = R\left(C_3 + \frac{C_1 C_2}{(C_1 + C_2)}\right)$ where R is typically 10^7 ohms. Thus, for a typical value for C_3 of 100 pF and for C_1 and C_2 of 1000 pF, the voltmeter decay time is 6 ms. In principle, one can use this technique, but in practice better methods are available. The above method has demonstrated how capacitive coupling can be used to measure DC voltage by creating a transient with a switch. When the impedance of the voltmeter goes to infinity this method becomes useful. The TReK^{TM} electrostatic voltmeter has (nearly) infinite input impedance and low (<10 pF) input capacitance. As mentioned earlier in the section II.C.3 a custom capacitance probe was built at USU to transfer the HV signals from the

sample surface to the TReK^{TM} probe outside the chamber. The TReK^{TM} probe was mounted outside the vacuum chamber, as was shown in fig. 2.14 (a). The probe's field plate will connect to a wire that passes through an insulator into the vacuum chamber.

In the vacuum chamber the wire will connect to a sample voltage sensor plate placed adjacent to the high-voltage surface of the sample. The wire is intended to deliver the voltage information to the field probe, but it adds two problems. First, a leakage current (both displacement current and mobile charge current) will flow to ground where the wire passes through the insulated vacuum feed through. Second, the capacitance of the wire decreases the amount of charge that is developed at the probe's field plate.

The equivalent circuit is shown in fig. 3.2. C_s is the capacitance of the surface of the sample to both its electrode and to ground. C_f is the capacitance of the surface of the sample to its nearby voltage sensor plate. C_w is the capacitance of the wire feedthrough to ground.

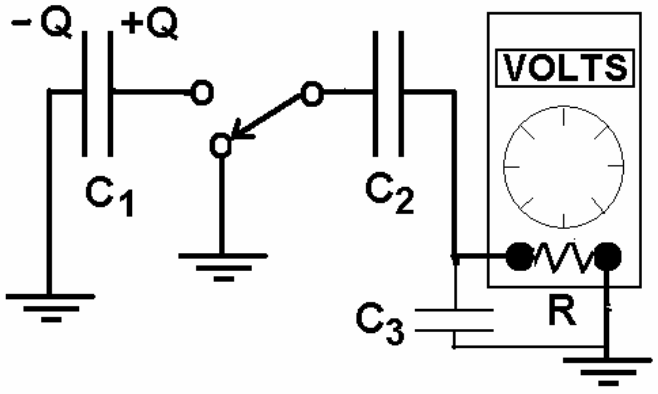

Fig. 3.1. Example circuit for determining capacitive coupling by measuring DC voltage created as a transient with a switch.

Since the TReK^{TM} probe adjusts its surface to nearly the same potential as that on the probe's field plate, there is negligible capacitance between the TReK^{TM} probe and the probe's field plate. R_i is the resistance of the wire to ground and is usually developed through the vacuum feedthrough insulator material. This resistance is not a constant. One may consider it to be an adjustable resistance for purposes of circuit analysis.

Figure 3.2 (a) shows the equivalent circuit when the sample electrode is grounded. If one suddenly changes the voltage on the sample by an amount V_s (see fig. 3.2 (b)), there will be an instantaneous but smaller change of voltage, V_p, measured by the probe. V_s is instantaneously greater than V_p because of the voltage dividing property (or equivalently, surface area ratio) of C_f and C_w. Instantaneously, a charge Q is developed across each capacitor:

$$V_p = Q / C_w \tag{3.6}$$

$$\text{and } V_s = Q / C_w + Q / C_f \tag{3.7}$$

$$\text{so that } \frac{V_s}{V_p} = \frac{C_w + C_f}{C_f} \tag{3.8}$$

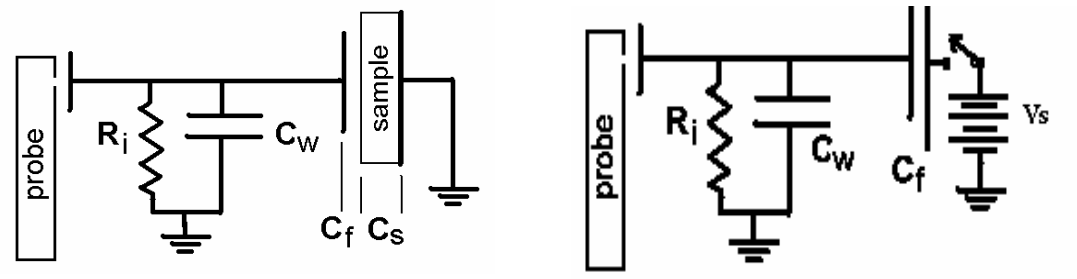

(a) (b)

Fig. 3.2. Equivalent circuit of charge probe assembly with the sample electrode (a) at ground (b) at voltage V_s.

In most cases, C_f and C_w will both be of order 10 picofarads (pF) and good experimental design will attempt to keep C_w as small as possible. As time passes, the charge Q on C_w will leak through R_i and the voltage V_p will approach zero. The value of R_i is exceedingly important because it limits the time duration over which a good measurement of the sample surface voltage may be obtained. If R_i were truly infinite and if the dielectric constant of C_w were truly constant, then V_p would not bleed-down. In fact, R_i is finite, and C_w increases with time after any voltage change. The value of R_i is actually only an effective resistance since decay occurring in the first minute or so is due to the polarization current which is not a resistive current.

The characterization of the probe was done by using a blank copper electrode in atmospheric conditions. The calculation of the value of this effective resistance is given under the following section on characterization of the probe.

2) Characterization of the TReK™ Probe at USU: The transfer probe which transfers the charge from the surface of the sample through the voltage sensor plate to the field plate outside the vacuum chamber (see fig. 2.15 (a)) needs to be characterized to calculate the conversion factor, i.e., to know what percentage of the surface voltage of the sample is reflected on the field plate and subsequently on the TReK™ probe. This characterization of the probe was done using a copper electrode under vacuum of approximately 10^{-5} Torr. The transfer probe was placed in front of a copper electrode mounted in the sample holder, and a known voltage was applied to the electrode. A 0 to 60 V DC power supply (Agilent model E3647A) was used for smaller voltage ranges and a ± 1 kV DC power supply (Bertan model 230-01R) was used for greater voltages. The ratio of the applied electrode voltage to the measured TReK™ probe voltage was then

recorded. (Note: In this section, further reference to sample implies the copper electrode.). This ratio would vary depending on the distance between the voltage sensor plate and the sample surface. The sensor plate was fixed at an optimum distance of 2 mm ± 0.5mm from the sample surface as determined by the experiments at JPL. The arrangement of the transfer probe assembly is shown in fig. 2.5 (a). Various experiments were performed using this arrangement to characterize the voltage data read by the TReK™ probe outside the vacuum chamber.

The entire setup for the transfer of charge from the surface of the sample to the TReK™ probe was subjected to various tests to gauge the reliability and reproducibility of the data obtained. The tests that were performed on the setup were as follows:

a) Arcing: As an initial step, it is essential to make sure that there is no arcing between the sample surface and the voltage sensor plate or the sample holder edges. If there is any kind of discharge through the electronics of the probe then serious damage can be caused to the expensive probe setup. Hence it might not be prudent to have the probe as a part of the arcing tests. The arcing phenomenon was monitored by using the applied voltage as a reference with time. Hence a maximum voltage of 1kV, in the steps of 10V, was applied to the sample in vacuum and the TReK™ probe response was monitored. But when the same experiment was conducted in atmosphere, the sample arced against both the sensor plate and the sample holder edges at a voltage of 637V. Figure 3.3 shows the applied voltage as function of time measured in atmosphere. This disparity is explained by Paschen's law where the breakdown voltage is a function of gas density and the distance between the two surfaces. In our case, the high vacuum environment does not allow the electrons to ionize gas molecules which would eventually

lead to breakdown.

b.) Decaying of the applied voltage: As mentioned earlier the presence of the capacitance and the resistance between the transfer wire and the ground might be a leakage path to the voltage applied to the sample. The characterization of this feature is extremely important as it would help us know how long the charge on the surface of the sample can be read without any error. To test this, the sample was held at a constant voltage of 300V for a period of approximately 20 minutes and the voltage shown by the TReK^{TM} probe was recorded. There was no substantial decay noticed in the data obtained. Figure 3.4 shows a plot with the applied voltage (read voltage) and the voltage recorded through the TReK^{TM} (TReK voltage).

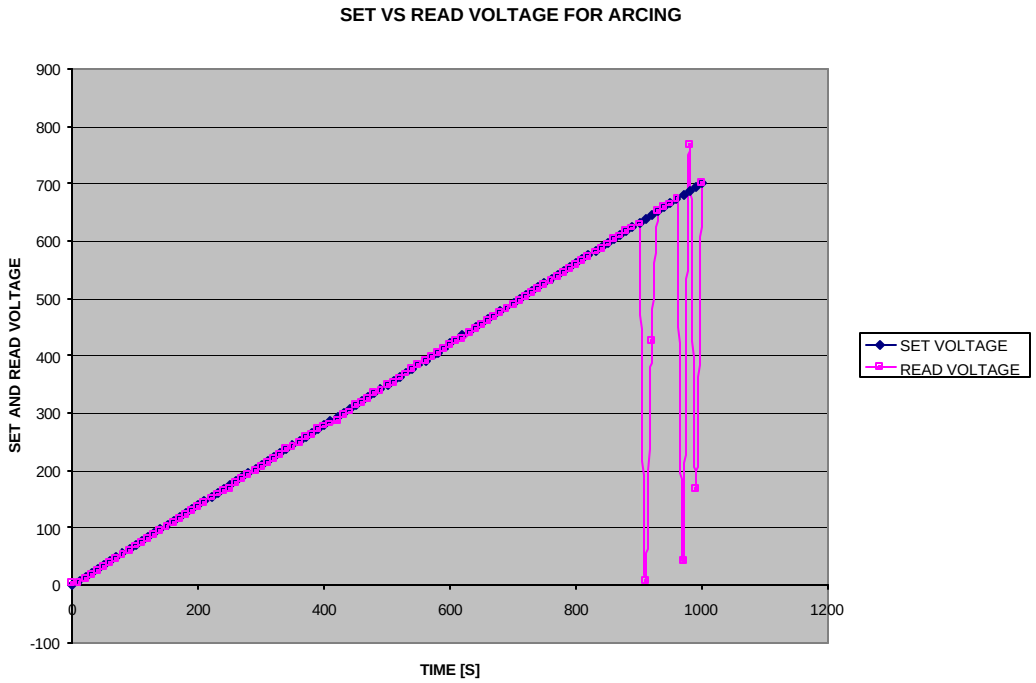

Fig. 3.3. Plot showing the behavior of the transfer probe when an arcing phenomenon occurs in atmospheric conditions.

Figure 3.5 shows a graph indicating the percentage discrepancy between the measured TReK^{TM} probe voltage and the voltage applied to the electrode as a function of elapsed time. The plot clearly shows that there is no more than a ± 2 % change in the measured voltage with respect to the applied voltage. Moreover this decay was performed on the transfer probe for a period of almost 1 day to monitor the long term change in the measured voltage through the probe. This measurement is shown by the plot in fig. 3.6. There is a decay that is observed through the resistance offered by the transfer wire to ground and from this plot one can calculate the effective resistance mentioned in the previous section by the simple capacitor model. From the plot of fig. 3.6 we can see that the decay time is $2x10^6$ sec. The total capacitance between the sample surface and the voltage sensor plate and the wire to the vacuum chamber wall ($C_f + C_w$) is found to be 10 pF. Hence from the values of the total capacitance and the decay time from the graph, the value of the effective resistance can be calculated as 5×10^{16} O.

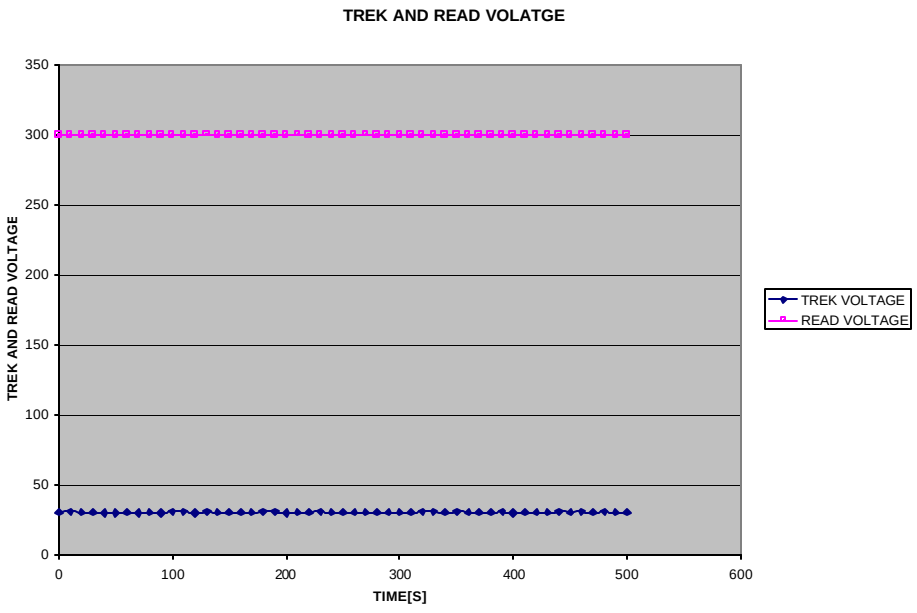

Fig. 3.4. Plot showing the applied voltage and the voltage read by the probe.

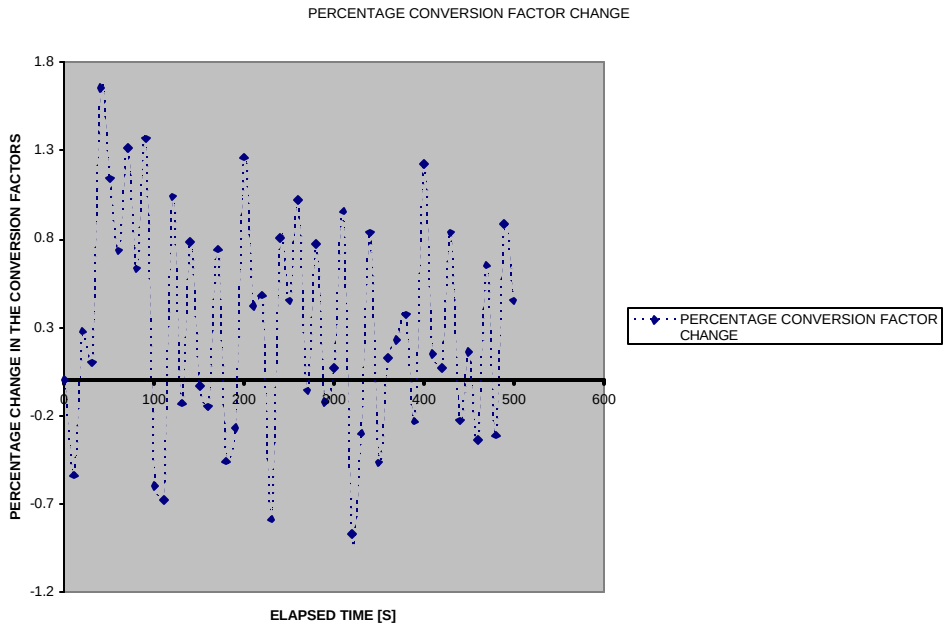

Fig. 3.5. Plot showing the percentage change in the voltage read by the probe from the sample.

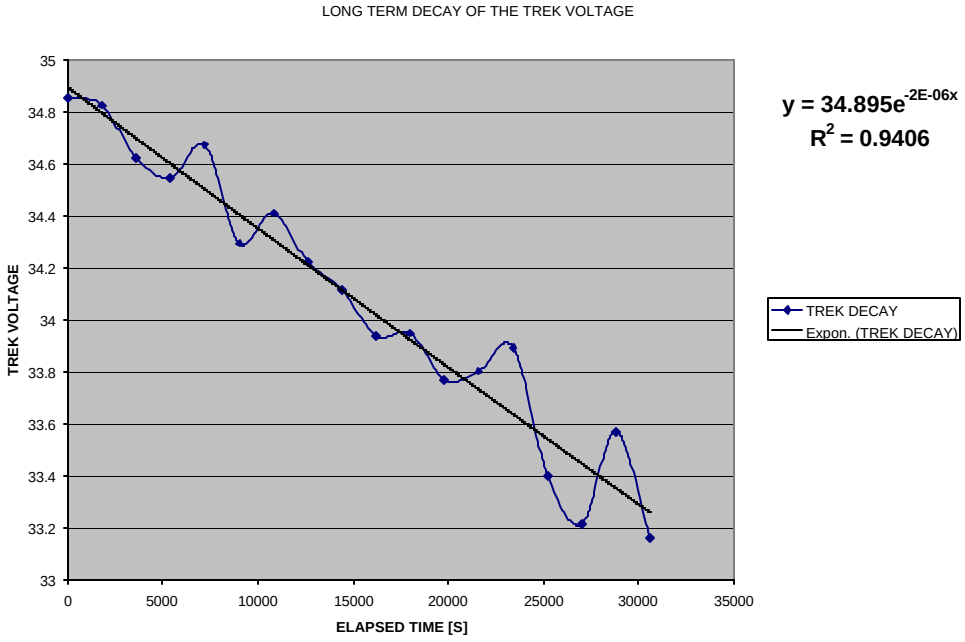

Fig. 3.6. Plot showing a long term decay of the probe voltage.

c) Linear calibration: In order to characterize the probe it is imperative to verify that the voltage read by the TReK^{TM} probe is linearly proportional to the voltage applied to the sample over the full range of voltages. The results obtained from the probe show that the voltages obtained are perfectly linear to what is applied to rear of the sample. The value of the slope of the plot between the applied voltage and the probe voltage is the calibration constant, a, of the transfer probe system. Equation 3.9 gives the calibration constant for the system in use. The surface voltage, $V_{surface}$, of the sample in relation to the voltage read by the probe and the offset voltage of the TReK^{TM} probe which is ideally zero, is given in equation 3.10. Figure 3.7 shows one of the linear plots obtained.

$$a = (7 \pm 0.8)\ V_{applied} / V_{probe} \tag{3.9}$$

$$V_{surface} = a\ V_{probe} + V_{probe\ offset} \tag{3.10}$$

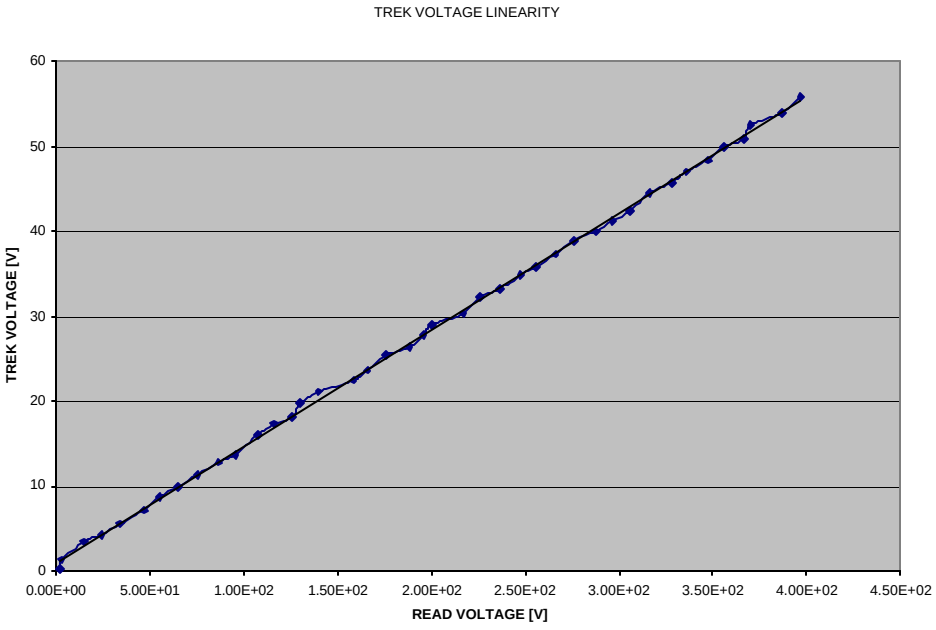

Fig. 3.7. Linearity plot between the applied voltage and the probe voltage.

B. Classical ASTM-IEC Resistivity Measurement Technique

1) Theory: As mentioned in the introductory portion of the thesis, the classical method of measuring the resistivity of the thin film insulators is based upon the measurement of current flow in a well defined structure where the relationship between the material's resistivity and the sample resistance can be determined [8, 9]. Figure 3.8 shows the preferred experimental arrangement for the ASTM-IEC or classical resistance method that is valid in the range of $10^5<?<10^{19}$ O- m [2, 5]. An adjustable high voltage is applied to one sample electrode. Current flow to a sample electrode held at ground is measured by a Pico-ammeter. The grounded guard ring serves to help define the volume of the material in which the measured current flows. The guard ring also helps to establish simple parallel electric field lines of uniform length where the measured current is flowing. The measured current flows in straight lines through the thickness of the sample and within an area, A_{eff}, slightly larger than the metal electrode area. The resistance of the sample is then given by $R = rd / A_{eff}$, where ρ is the resistivity (O-m), A_{eff} is the effective area (m^2) of the metal electrode and d (m) is the sample thickness. The resistance R is determined simply from the current and from the applied voltage using Ohm's law. The guard ring, therefore, brings the mathematical model into "similarity" with the actual process of current flow in the sample [2].

Classical resistivity measurements can vary appreciably—from factors of two to two orders of magnitude—due to variations in sample environments and test conditions [8]. Most reported ? values are derived from measurements made at ambient temperature and relative humidity, which is not representative of the wide temperature range and vacuum conditions in which space hardware operates.

Temperature variations can often be described as Arrhenius behavior of the form $r = r_o \exp[E_A / k_B T]$, where ?o is a material parameter and E_A is an activation energy characteristic of a particular energy absorption process. Resistivity also changes appreciably—often orders of magnitude—with relative humidity or moisture content, particularly for thin film samples. Both ambient humidity and drying during sample conditioning need to be considered [8]. For example, resistivity has been shown to vary with time to the ½ power, as water diffused into or out of the sample [24]. Up to two orders of magnitude increase in ? have been observed during vacuum pump down of polymer films [24]. Further, dielectric resistivity often depends on duration and magnitude of the applied sample voltage. The observed decrease in current with time is due primarily to dielectric absorption (*e.g.,* interfacial polarization, volume charge, rearrangement of dipoles on the molecular level, etc.,) and ion migration into the electrodes; it usually has the form $I(t)=At^{-m}$, where $0<m<1$.

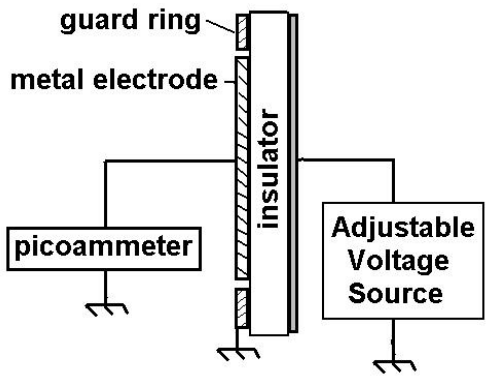

Fig. 3.8. Preferred sample design for ASTM-IEC method for measuring resistivity of thin insulators.

Excessive voltage produces high internal electric fields, resulting in breakdown of the insulator when the dielectric strength is exceeded (typically, when the field exceeds 10^7 V/m) [10]. Sample impurities or surface contamination are known to substantially affect bulk resistivity and surface resistivity, respectively. Given the substantial variability in resistivity from these factors, it is essential that the sample preparation, conditioning history, and environment be well characterized and controlled for such measurements.

2) Description of the Capacitive Resistance Apparatus: The capacitive resistance apparatus (CRA) at USU is designed as a more versatile instrument for classical resistance measurements under more tightly controlled conditions (see fig. 3.8). The sample environment—including sample temperature, ambient vacuum or background gas, and humidity—can be strictly controlled. Computer automation of voltage and current measurements, together with environmental parameters, allow rapid and prolonged resistance measurements. Thus, the apparatus is capable of parametric studies of variables that influence the resistivity, including sample material and thickness, applied voltage magnitude and duration, sample temperature, ambient gas or vacuum, and humidity.

Two independent thin film insulator samples of up to ~1 mm thick can be mounted in the apparatus simultaneously; these are stretched over an electrically and thermally isolated Cu high voltage electrode and held smoothly in place with two polycarbonate sample clamps each. An adjustable voltage is applied using either a 0 to ±110 VDC, a 0 to 1 keV, or a 0 V to ±50 keV computer-controlled power supply, depending on the range required. Wiring to the high voltage electrode uses corona-free high voltage Teflon-

insulated wire to a standard 15 kV coaxial SHV vacuum feedthrough. Current flow through the samples to two independent sample inner electrodes held at ground is measured by a dual channel pico-ammeter [10]. The unit is also designed to measure the punch through voltage of thin insulating films, by monitoring current across the sample while applying up to ±15 keV across the sample electrodes [5]. Figure 3.9 shows the capacitive resistance apparatus showing the electrodes and the guard rings with the base plate that will be grounded.

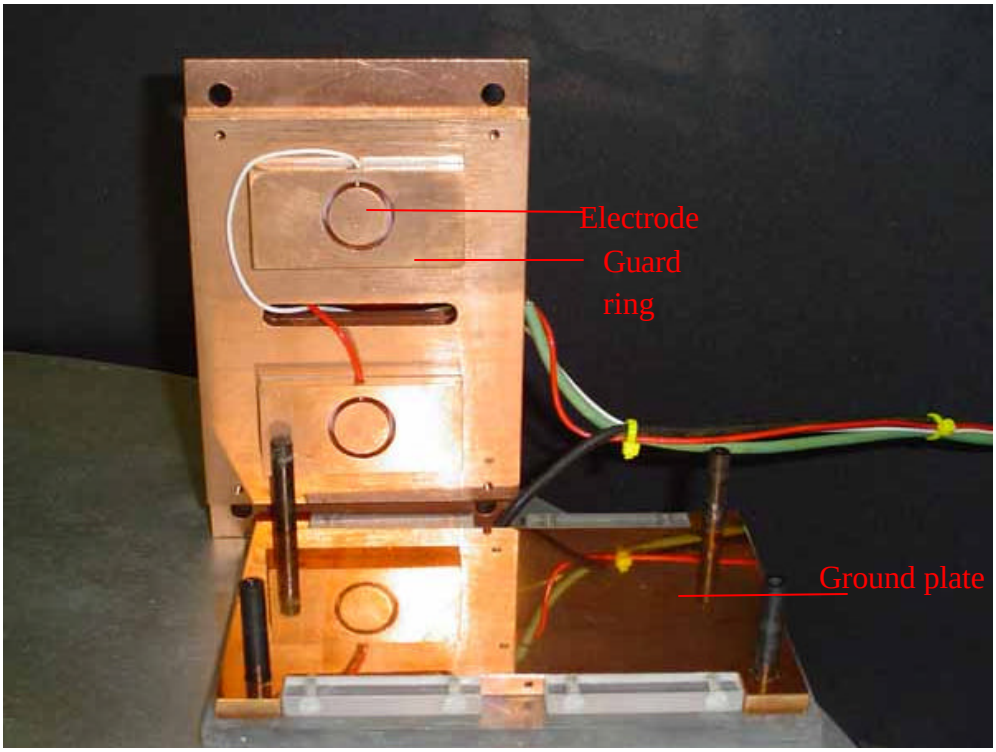

Fig. 3.9. The capacitive resistance apparatus.

The unit is designed to control the temperature of the electrodes and the sandwiched samples to ~ ±2 °C using a standard PID temperature controller and platinum resistance thermometers. Two 70 W thermoelectric Peltier cooling units are mounted above the sample electrodes. In cooling mode, the Peltier coolers are designed to cool the sample to –100 °C and exhaust excess heat via a copper braid to an external heat sink through a O-ring-sealed compression port. In heating mode, the Peltier coolers are run with reverse voltage, drawing heat from the external heat sink. In this mode, the unit is designed to heat the electrodes up to +100°C [2]. Figure 3.10 (a-b) show data obtained at USU using the classical resistance method following the ASTM D 257-99 standard method [8] for Sheldahl thermal control blanket material at 26±2 °C in ambient room light at 30±5% ambient relative humidity with wet electrodes for a range of voltages. The curves showed linear behavior on a log-log plot with a slope of ~½ and converged to ~ (3±1) x10^{+14} O-m at ~½ hr. The published resistivity value for Dupont Kapton HN is 1x10^{14} O-m.

The CRA aluminum-walled vacuum chamber is pumped with the same system used for the charge storage chamber (see section II.B.1). Vacuum connections between to the CRA chamber are made using standard Quick Connect and Conflat^{TM} fittings. The CRA vacuum chamber is also connected to a stainless steel gas handling system to allow control of the ambient gas environment composition and pressure; pressure is monitored by a standard vacuum thermocouple gauge (1 atm to 1 mTorr), a capacitance manometer (100 to 0.1 Torr), and a high pressure Si strain gauge transducer [10^{+6} to 10^{0} Torr]. Figure 3.11 (a) shows a photograph of the vacuum chamber. The CRA has been designed in such a way that there is an easy access to the plates between which the samples are held.

The sliding mechanism is shown in Figure 3.11(b). The results produced by this apparatus will be used for comparison of the data obtained from the charge storage system.

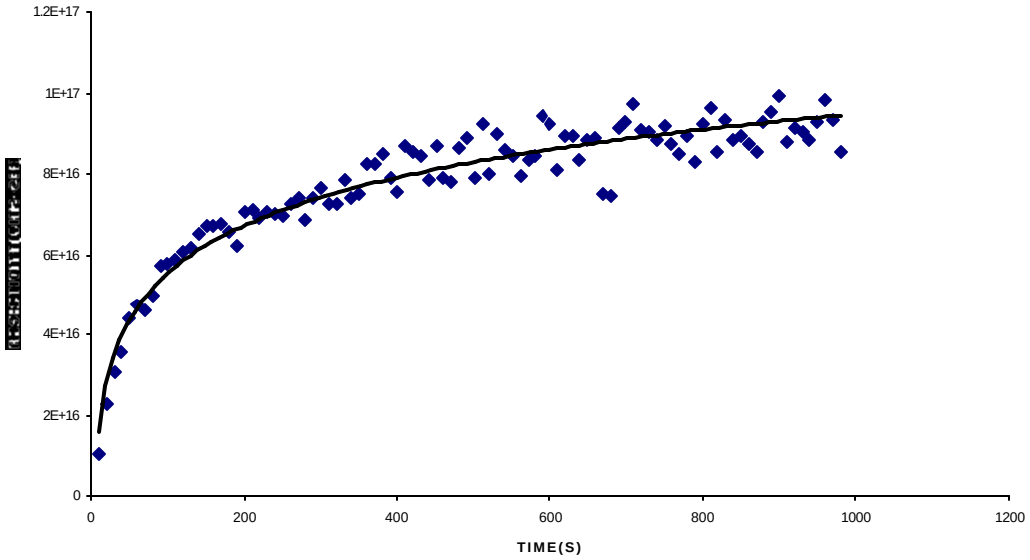

(a)

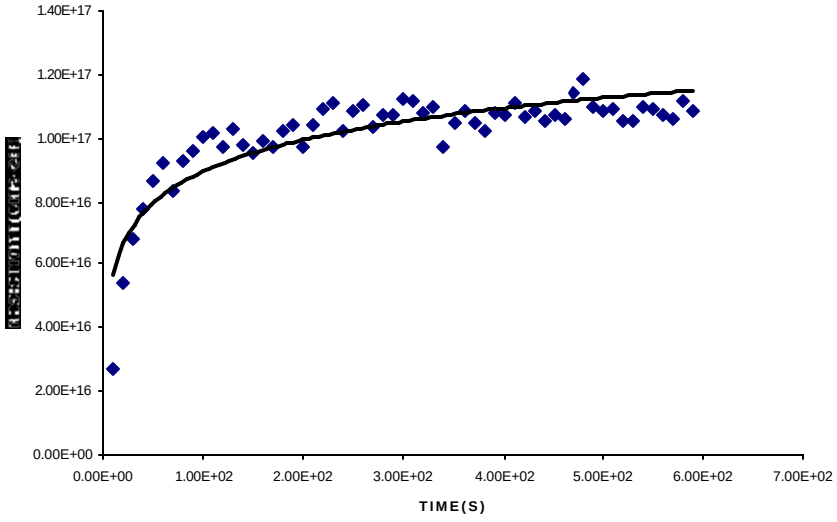

(b)

Fig. 3.10. Plots showing resistivity values obtained for a Kapton sample from the capacitive resistance apparatus for (a) 400 volts (b) 500 volts.

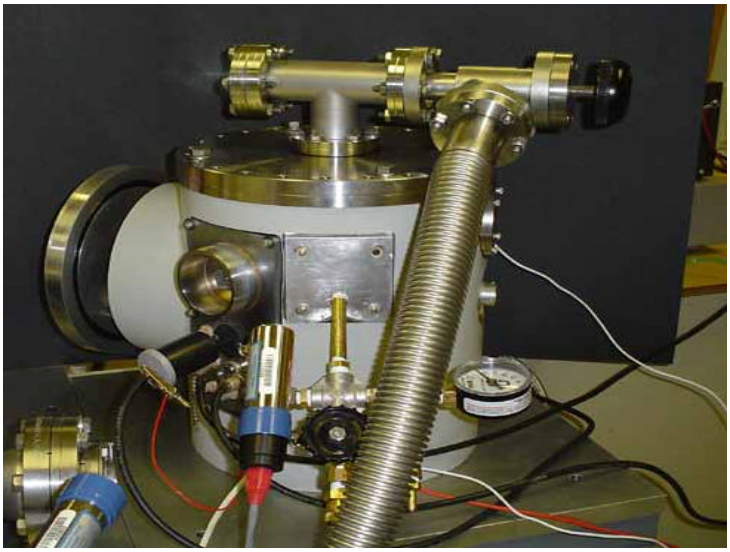

(a)

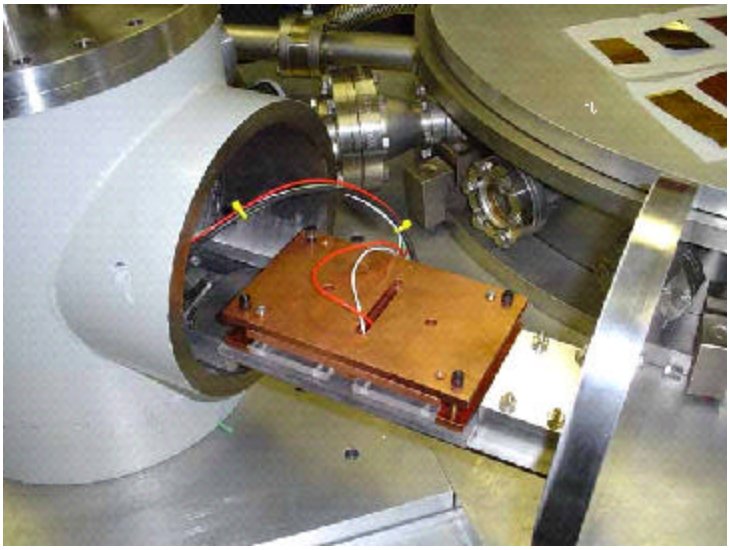

(b)

Fig. 3.11. (a) CRA vacuum chamber (b) Sliding mechanism providing easy access to the plate holding the samples.

C. Gas Handling System

The space environment contains different types of gases which have varied effects on the resistivity of the insulators aboard the spacecraft. In order to accurately characterize and document this behavior a system called as the *gas handling system* (GHS) has been developed at USU which is attached to the vacuum chamber to dose the samples with accurate amounts of gas. It can be used to administer a single dose of gas to a system or to do isotherms, which require many doses administered sequentially. This section provides an overview of the system and its capabilities. The gas handling system has also been automated using the LabVIEW. Figure 3.12 shows the photograph of front view of the gas handling system.

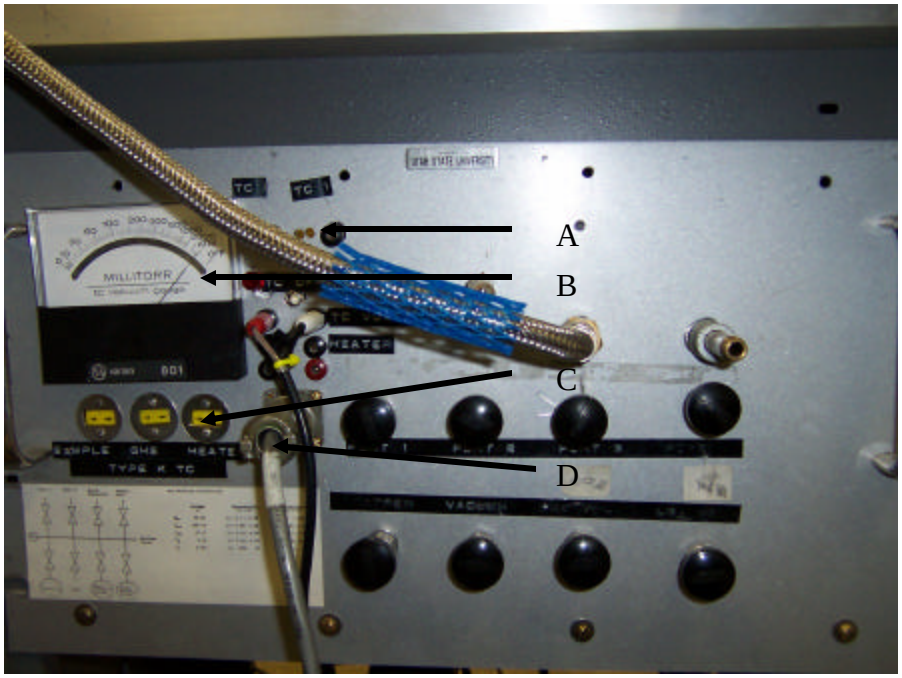

Fig. 3.12. Front view of the gas handling system.
A) represents the thermocouple output voltages monitored by the computer B) millitorr range vacuum gauge (Varian model 801) C) RTDs D) MKS Absolute pressure gauge input (Baratron model 122A).

GHS is mainly built from the 0.3 cm NPT stainless steel pipe fittings. Figure 3.13 shows the rear view of the system. The GHS has two pressure gauges one is an absolute pressure gauge and the sec second is a differential pressure gauge(C and D in fig. 3.13).There is standard cylinder of known volume to hold the required gas (A in fig. 3.13). The entire system is enclosed in a foam box for temperature stability (F in fig. 3.9).The temperature control for the system is achieved by an Omega temperature controller (Model CN9000). This interfaces with two heaters and a thermistor. The temperature controller delivers the current to the heaters proportional to the resistance of the thermistor and tries to achieve and maintain a constant temperature. The temperature can be set by entering the temperature in the digital display the controller has. The temperature controller was shown in fig. 2.11.

Fig. 3.13. Rear view of the gas handling system.
A) standard volume cylinders for holding gas B) heat sink C) Baratron absolute pressure gauge D) MKS differential pressure gauge E) RTDs F) foam box for temperature stability.

D. Sample Selection

The charge storage method of calculating the resistivity has to be tested on different samples that are likely to be flown in severe electron environments. The resistivity values and the corresponding decay time predictions need to confirmed. There is a wide range of samples on which the resistivity measurements are currently being performed so that a good resistivity database can be set up. Four specific sample sets have been identified and will constitute the majority of the samples selected for testing in this project. These are:

1. Samples from the *Europa Orbiter*. The most critical materials have been chosen from that list, and a testing program for these is being pursued for the data itself, and as a training process for USU personnel.
2. CRRES/IDM flight spares samples. The original CRRES/IDM flight spares samples are available for testing. It is possible to compare the resistivity measurements performed in this project with actual in-space results for the CRRES/IDM materials.
3. USU/SEE Materials Database. Tests are ongoing with insulating thin-film spacecraft materials samples that have been included in the USU Materials Database of Electronic Properties in the SEE Charge Collector Knowledgebase. These include Polyimide (PI) on Aluminum (Al), Polyethylene Terephthalate (PET) on Al, Fluoro ethylene propylene (FEP) on Al, PI on Ag/Inconnel, Anodized Al (Cr), Anodized Al (S), and Room Temperature Vulcanized (RTV) Silicone on Cu.

4. Sheldahl Technical Materials Samples. A large sample set of thin film insulator spacecraft materials from Clare Sokup, Applications Engineer at Sheldahl Technical Materials. Specifically, this large sample set will allow us to test various insulating materials, thickness of insulating materials, and conductor backing material.

Table IV shows the initial sample set for the USU chamber. A 25 μm thick thin film Kapton sample with aluminum vapor deposited on the back (Sheldahl Materials # G405110) will be used for initial measurements. This test matrix will provide initial analysis for the effects of the following parameters:

- Reproducibility of results—Four similar identical samples (4,5,6,7), duplicates of 9 other materials (15-23 and 24-32).
- Insulator thickness – Six different thickness of PI on Al (4-12).
- Insulator type – Four common insulators (PI, PET, FEP, SiO_x) and seven additional spacecraft materials.
- Conductor type – Al, Au and Inconnel/Ag on PI.
- Initial charge deposition – Large (4, 5) and small (6, 7) charge deposition on identical samples.

TABLE IV

SAMPLE MATRIX TESTED AT USU IN THE CHARGE STORAGE CHAMBER

Sample Position	Material	Material Properties
1	Blank electrode	
2	Faraday Cup	
3	Optical Photocell	
4*	Single sided Al on PI	~1000 Å Al on 1.0 mil PI, large charge
5*	Single sided Al on PI	~1000 Å Al on 1.0 mil PI, large charge
6*	Single sided Al on PI	~1000 Å Al on 1.0 mil PI, small charge
7*	Single sided Al on PI	~1000 Å Al on 1.0 mil PI, small charge
8	Single sided Al on PI	~1000 Å Al on 0.3 mil PI
9	Single sided Al on PI	~1000 Å Al on 2 mil PI
10	Single sided Al on PI	~1000 Å Al on 5 mil PI
11	Single sided Al on PI	~1000 Å Al on 10 mil PI
12*	Thick PI	~250 µm
13	Single sided Au on PI	~900 Å Au on 0.3 mil PI
14	Single sided Au on PI	~900 Å Au on 5.0 mil PI
15*	Inconnel/Ag on PI	~275 Å Inconnel on ~1500 Å Ag on PI
16	Nova Clad G2300	17 µm Cu on 50 µm PI
17	Silicone PSA on PI on Au	1 mil Silicone PSA on 1 mil PI on ~900 Å Au
18	966 Acrylic PSA on PI on Au	966 Acrylic PSA on 1 mil PI on ~900 Å Au
19	Atomic Oxygen Resistant PI	AOR on PI on AOR
20*	Single sided Al on PET	~1000 Å Al on 1.0 mil PET
21*	Single sided Al on FEP	~1000 Å Al on 5.0 mil FEP
22*	DC93-500 RTV on Cu	~25 µm DC93-500 on thick Cu
23*	CV-1147 RTV on Cu	~25 µm CV-1147 on thick Cu
24*	Inconnel/Ag on PI	~275 Å Inconnel on ~1500 Å Ag on PI
25	Nova Clad G2300	17 µm Cu on 50 µm PI
26	Silicone PSA on PI on Au	1 mil Silicone PSA on 1 mil PI on ~900
27	966 Acrylic PSA on PI on Au	966 Acrylic PSA on 1 mil PI on ~900 Å Au
28	Atomic Oxygen Resistant PI	AOR on PI on AOR
29*	Single sided Al on PET	~1000 Å Al on 1.0 mil PET
30*	Single sided Al on FEP	~1000 Å Al on 5.0 mil FEP
31*	DC93-500 RTV on Cu	~25 µm DC93-500 on thick Cu
32*	CV-1147 RTV on Cu	~25 µm CV-1147 on thick Cu

PET-Polyethylene Terephthalate *Sample tested in USU/SEE Materials Testing
PI – Polyimide (Example: Kapton) FEP- Fluoro ethylene propylene (Example: Teflon)

CHAPTER IV

RESULTS, FUTURE WORK AND CONCLUSIONS

The previous chapters detailed the necessity to characterize the resistivity of insulators used for the spacecraft applications and described the instrumentation that was built at USU to measure the insulator resistivity under typical space environments. It also etched out the requirements of the instrumentation and calibration of various instruments. This chapter reports on the resistivity values obtained from the samples placed inside the system developed and the how those values compare with values obtained with the classical method [8, 9]. It also contains a section on the analysis of the results obtained and the improvements that could be carried out further with the system, so that one could precisely characterize the spacecraft insulators and to an extent predict the anomalies that could occur because of the spacecraft charging.

A. Measurement of Surface Voltage Decay

As mentioned in section II.B.3, a custom made electron gun was used for charging the samples. The sample that was chosen for the measurement using charge storage, was a Kapton sample 5 mil thick with aluminum conductor backing. The procedure for charging and measuring the surface voltage of the samples is given in fig. 4.1. The insulated surface of the sample faces the electron source or the field probe. The other surface of the sample is metalized (aluminum backing in this case) and connected to wiring so that it can be biased relative to ground, and relative to the electron source, or monitored for currents. With a hot tungsten filament in front of the sample, and by slowly raising the voltage source, one gently charges the sample.

The probe is initially calibrated in front of the ground reference before the surface voltage is read from the sample. Imagine that the sample is a perfect insulator. If the charging voltage at the back of the sample is set to, say, +100 volts the field probe will measure "100-volts" (in the ideal case, with the conversion factor being 1). The sample is then moved in front of the electron gun. One then turns on the filament and the electrons emitted by the filament travel to the surface of the sample and "ground" the surface of the insulating sample. This establishes 100 volts across the sample. The filament is then turned off and 100 volts remains across the sample. The sample may then be moved to face the field probe and confirm the fact that the sample surface is grounded by measuring 0 volts.

One then grounds the rear electrode of the sample and instantly the field probe should register –100 volts as the surface voltage on the insulating sample. If the sample is leaky, the –100 volts decays through the sample bulk and into the ground wire, and its decay time constant is measured. And as mentioned earlier, the resistivity of the sample is determined from its decay time constant, t = ?e=RC.

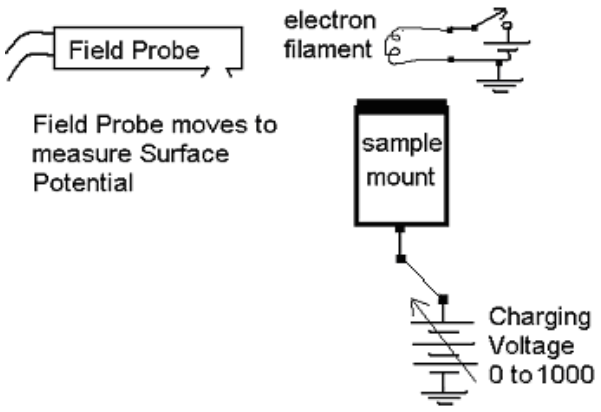

Fig. 4.1. Apparatus for measuring surface potential of the sample surface in vacuum.

The 5 mil Kapton sample was charged with low energy electrons, 50-500 eV. This was accomplished by biasing the rear copper electrodes at +500 volts and lighting the electron-emitting filament in the vacuum spaced about 10 cm from the sample's front faces. One needs to make sure that the electrons are just placed or “dusted” on the surface. The procedure that is followed is to have the rear electrode charged in steps of 40-50V until 500V is reached. At each and every step of potential increase on the rear electrode, one needs to make sure that the field probe continues to read zero. The surface of the sample is thereby charged to approximately minus 500 volts relative to the copper electrodes on the rear faces of the samples.

Five hundred volts was chosen for a good reason. Generally, conductivity in dielectrics increases and resistivity decreases with increasing electric field strength. Five hundred volts is close to the maximum electric field that can safely be placed on this material for many years without generating partial discharges that could harm sensitive electronics [1].

B. Results

The potentials of the sample surface were periodically monitored for a period of about a week at room temperature. Initially there was a steep decline of surface voltage, on the Kapton sample during the first day itself. The early decay is shown in fig. 4.2. This initial decline in the surface voltage can be attributed to the polarization [10] of the molecules in the dielectric. Hence this initial decay in the surface voltage cannot be taken as the leakage that corresponds to the resistivity of the sample. It is important to note here that the ASTM methods measure decay with 10 minutes of bias application.

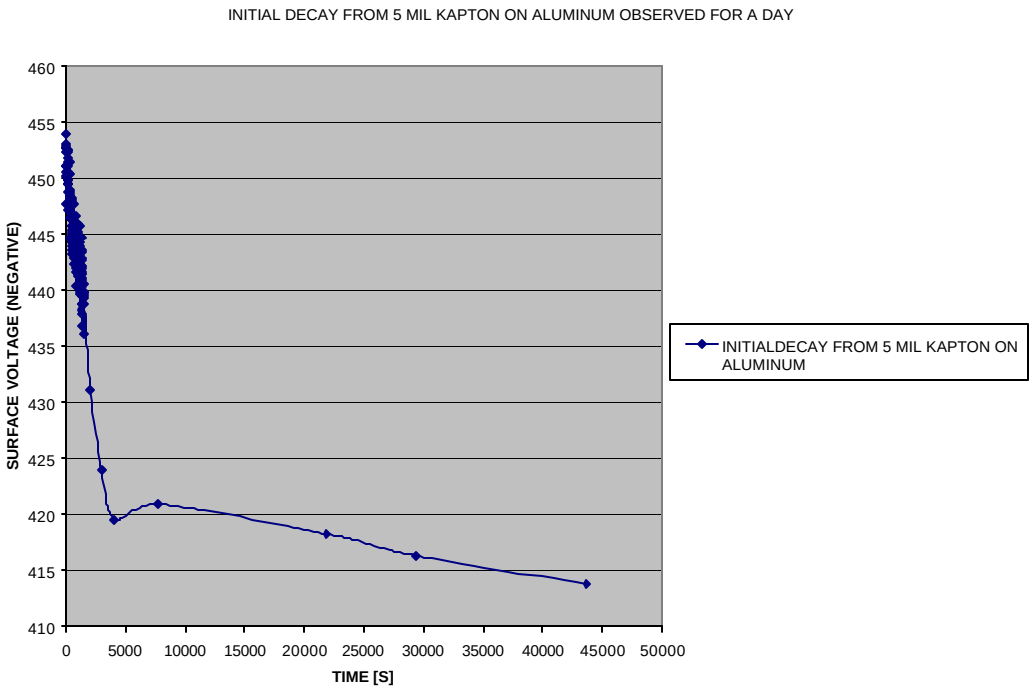

Fig. 4.2. Plot showing the initial surface voltage decay observed for a day.

One can also notice that though the leakage current is substantial at ten minutes (600 seconds) it is significantly reduced after a few hours time. This confirms the notion that the decay measured through the classical methods is because of the polarization current rather than the actual resistivity. The current associated with an increasing polarization cannot proceed forever. Hence it is imperative to wait until we get the decay due resistivity. After some time, all of the polar molecules would have transitioned to full polarization and additional polarization will not occur. Similarly, injection of ions may slow if they become trapped near the electrodes and "repel" further injection. Electron and hole injection may slow down as the junction field is developed under conditions of slow trapping build-up [10]. The classical method performed over very long time-duration finds that the current decays well beyond that at the classical time duration of 10

minutes. Figure 4.3 shows the surface voltage decay for the Kapton sample for a period of 1 week at room temperature.

From the plot in fig. 4.3 one could see that the surface voltage has a steep decline initially, followed by a slow decay period before settling on a resistivity curve. This is the curve that is used for the evaluation of the resistivity. The calculation of the resistivity and the value obtained are given in the following section.

Assume that the sample is a simple uniform parallel-plate leaky capacitor. Apply a voltage, Vo, until time t=0.

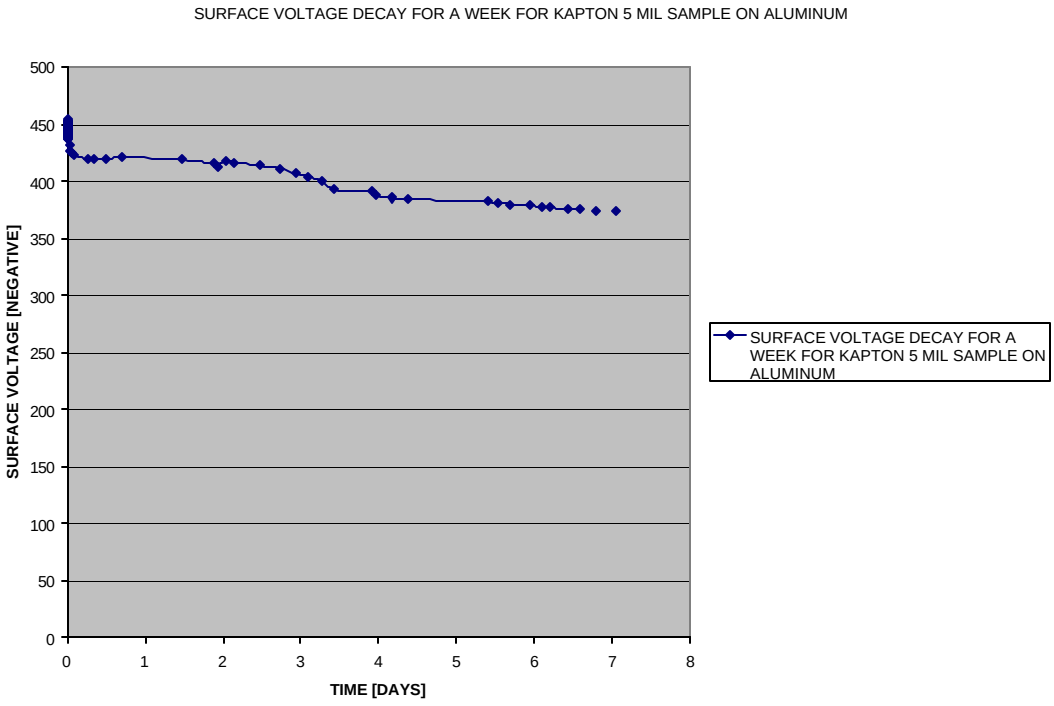

Fig. 4.3. Plot showing the surface voltage decay observed for a period of one week.

At t=0 disconnect the voltage source from the capacitor so that the following function holds.

$$V = Vo \exp [-t/\rho\varepsilon] \quad (4.1)$$

where ρ is the resistivity of the sample material, ε is its permittivity.

For small $-t/\rho\varepsilon$, $\exp [-t/\rho\varepsilon] = 1 - t/\rho\varepsilon$.Our experiments always deal in the regime where $t << \rho\varepsilon$ and the decay is only a small percentage of the initial surface voltage.

$$dV/dt = [-1/\rho\varepsilon] Vo \exp [-t/\rho\varepsilon] \quad (4.2)$$

Then $(1/Vo)(dV/dt) = (-1/\rho\varepsilon) \exp[-t/\rho\varepsilon] = (-1/\rho\varepsilon) [1 - t/\rho\varepsilon]$. Note that this function is very nearly equal to $(-1/\rho\varepsilon)$.

Therefore,

$$\rho = -1/ [\varepsilon (1/Vo) (dV/dt)] \quad (4.3)$$

Thus a tabulation of (1/Vo) (dV/dt) provides the simplest evaluation of the resistivity, ρ of the insulator sample. The dielectric permittivity, ε for the polyimide sample used here is taken to be a constant approximately equal to 3.09×10^{-11} F/ m. Here the initial voltage, Vo, is the voltage at which the resistivity curve begins. Figure 4.4 shows the evaluation of the slope dV/dt from the resistivity curve. From the plot the slope of the curve is $-6x10^{-05}$ V/sec. The initial voltage at which the resistivity curve begins is 391.15 V.

Figure 4.5 shows a plot indicating that the resistivity continues to increase after the initial charge on the sample.

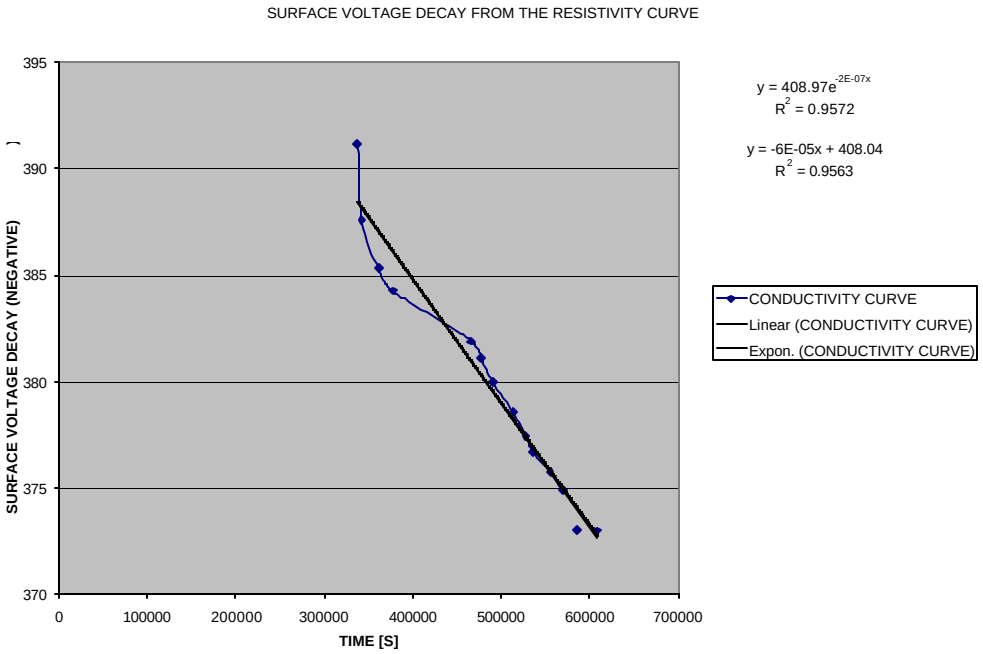

Fig. 4.4. Plot showing the resistivity curve for the Kapton sample.

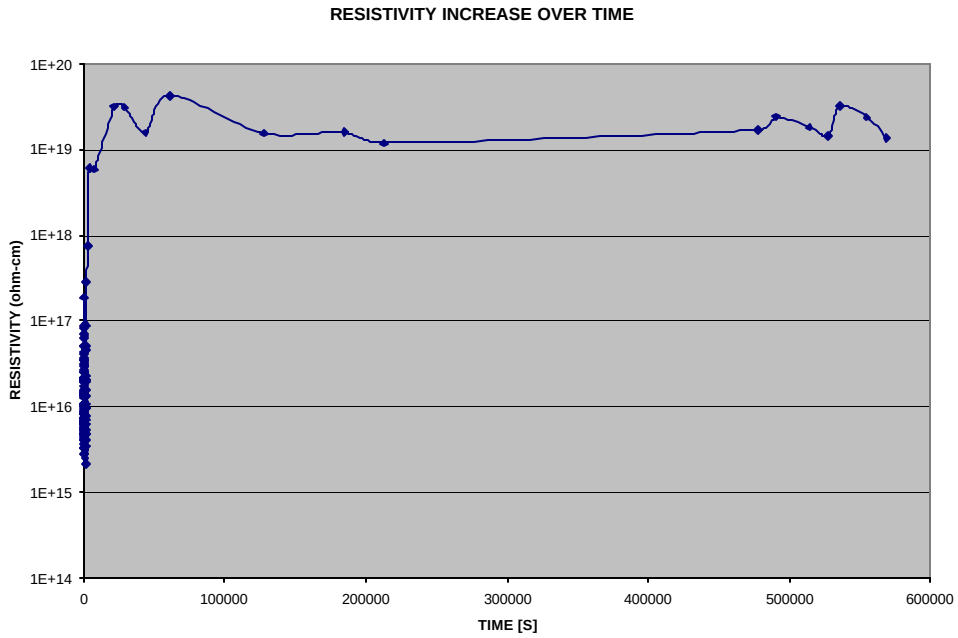

Fig. 4.5. Plot showing the increase in the resistivity value over time after initial charge deposition.

One could also calculate the resistivity value by fitting an exponential trend line to the curve and equating that to equation 4.1. By calculating the resistivity value using equation 4.3 we get 2.1097 x 10^{17} O-m which is a value which is at least 10^3 larger than the resistivity values given in the classical method. This in turn increases the relaxation time by the same amount, which would make a big difference in the prediction of pulses when the sample is placed in the space environment. This value is similar to what was obtained at JPL when similar charge storage test was performed on the same sample.

C. Future Work

The future work of the project can be divided into two categories. First would be to upgrade the instrumentation that is already present. Second would be to improve upon the existing methodology by performing several tests on different samples.

1) Instrumentation Upgrades: The most important portion of the upgrade is to assemble various instruments into the existing system. The devices for temperature control of the system needs to be plugged in the chamber along with the instruments for monitoring humidity variations inside the chamber. The automation of the electron gun and electron gun controller has to be completed in the future.

2) Improvements on Experimentation: The resistivity and decay curves need to be done for a large number of samples to confirm reliability and reproducibility. Dielectric resistivity measurements with longer test runs should be done. The resistivity values have to be documented for future references for modeling spacecraft. The dependence of resistivity with variations in parameters like temperature, humidity, initial charge, conductor backing, sample thickness, etc., have to be addressed. The effect of space environment contaminants on the dielectrics is an area of research one can use this

measurement technique. One can analyze the variations in dielectric resistivity, breakdown voltage and interaction with plasma based on the kind of contaminant one has on the surface of the dielectric and how thick the contaminant is. It is also important to study if the surface voltage measurement proposed in the thesis would still hold good for thick contaminants. It is also possible to know if the contaminant is conducting or non-conducting from the kind of decay curves that we get.

It might also be interesting to study the degradation in measurements due to the presence of some physical defects on the surface of the dielectric. Depending on the results we get it might also be possible to predict the kind of interactions the plasma would have with the dielectric and also if there could be discharges within the sample surfaces if the defects are large enough. These interactions can be studied with scribe lines equally spaced, in a tic-tac-toe format, etc., on the surface of the sample.

D. Conclusions

It is important that the resistivity measurements for dielectrics used for spacecraft applications are tested in conditions similar to those, which these materials are exposed to in space. But the classical methods are performed in atmospheric conditions with a set up that does not replicate the charging phenomenon in space. The classical method was repeated at USU and the resistivity values were found to be $3x\ 10^{14}$ O-m which is at least 10^3 smaller than the value obtained by the charge storage method. The classical resistivity values have been imported from the ASTM/IEC [8, 9] handbooks thus far and hence lead to poor prediction of decay times as the resistivity values are not correct. At USU tests have been performed to measure the resistivity by the charge storage method which emulates the space environment by developing the instrumentation and charging the

samples in the same way as dielectrics exposed to plasma are charged. The tests have also shown the resistivity continues to increase even for a couple of days after charging the sample. This is the typical scenario that takes place in the space environment. The classical methods do not take this into consideration. Hence the charge storage method is a better way to characterize the resistivity of the spacecraft insulators and the calculation of the decay time would enable us to predict the discharge pulses. This would be a significant step forward in modeling the future spacecrafts, especially in knowing which insulators could be used in the orbits. There is a definite need for a database of resistivity values of spacecraft insulators so that modeling of spacecrafts become more accurate.

There were several key features that were reported in this thesis. They can be summarized as follows:

1.) Classical methods for the measurement of resistivity of spacecraft dielectrics fail to take a few factors into consideration like the conditions of testing, method of charging the dielectrics, decay of the charge and duration of measurement. These factors play a very vital role in deciding the resistivity value.

2.) A new method was introduced which would have only one surface of the dielectric exposed and charged without any surface contact. The surface charge decay from the sample is monitored and this decay is used in the calculation of resistivity.

3.) A different way of surface voltage monitoring and transferring from the sample surface to the capacitance probe was discussed. This method has several inherent advantages. Here the high voltage capacitance probe is not placed

inside the vacuum as is the case with earlier research works [17]. Instead a new mechanism was built to transfer surface voltage to the probe placed in atmosphere, so that in case of repairs, one can work on the probe without breaking vacuum. Moreover it also avoids the possibility of stray charges driving the probe off-scale.

4.) Proper guidelines need to be set before instrumentation is developed for the measurement of resistivity to make sure we emulate space conditions.

5.) Resistivity values obtained by the new charge storage method are at least 10^2 to 10^4 times higher than those obtained by classical methods. This huge difference in turn affects the calculation of relaxation time which is extremely critical in the prediction of discharges. Also the resistivity value continues to increase even after a day since the initial charge.

REFERENCES

[1] A. R. Frederickson, C. E. Benson, and J. F. Bockman, "Measurement of Charge Storage and Leakage in Polyimides," *Nuclear Instruments and Methods in Physics Research Section B: Beam Interactions with Materials and Atoms*, vol. 208, no. 7, pp. 454-460, Aug. 2003.

[2] Prasanna Swaminathan, A. R. Frederickson, J. R. Dennison, Alec Sim, Jerilyn Brunson, and Eric Crapo, "Comparison of Classical and Charge Storage Methods for Determining Conductivity of Thin Film Insulators," *8th Spacecraft Charging Technology Conference*, Oct. 2003.

[3] K. E. Holbert, Spacecraft Charging Tutorial. [Online]. Available: http://www.eas.asu.edu/~holbert/eee460/spc-chrg.html. Sep. 2003.

[4] H. B.Garrett, "The charging of spacecraft surfaces," Reviews of Geophysics and Space Physics, vol. 19, no. 4, pp. 577-616, Nov. 1981.

[5] J. R. Dennison, A. R. Frederickson, and Prasanna Swaminathan, "Charge storage, conductivity and charge profiles of insulators as related to spacecraft charging," *8th Spacecraft Charging Technology Conference*, Oct. 2003.

[6] J. P. Estienne, *Space Environment and EMC/ESD Phenomena*, *The Behaviour of Systems in the Space Environment*, 1st ed. Boston: Kluwer Academic Publishers, 1993, pp. 513-564.

[7] M. Romero and L. Levy, *Internal Charging and Secondary Effects, The Behaviour of Systems in the Space Environment*, 1st ed. Boston: Kluwer Academic Publishers, 1993, pp. 565-580.

[8] ASTM D-257-91, "Standard test methods for DC resistance or conductance of insulating materials," Feb. 1991.

[9] IEC-93, "Methods of test for volume resistivity and surface resistivity of solid electrical insulating materials," Mar. 1980.

[10] A. R. Frederickson and J. R. Dennison, "Measurement of conductivity and charge storage in insulators related to spacecraft charging ," *IEEE Trans. Nuclear Sciences*, vol. 50, no. 6, pp. 2284-2291, Dec. 2000.

[11] A. R. Frederickson and D. H. Brautigam, "Mining CRRES IDM pulse data and CRRES environmental data to improve spacecraft charging and discharging models and guidelines," Final Report, NASA SEE Program Contract no. NAS7-1407, To be published.

[12] A. R. Frederickson, "Radiation induced electrical current and voltage in dielectric structures," *Physical Sciences Research Papers*, no. 613, pp. 1-59, Nov. 1974.

[13] D. M. Taylor and T. J. Lewis, "Electrical conduction in polyethylene teraphthalate and polyethylene films," *Journal of Applied Physics*, vol. 4, no. 9, pp. 1346-1357, Sep. 1971.

[14] D. K. Das Gupta and K. Joyner, "On the nature of absorption currents in polyethylene terephthalate (PET)," *Journal of Applied Physics*, vol. 9, no. 5, pp. 829-840, Apr. 1976.

[15] T. J. Sonnonstine and M. M. Perlman, "Surface potential decay in insulators with field-dependent mobility and injection efficiency," *Journal of Applied Physics*, vol. 46, no. 9, pp. 3975-3981, Sep. 1975.

[16] E. A. Baum, T. J. Lewis, and R. Toomer, "Decay of electrical charge on polyethylene films," *Journal of Applied Physics*, vol. 10, no. 4, pp. 487-497, Mar. 1977.

[17] L. Levy, D. Sarrail, and J. M. Siguier, "Conductivity and secondary electron emission properties of dielectrics as required by NASCAP," *Third European Symposium on Spacecraft Materials in Space Environment*, pp. 113-123.

[18] TReK, Inc., Operators Manual: Model 341A, High Voltage Electrostatic Voltmeter [Online]. Available: www.trekinc.com, Sep. 2002.

[19] R. Coelho, L. Levy, and D. Sarrail, "Charge decay measurements and injection in insulators," *Journal of Applied Physics*, vol. 22, no. 9, pp. 1406-1409, Sep. 1989.

[20] A. R. Frederickson, "Radiation induced voltage on spacecraft internal surfaces," *IEEE Trans. Nuclear Science*, vol. 40, no. 6, pp. 1547-1553, Dec. 1993.

[21] A. C. Whitlesey, A. R. Frederickson, and H. B. Garrett, "Comparing CRRES internal discharge monitor results with ground tests and published results," *7th Spacecraft Charging Technology Conference*, pp. 265-275, Apr. 2001.

[22] Maxim Integrated Products, DG 303A Data sheet. [Online]. Available: http://www.maxim-ic.com, July 2004.

[23] Clint D. Thomson, "*Measurements of Secondary Electron Emission Properties of Insulators,*" PhD. Dissertation, Utah State University, Logan, UT, 2004.

[24] J. M. Bodeau, private communications.

APPENDICES

APPENDIX I

LABVIEW DATA ACQUISITION DETAILS

LabVIEW is a graphical programming language that has been widely adopted throughout industry and academia for data acquisition, instrument control software and analysis software. The Charge Storage Chamber (CSC) has many types of equipment which requires deft and precise handling for long term usage. Most of the experiments performed in the CSC are done for a period of over a month. It is extremely difficult to consistently take data from these equipments and also monitor them for that period of time. Hence it was decided that an automated software controller be built using LabVIEW for monitoring the CSC. The objective of this appendix is to introduce the programming methodology followed in the design of the software for the CSC.

A. Features

There are a variety of equipments that are being monitored and controlled by the LabVIEW graphical program. The important features of the software written are as follows:

- Communication with serial, GPIB and Data Acquisition and Control (DAQ) interface connections, with configurable GPIB and DAQ addresses using a configure manager.
- The program has been written with an online control where the instruments can be controlled from anywhere in the network.

- A help menu has been created for easy understanding of the system control and acquisition.
- It provides pump-down control of the chamber and can also shut down by itself in case of any foreseeable problem.
- The system can be paused at any stage of the experiment allowing manual control of the experiments also.
- It has a front panel control of each equipment with indicators and buttons.
- Provides voltage profile management which lets the user to :
    a) Create a new voltage profile with variations in,
        - the time step (time interval between each data is sampled and reported)
        - voltage step (steps by which the voltage needs to increase or decrease)
        - range of voltages
        - multiple data lines for manipulation
    b) View the created profile
    c) Saving and retrieval of previous data profiles
- The complete programming control is being done by an Active-X interface.
- Data speed in the GPIB interface is limited by the return time of the instruments connected to it. The minimum step time for the currently connected equipments has been experimentally found to be approximately 10s.

B. Inputs to the LabVIEW Control

The control is being provided by the program through the National Instruments boards NI 6014, GPIB interface card (Axiom Model AS50999), RS 232 and USB ports. It is designed to acquire current data decaying from the samples, the voltages applied to the sample copper electrode and the pressure and the temperature of the chamber. The instruments attached to the NI board are the BERTAN ±1kV high voltage supply (Model 230-01R), Baratron absolute pressure gauge (MKS Model 122A), TReK^{TM} capacitance voltage meter (TReK^{TM} model 341A), temperature sensors like the RTDs, gas handling system (see Chapter III), other pressure sensors, the humidity sensor (Honey well model HIH-3610-001 environment condition sensor), etc., The RS 232 port is used to control the vacuum gauge controller (Stanford Research Systems IGC 100). The GPIB interface is used to control the 60V DC power supply (Agilent Model 3647A), the electrometer (Keithley Models 619), a ±100 VDC power supply (Keithley Model 237), a 6-digit multimeter (Keithley Model 196), an electrometer (Keithley Models 619) and the pico-ammeter (Keithley model 6485). The USB port is used to control and monitor the Intel PLAY QX3 computer microscope.

C. Programming

The LabVIEW code was written using the state machine architecture. The program flow is controlled by the inputs of the step time and the voltage steps. A simple state machine program representing the one developed for the CSC is provided below:

State A: Check if the values are entered

If (time > step time) then

voltage output = step voltage

next state

else wait

State B: If state A then

Read data

return

Load read data into a cluster array-continue the steps

State C: If the output voltage >= range provided by the user

Exit and save data in the Excel file

else State A

D. Operation Outline

The program developed is operated in the following phases:

1.) Initialization

2.) Data Profile Management

3.) System Configuration

4.) Start the Experiment from the Front Panel

1) Initialization: When the program starts there is a front panel display for the user. On clicking the initialize button from the panel it allows the user to enter information regarding the operator, type of samples used, and the environment of the experiment. The information entered is used to set-up a folder in which the data collected would be stored.

2) Data Profile Management: As mentioned earlier, the data profile lets the user choose the number of data points the samples is subjected to, the step time, range of voltages (start voltage and the end voltage). It also lets the user view the profile of the points entered.

3) System Configuration: System configuration provides a menu for choosing appropriate instruments for the experiments. The panel has been set-up in such a way that the instruments connected to the GPIB interface can be chosen from the drop down menus and the one connected to the DAQ boards are chosen by toggle buttons.

4) Start the Experiments from the Front Panel: Once the configuration of the instruments is done the control moves to the front panel again where the user can either start or exit the program. The LabVIEW front panel windows below show a step by step transfer of control from the front panel to various blocks before going back to proceed on to the front panel for data acquisition:

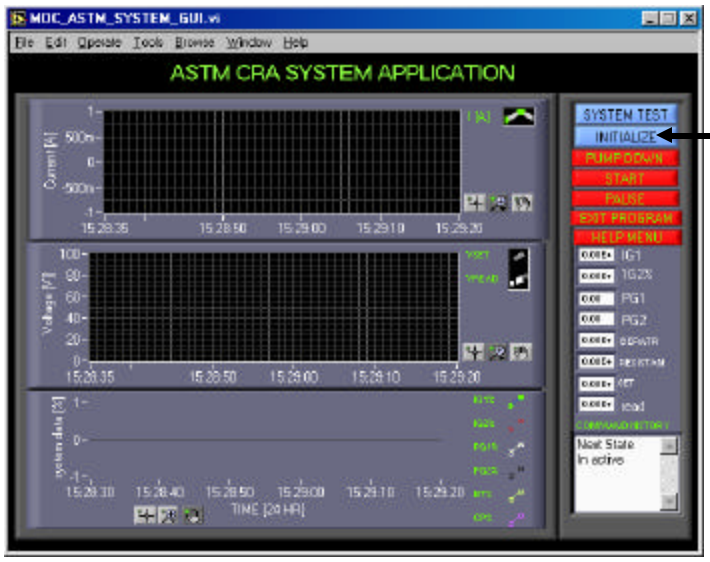

Step 1: Initialization, the arrow indicates the initialization button to get started in the front panel of system monitoring.

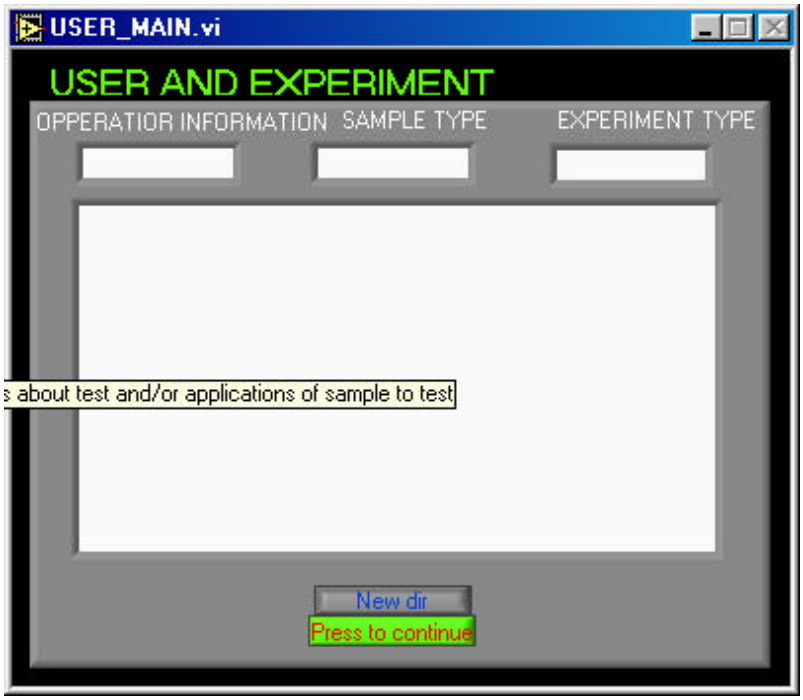

Step 2: Operator and experiment information. One can enter the notes regarding the type of environmental conditions, etc.,

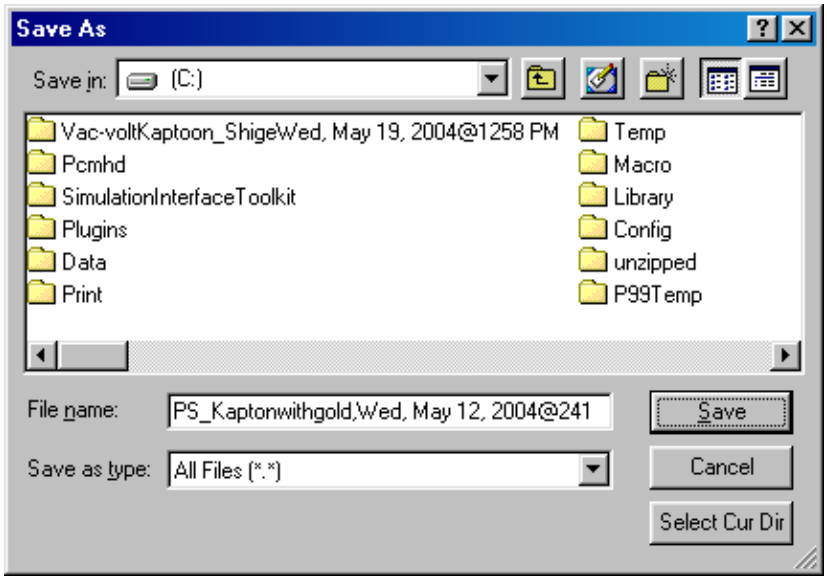

Step 3: Saving the data by creating folders exclusively based on the information entered by the user.

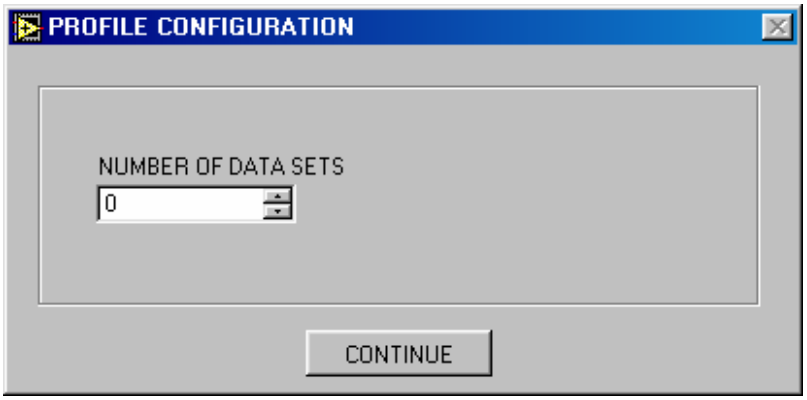

Step 4: Profile management, this window lets the user select the number of data lines that are to be processed.

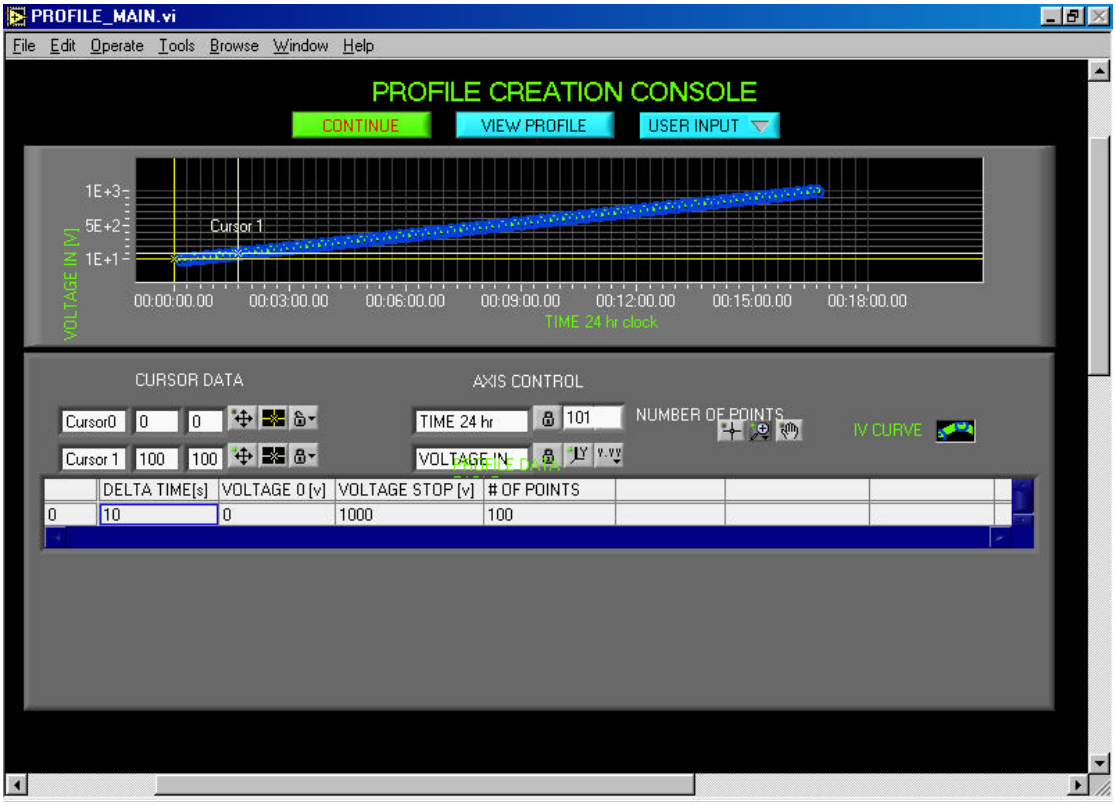

Step 5: Entering the delta times and the start and stop voltages with number of sample points.

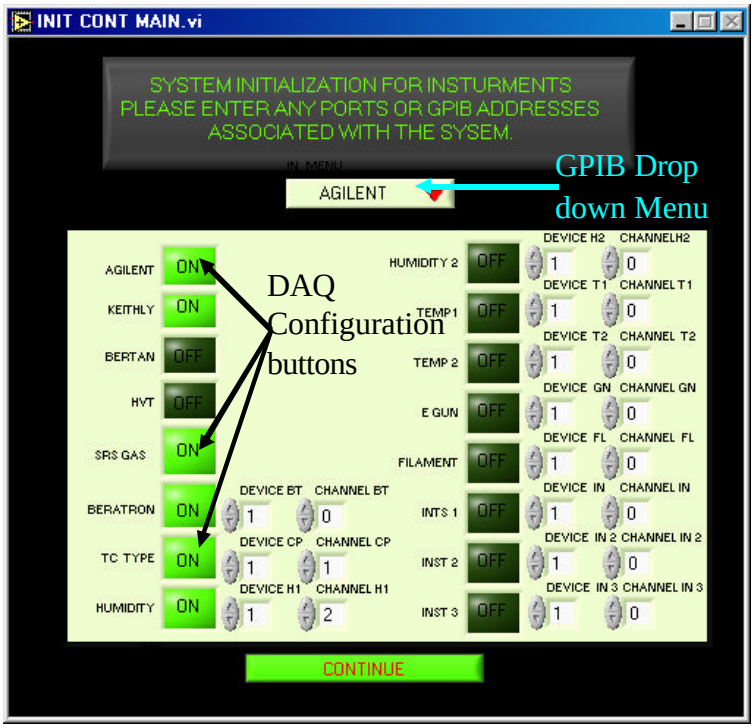

Step 6 : Choosing on the instruments that need to operate for the ongoing experiment.

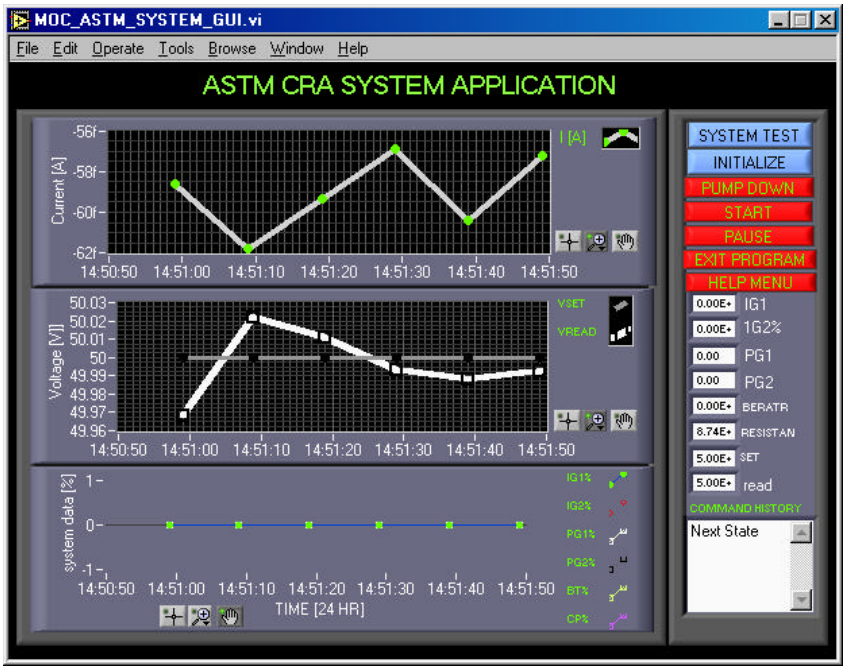

Step 7: Control transferred from the configuration menu to the front panel where user needs to press “Start “ to begin the experiment or “Exit program” to abort

APPENDIX II

CHARGE STORAGE SYSTEM AT JET PROPULSION LABORATORY

A. Experimental Setup of Charge Storage Method at JPL

The charge storage chamber at JPL is a sample handing system integrated into an existing vacuum chamber. At JPL the chamber provides the surface voltage measurements, and, in addition, provides energetic electron irradiations to samples that are large enough to simulate pulsed discharges by materials flown on spacecraft. This extra constraint causes the JPL chamber to differ from that at Utah State University (USU) [2]. The JPL samples will sometimes be as wide as 10 cm. Also, the vacuum space in front of the sample must be large enough to simulate the pulsed discharge phenomena that occur near insulator surfaces on spacecraft, constraining them to provide at least 10 cm of empty vacuum in front of the sample for pulsed discharges to propagate.

Figure 1.8 represented the arrangement of the vacuum chamber at JPL. Figure II.1 gives the detail of the entire charge storage set up at JPL.

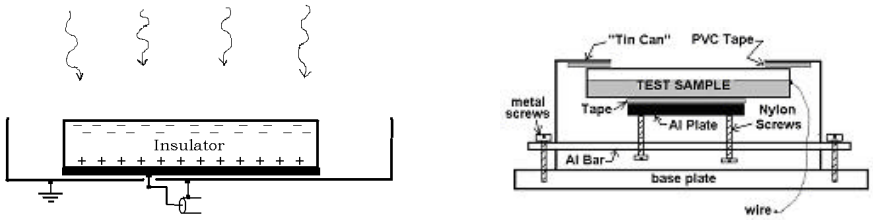

(a) (b)

Fig. II.1. JPL charge storage chamber design.
(a) Detail of sample mount for sample open to vacuum (b) Detail of the "tin can" sealed sample mount.

As was shown schematically in fig. 1.7, the chamber contains a broad-beam electron gun with accelerating potentials from 0 to 75 keV , a plasma source with bias capability, an electron-emitting filament, a light source, a sample surface voltage-sensing device, and temperature probes. The sample electrode can be attached to an oscilloscope, a current monitor, a voltage source or a voltmeter. The grounded grid across the center of the chamber prevents electric fields developed by the electron gun and the plasma source from affecting the sample.

1.) Sample Carousel and Sample Holder Design: The chamber at JPL is designed in such a way that there can be three to five samples in the JPL chamber. The fifth object is a Faraday plate in a can to measure beam current [2].A cross-sectional view of the sample holder is shown in the fig. II.1 (b). Different sensor plates, carousels and sample plates can be configured for different samples in the JPL design [see fig. II.2 (c)]. The sample mount assembly and the sample carousel are intended to avoid things that will charge up and try to provide electrical shielding for the probes and current sources as well as each sample. Note that electrons in the vacuum chamber can access only the exposed portion of the insulator surface and cannot get to the rear sample electrode at all. There are no insulating surfaces visible by line-of-sight from the sample surface that can accumulate charge and produce perturbing electric fields. Charge accumulation on the sample electrode can create a tangential field adjacent to the front insulator surface, making characterization of the surface voltage difficult. Stray charge accumulation on the sample electrode also interferes with measurement of the current to the front of the sample surface during sample charging. Further, the design allows for no sources of light visible from the sample surface that could charge or discharge the sample surface; this

requires a nearly light tight seal for each sample. Finally, RF signals emanating from the sample surface can get to the outside world only by coupling to the wire from the back of the sample [2]. If such a path exists, then the DC sample bias during charging will also cause charging on the polycarbonate and distort later field measurements. The tin can, the base plate and the PVC tape provide an "air-tight" enclosure protecting the sides and back of the sample from electrons in the vacuum. Additionally, the wire can be brought through the base plate as a shielded coaxial cable so that electrons in the vacuum cannot "connect" to the wire. Alternatively, the region below the base plate may be free of electrons. The PVC tape provides a soft surface for the insulator under test to press against. The Nylon screws compress the Al Plate and its insulating tape against the electrode of the sample, and press the sample against the PVC Tape [2]. When using this sample holder, one must be aware of the effects of the PVC tape and the close vicinity of the tin can to the charged sample surface. Specifically, one must consider: (a) the insulating strength of the PVC tape and the insulator sample, together, must withstand the voltage applied to the sample electrode at the rear of the sample; (b) the PVC tape must be thin enough that, even if it is charged, it does not contribute any charging signal to the TreK^{TM} probe; and (c) when the insulator is highly charged, the close proximity of the tin can may induce pulsed breakdowns at the edges of the sample.

2.) TreK^{TM} Probe Assembly: An electrostatic voltmeter [18] is used at both JPL and USU, that can sense surface voltages from –20 kV to +20 kV relative to local "ground", and from this infer local surface charge distributions. The TreK^{TM} probe arrangement, its dimensions and the chamber photographs at JPL are shown in fig. II.3. The TreK^{TM} voltmeter is actually composed of an electric field sensor and an adjustable voltage

source. An internal sensor monitors the electric field that penetrates into the hole in the face of the TreK™ probe's metal box.

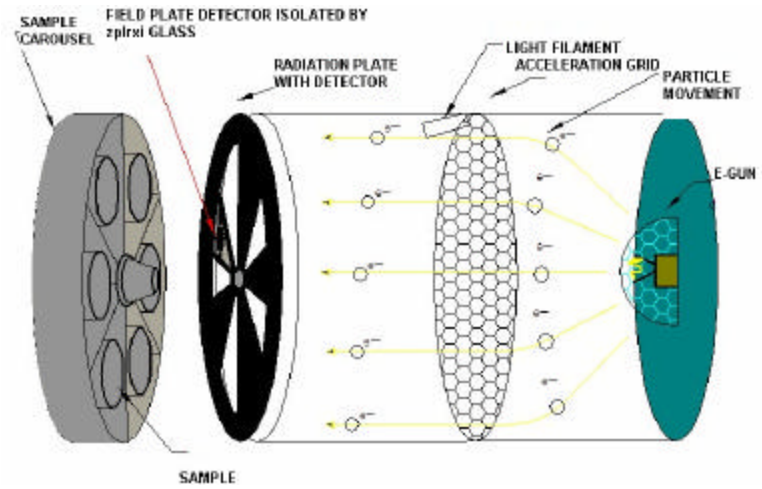

(a)

(b)

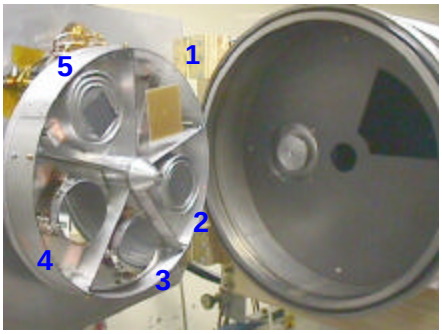

(c)

Fig. II.2. Chamber design at JPL.
(a) Internal design of JPL charge storage chamber. (b) Photograph showing JPL chamber with door closed. (c) Carousel mounted to the door of the vacuum chamber on left half; the body of the vacuum chamber on right. Five samples are on this carousel: clockwise from 1-o'clock: (1) a square sample of circuit board material in the fully open mounting; (2) the mirror in the "air-tight" can; (3) and (4) two mirrors in an open configuration; and last (5) a carbon-coated metal in a can acting as a beam current monitor. When the door is closed, the carousel extends about 8 cm into the vacuum chamber and rubs against a carbon-coated aluminum plate called the shutter. The shutter is tightly affixed to the walls of the chamber.

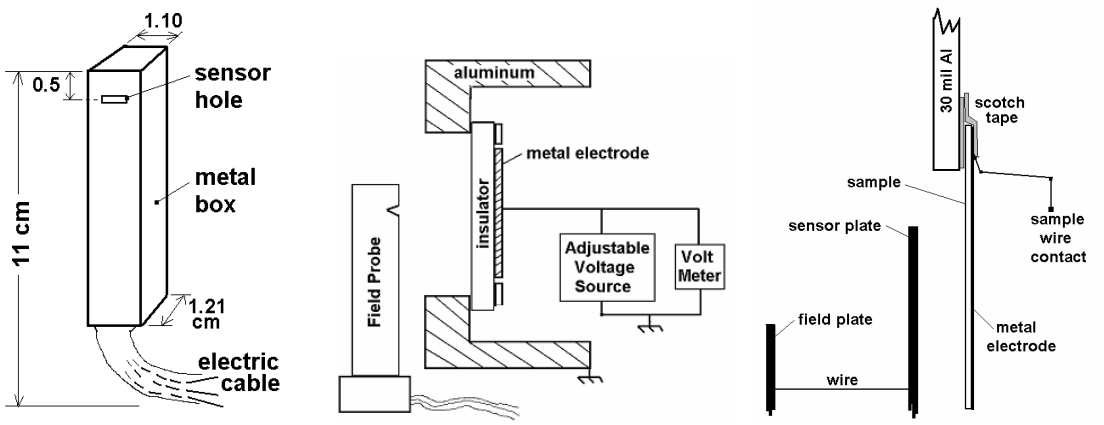

(a) (b) (c)

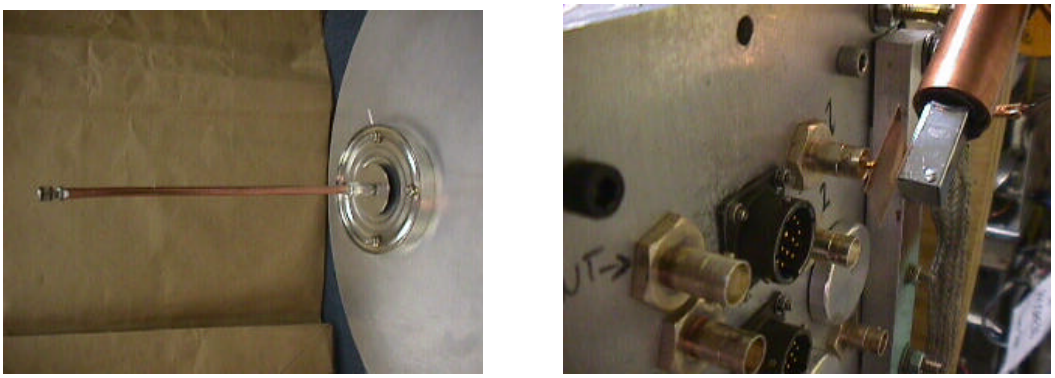

(d) (e)

Fig. III.3. TreK^{TM} probe assembly at JPL.
(a) Diagram of TreK^{TM} probe dimensions. (b) Schematic of the TreK^{TM} field probe and the sample configuration. (c) Details of the samples suspended across an opening in a thin aluminum plate with adhesive tape. (d) Structure of JPL can sample holder and field plate assembly inside the vacuum. The can covers the PMMA and its interior baffle. The grounded can does not contact the baffle nor the center screw that is connected to the sensor plate nor the PMMA. The second "baffle" and the stiff copper sensor wire are attached to the sensor plate screw and connect to the field plate via a short flexible clip lead and the center conductor of a BNC vacuum feed through. (e) One-inch copper field plate close to the TreK^{TM} probe outside the vacuum.

The circuits adjust the potential of the metal box until it attains nearly the potential of the nearby high voltage (HV) surface, at which condition there is zero field penetrating into the small hole. A standard voltmeter is used to measure the potential of the box, and the sample surface potential is proportional to the box potential. No electrical contact is made to the nearby HV surface. In addition, as the box voltage approaches the nearby HV surface voltage, the effective capacitance of the box to that surface approaches zero.

The electron beam, low-energy electron treatments, light photon treatments, thermal treatments, or other treatments of the samples must not affect the capacitor sensing circuit that brings the sample surface voltages out of the vacuum chamber. At JPL a custom capacitance transfer probe was constructed to make electric field measurements at sample surfaces *in situ* in the vacuum chamber, using a TreK™ probe external to the chamber; this isolates the sensitive TreK™ probe from the sample treatments.

Figures II.3 (c), (d) and (e) shows the JPL sample arrangement, TreK™ probe structure and the probe outside the vacuum. Key aspects of the design are the geometry, construction and materials of the field probe, voltage sensor plate, connecting wire, and wire vacuum feedthrough. In addition, the coupling to the charge probe assembly - particularly the voltage sensor plate - to the sample and sample electrode are important. Both the mountings and the samples themselves must be coordinated so that the measurement technique corresponds to the physical and mathematical modeling. The spacing between the biased field-generating plate and the field probe is much smaller than the extent of the probe. Therefore, between the flat surface of the probe and the flat

plate the electric field is plane-parallel. Note that surfaces at other voltages must be relatively far from the flat plate so as not to alter the field between the plate and the probe. We determined that a 12 mm x 12 mm flat plate spaced 3 mm from the probe satisfied this condition, even with most of the probe surrounded with protective copper pipe.

3.) Sample Treatment: The arrangement for charging and measuring the voltage on an insulated surface at JPL was defined in fig. 2.15 (a). The insulated surface of the sample faces the electron source and/or the field probe. The other surface of the sample is metallized and connected to wiring so that it can be biased relative to ground, and relative to the electron source, or monitored for currents. The diameter of the center electrode on the sample is 4.6 cm and its area is 16.6 cm^2. The diameter of the opening on the aluminum mount is 5.08 cm. A grounded reference sample is used to establish the zero of the field probe.

An electron-emitting filament is used to provide uniform surface charge that does not penetrate far into the sample. A positive bias is applied to the rear sample electrode. The filament source is used to inject electrons into the vacuum; slowly raising the sample electrode voltage to, say, 1 kV, one gently charges the sample with electrons that impact the sample with less than 25 eV and develops 1 kV across the sample. The filament source is then turned off, the rear sample electrode grounded, and a 1 kV voltage is measured on the front surface of the insulator sample with the capacitance transfer probe and TReK^{TM} probe. This method places the electrons gently onto the front surface, not deeper into the bulk of the insulator. The field in the sample is therefore ideal for our measurements. Measurement of total current flow with an electrometer as the sample

electrode is changed from 1 kV to ground, as well as the sample electrode voltage, can be used to determine the current required to charge the sample and to estimate the sample dielectric constant.

Alternately, a broad-beam electron gun with accelerating potentials from 0 to 75 keVA is available on the JPL chamber for uniform, stable charge deposition at energies in the few keV regimes near the second crossover energy and at higher energies for study of internal sample charging [see fig. II.2 (a)]. Charging induced by electron irradiation is strongly modified by the electron-hole pairs that the irradiation generates in the insulator. High field effects at 10^8 V/m act strongly on the electron-hole pairs and on electrons in shallow traps to provide extended conductivity. Visible light can be used to investigate conduction by electrons (or holes) emitted from shallow trapping levels. The qualitative physics of such processes in solid dielectrics has long been known, and some instrumentation is developed here for measuring the effects in practical spacecraft charging applications.

As was shown in fig. 1.7, the JPL chamber also has an integral plasma source with bias capabilities, plus W-filament and UV light sources. Charging with electrons from the plasma can, in general, be accomplished more effectively with the low energy flood gun described above. But charging with positive ions is best accomplished with a plasma source. The plasma source is used while rear sample electrode is biased negative in order to get ions onto the surface. This is useful, for example, to see if ions chemically diffuse and produce conduction in insulating polymers when electrons do not, or to study about atomic diffusion in dielectrics.